FABRICATION OF NANOCOMPOSITE ELECTRODE FOR EFFICIENT ELECTROCHEMICAL CONVERSION OF CARBON DIOXIDE TO VALUE-ADDED HYDROCARBONS

BY

RAMADAN ABDELMONEM RABIE MOHAMED GEIOUSHY

A Dissertation Presented to the

DEANSHIP OF GRADUATE STUDIES

KING FAHD UNIVERSITY OF PETROLEUM & MINERALS

DHAHRAN, SAUDI ARABIA

In Partial Fulfillment of the
Requirements for the Degree of

DOCTOR OF PHILOSOPHY

In

CHEMISTRY

APRIL 2017

KING FAHD UNIVERSITY OF PETROLEUM & MINERALS

DHAHRAN- 31261, SAUDI ARABIA

DEANSHIP OF GRADUATE STUDIES

This thesis, written by **RAMADAN ABDELMONEM RABIE MOHAMED GEIOUSHY** under the direction his thesis advisor and approved by his thesis committee, has been presented and accepted by the Dean of Graduate Studies, in partial fulfillment of the requirements for the degree of **DOCTOR OF PHILOSOPHY IN CHEMISTRY.**

Dr. MAZEN KHALED
(Advisor)

14/5/2017

Dr. ABDULAZIZ AL-SAADI
Department Chairman

Dr. ABDALLA ABULKIBASH
(Member)

Dr. Salam A. Zummo
Dean of Graduate Studies

Dr. ANVARHUSEIN ISAB
(Member)

18/5/17

Date

Dr. BASHEER CHANBASHA
(Member)

Dr. KHALID ALHOOSHANI
(Member)

I dedicate this work to the almighty ALLAH, the source of wisdom, the light of understanding and inspiration, who has been the reason for my success in my life. Also, I dedicate to my beloved family

ACKNOWLEDGMENTS

My great thanks to ALLAH who gave me the strength and the patient throughout my academic pursuits, for the completion of the doctoral research work, and subsequent award of the doctor of philosophy degree in chemistry.

I wish to acknowledge King Fahd University of Petroleum and Minerals (KFUPM) and the ministry of higher education for providing me the PhD scholarship. Also, I would like to thank the rector of KFUPM (Dr. Khaled Al-Sultan); the past (Dr. A. Hamdan) and present (Dr. Abdulaziz Al-Saadi) Chairmen, Department of Chemistry, KFUPM for hosting and providing the needed facilities for my PhD research work. I wish to thank the Dean of Graduate Studies, Dr. Salam A. Zummo for his encouragement in this program; his advice have helped in so many ways regarding the program schedules and general academic performance.

I express my deepest gratitude to my research advisor, Prof. Mazen Khaled for his instructive guidance and encouragements, constructive criticism and insights, and patience in training throughout the research work. I am also grateful to my committee members: Prof. Abdalla Abulkibash, Prof. Anvarhusein Isab, Dr. Basheer Chanbasha, and Dr. Khalid Alhooshani for their assistance and advice in keeping with the progress of work on schedule and the reading, correction of this thesis. Special thanks goes to the graduate students' coordinator (Prof. Bassam El-Ali), all chemistry faculty members, and chemistry department stuff.

I gratefully acknowledge the assistance of Center of Research Excellence in Nanotechnology, Dr. Abbas Hakeem, (CENT) for allowing me the use of equipments for characterization of the synthesized materials.

I would like to thank my home institute; Central Metallurgical R & D Institute (CMRDI), Egypt for the permission to complete my graduate study at KFUPM.

I wish to thank and appreciate the members of my dear family; mother, father, brothers, and sister. My deepest thank to my wife and my lovely daughters (Leena & Rawda) for their love, patience and the source of inspiration and peace.

TABLE OF CONTENTS

LIST OF TABLES

LIST OF FIGURES

LIST OF ABBREVIATIONS

CO_2	:	Carbon Dioxide
CCS	:	Carbon capture and sequestration
IEA	:	International energy agency
WEO	:	World energy outlook
CO_2RR	:	CO_2 reduction reaction
HER	:	Hydrogen evolution reaction
FE (%)	:	Faradaic efficiency
j	:	Current density
XRD	:	X-ray diffraction
SEM	:	Scanning electron microscope
EDS	:	Energy dispersive scattering
TEM	:	Transmission electron microscope
HRTEM	:	High resolution transmission electron microscope
XPS	:	X-ray photoelectron spectroscope
GCMS	:	Gas chromatography mass spectrometer
SCE	:	Saturated calomel electrode
RHE	:	Reference hydrogen electrode
Ag/AgCl	:	Silver/silver chloride reference electrode
NFs	:	Nanoflowers
LSV	:	Linear sweep voltammetry

DFT	:	Density functional theory
GCE	:	Glassy carbon electrode
CV	:	Cyclic voltammetry
CNF	:	Carbon nanofiber
GO	:	Graphene oxide
GN	:	Graphene
NPs	:	Nanoparticles
SDS	:	Sodium dodecyl sulfate
Sample S1	:	Composite with ZnO/Cu_2O weight ratio of 2:1
Sample S2	:	Composite with ZnO/Cu_2O weight ratio of 1:2

ABSTRACT

Full Name : [Ramadan Abdelmonem Rabie Mohamed Geioushy]

Thesis Title : [Fabrication of Nanocomposite Electrode for Efficient Electrochemical Conversion of Carbon Dioxide to Value-Added Hydrocarbons]

Major Field : [Chemistry]

Date of Degree : [April 2017]

Electrochemical reduction of carbon dioxide to valuable fuel is one of the most promising and rapid approaches to reduce CO_2 emission in atmosphere beside store energy in the form of liquid fuels. Due to the drawback of the high cost of hydrogenation and low yield of photochemical processes, electrochemical reduction of CO_2 is the most common, simple, and high product yield process. Comparing to different renewable energy sources such as, solar and hydrogen energy, conversion of CO_2 to liquid fuels is superior and more convenient way to store energy due to the high density per weight and per volume which render CO_2 conversion come on top of other renewable energy sources. In this study, we fabricated graphene(GN)/metal oxide nanocomposites such as GN/Cu_2O, GN/ZnO, and G/ZnO/ Cu_2O-based electrode where graphene is known to be the most efficient cathode due to its large surface area and high electron mobility due to its extended pi-bond structure. Cu_2O is a universally agreed form of copper (I) oxide to be the most efficient metallic oxide that aid in the transformation of the CO_2 to methanol specifically. Graphene/Cu_2O based electrode showed high catalytic activity for CO_2 reduction towards ethanol in compare to Cu_2O. Also, the contribution of Cu_2O into graphene/ZnO composite showed a reasonable enhancement in the cathodic reduction current density. Different ZnO/Cu_2O weight ratios has been tested, and the results indicated the conversion of CO_2 to n-propanol.

ملخص الرسالة

الاسم الكامل: رمضان عبد المنعم ربيع محمد جيوشى

عنوان الرسالة: تصنيع أقطاب ذات كفاءة عالية لتحويل ثانى أكسيد الكربون الى هيدروكربونات عالية القيمة

التخصص: الكيمياء

تاريخ الدرجة العلمية:أبريل 2017

يعتبر الاختزال الكهروكيميائى لغاز ثانى أكسيد الكربون الى مواد ذات قيمه عاليه هى واحدة من اكثر الاساليب الواعدة للحد من انبعاثات ثانى اكسيد الكربون فى الغلاف الجوى بجانب انها احدى الطرق لتخزين الطاقة فى شكل وقود سائل. هناك طرق اخرى لتحويل ثانى اكسيد الكربون الى مواد عالية القيمة مثل الهدرجة والعمليات الكهروضوئية ولكن بسبب التكلفة العالية لعملية الهدرجة والعائد القليل الناتج من العملية الكهروضوئية لذلك طريقة الاختزال الكهروكيميائى هى العملية الشائعه وبسيطه وتنتج عائد عالى. فى نفس الوقت مقارنة لمختلف مصادر الطاقة المتجددة مثل الطاقة الشمسة والهيدروجين تأتى عملية اختزال غاز ثانى اكسيد الكربون كوسيلة ملائمة وممتازة لتخزين الطاقة. ولذلك هذا الاقتراح يهدف الى تصنيع الكترود قائم على مادة الجرافين مع بعض اكسيد العناصر النانومترية مثل اول اكسيد النحاس واكسيد الزنك كل على حدة. حيث تأتى مادة الجرافين على رأس المواد ذات مساحة سطح كبيرة جداً بجانب سهولة وسرعة انتقال الالكترونات بين طبقات الجرافين لتسهيل عملية اختزال ثانى أكسيد الكربون. أيضاُ اشباه الموصلات مثل أول اكسيد النحاس ذات فجوة الطاقة 2.14 فولت والمعروف بفعاليتة العالية لتحويل ثانى أكسيد الكربون الى ميثانول بجانب الاكسجين الذى يزيد من فجوات الالكترونات ومن خلالها تزيد امتصاص ثانى اكسيد الكربون على سطح الالكترود. لذلك من خلال جمع الخصائص لكل من الجرافين واشباه الموصلات للاكأسيد المذكورة داخل المقترح مع المنهجية الخاصة بنا فاننا نتوقع تعزيز كبير للانتقائية والانتاج العالى والكفاءة الفارادية العالية لانتاج هيدروكربونات ذات قيمة عاليه من غاز ثانى أكسيد الكربون. وقد أثبتت تلك الدراسة كما سيتضح من خلال النتائج المعروضة قدرة الالكترود مصنوع من الجرافين/اول اكسيد النحاس على اختزال ثانى أكسيد الكربون الى الكحول الايثيلى. كما تم تققيم الكترود مصنوع من الجرافين/ اكسيد الزنك/ أول اكسيد النحاس لتحويل ثانى أكسيد الكربون الى البروبانول.

CHAPTER 1

INTRODUCTION

1.1 Carbon Dioxide

CO_2 occurs naturally in small amounts (about 0.04%) in the atmosphere. As a major greenhouse gas, CO_2 acts to maintain the natural greenhouse effect that keeps our planet hospitable to life. CO_2 is added to soft drinks to make them bubbly. CO_2 is also used in fire extinguishers. Every day, millions of tons of CO_2 are injected into underground geologic zones to help produce oil in a well-known industry practice called "CO_2 flooding" or enhanced oil recovery.

1.2 Is CO_2 a Pollutant?

CO_2 formed by human action is called anthropogenic CO_2. Plowing the land, making cement, and burning fossil fuels for energy all generate anthropogenic CO_2, which adds carbon to the global carbon cycle. Between 1751 and 2013, approximately 1440 billion metric tons of CO_2 has been emitted to the atmosphere from these sources. This raises concerns about climate change. The U.S. Environmental Protection Agency has considred CO_2 a pollutant in order to be able to regulate anthropogenic CO_2 emissions from human activities under the Clean Air Act of 1970.

1.3 Carbon capture and sequestration (CCS)

Since the industrial revolution in the 19th century, the fossil fuels (petroleum, coal, and natural gas) are burned in the power plants to produce energy. On the other hand, the global demand for energy is increasing in parallel with the fast development of economy and population. In addition, the fossil fuels as non-renewable resources are excessively depleted, leading to an energy crisis. Also, the huge consumption of fossil fuels causing large amounts of CO_2 accumulation in the atmosphere [1]. Around 496 gigatonnes of CO_2 was predicted to produce from many factories, vehicles, chemical and power plants in the coming few decades. As a result, the atmospheric CO_2 concentration has far exceeded the upper safety limit of 350 ppm. Recently, the International Energy Agency (IEA)-World Energy Outlook (WEO) revealed that by 2030 CO_2 emissions will attain 63% from today's level, which is almost 90% higher than those of 1990. Carbon dioxide is the major greenhouse which contributes significantly to the global warming [2][3][4][5]. On the other hand, CO_2 is a typical renewable feedstock for manufacturing chemicals such as; hydrocarbons and alcohols. The scientists believe that the average temperature will rise up if CO_2 concentration reaches 550 ppm, which could disrupt our eco-environment system. It was agreed by 195 nations in Paris agreement on climate change to keep a global temperature rise this century well below 2 degrees Celsius.

To mitigate CO_2 emission, during the previous decades, fossil fuels have been replaced by clean and renewable energy sources. Solar and wind energy were considered the most viable option to drive clean and renewable energy demand, but the challenges associated

with storage and the utilization of these sources require the development of economically viable technology. Figure 1.1. shows the concept of restoring balance in CO_2 cycle [6].

Later, carbon capture and sequestration (CCS) was the common and essential way to prevent the release of large amount of CO_2 into the atmosphere. Nevertheless, there are some limitations of CCS technology, such as energy consumption and high cost in addition to the leakage of stored CO_2. Recently, conversion of carbon dioxide to useful organic molecules like hydrocarbons or alcohols received more attention as an ideal solution to reduce the amount of atmospheric CO_2 level and assist in switching from fossil fuels to renewable energy sources[7][8][9][10], thus overcomes the energy storage problem as it provides the suitable potential solution to store the renewable energies in chemical forms as shown in figure 1.2.

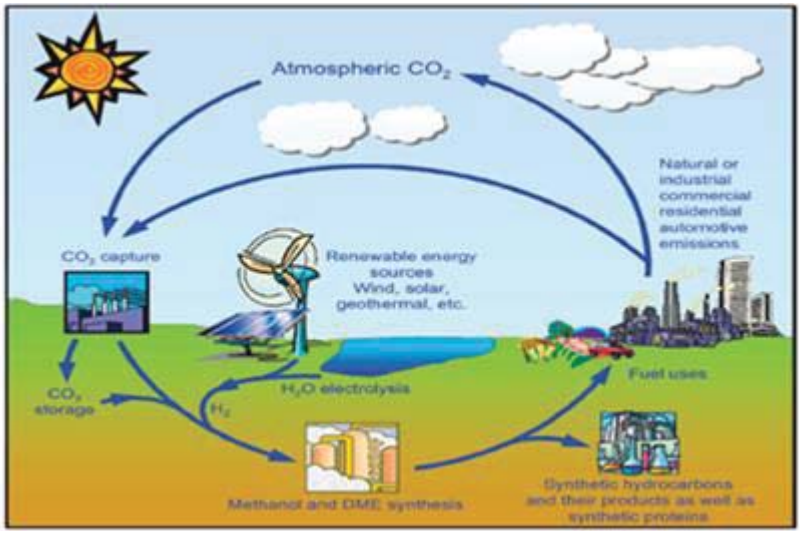

Figure 1.1 The carbon dioxide cycle in life [6].

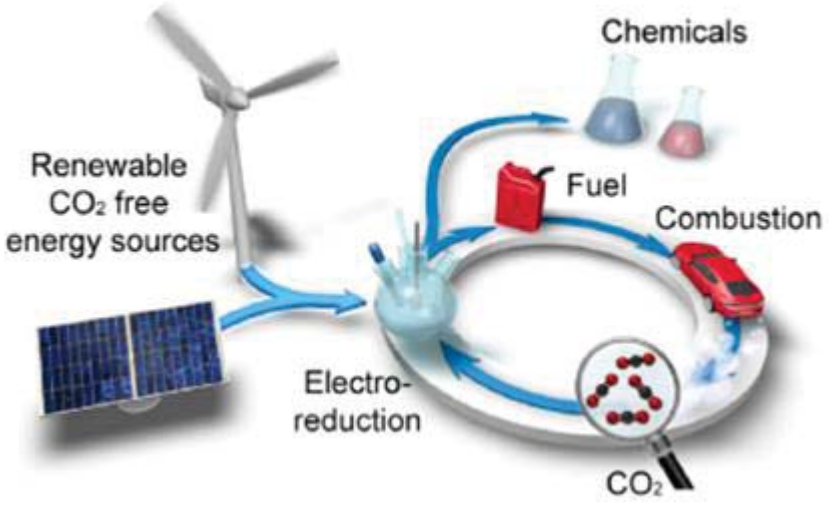

Figure 1.2 Possible pathways to convert carbon dioxide to chemicals [8].

1.4 Thermodynamic considerations of CO_2

$$CO_{2(g)} + 3H_{2(g)} \rightarrow CH_3OH_{(l)} + H_2O_{(l)} \qquad \Delta H = -131.0 \text{ kJ mol}^{-1}$$

The above equation shows the reaction between carbon dioxide and hydrogen to form stable products and it is considered to be thermodynamically favorable. So that the limited use of CO_2 is more likely kinetic. Both terms (ΔS and ΔH) of the Gibbs free energy (ΔG) are not favorable for converting CO_2 to other molecules [11]. The carbon-oxygen bonds are relatively strong and substantial energy has to be supplied for their cleavage. The entropy contribution through the term (- $T\Delta S$) makes little contribution to the thermodynamic driving force for any reaction involving CO_2 so that the value of the enthalpy change AH is a good guide to the thermodynamic feasibility. Table 1.1 shows thermodynamic terms for several CO_2 reactions. The kinetics are favorable CO_2 reduction may also be possible at metallic surfaces where the free energy of oxide formation is highly favorable.

Table 1.1 Thermodynamics of CO_2 reactions [11].

	ΔH	-TΔS	ΔG
$H_{2(g)} + CO_{2(g)} \rightarrow CO_{(g)} + H_2O_{(g)}$	41.2	22.6	18.6
$H_{2(g)} + CO_{2(g)} \rightarrow CO_{(g)} + H_2O_{(l)}$	-2.8	22.8	20
$H_{2(g)} + CO_{2(g)} \rightarrow HCOOH_{(l)}$	-31.2	64.2	33
$2H_{2(g)} + CO_{2(g)} \quad \backslash CH_2O_{(g)} + H_2O_{(L)}$	-9	55	44
$3H_{2(g)} + CO_{2(g)} \quad \backslash CH_3OH_{(l)} + H_2O_{(l)}$	-131.3	122.1	-9.2
$4H_{2(g)} + CO_{2(g)} \quad \backslash CH_{4(g)} + 2H_2O_{(L)}$	-252.9	122.1	-130.8

1.5 Molecular orbitals of CO_2

CO_2 contains 22 electrons, 16 of which are valence electrons (4 e^- from C + 12 e^- from 2 O) accommodating four σ orbitals (eight electrons) and two π orbitals (eight electrons) in which four bonding pairs and four non-bonding pairs as shown in figure 1.3. The unoccupied $2\pi_u$ molecular orbital is the only valence orbital for which the bent molecule is strongly favored. Processes at surfaces involve electron transfer from a substrate into the CO_2 molecule which in turn would lead to occupation of this orbital via the formation of a CO_2 anion ($CO_2 + e^- \rightarrow CO_2^-$). The undistorted CO_2 molecule exhibits two bonding modes, namely via the oxygen atom(s) forming a linear CO_2-metal bond or via the pi-bonds of the CO_2 molecule. In comparison, anionic CO_2 molecule could exhibit three modes of coordination: (a) a pure carbon coordination, or (b) a pure oxygen bidentate coordination, or (c) a mixed carbon-oxygen coordination.

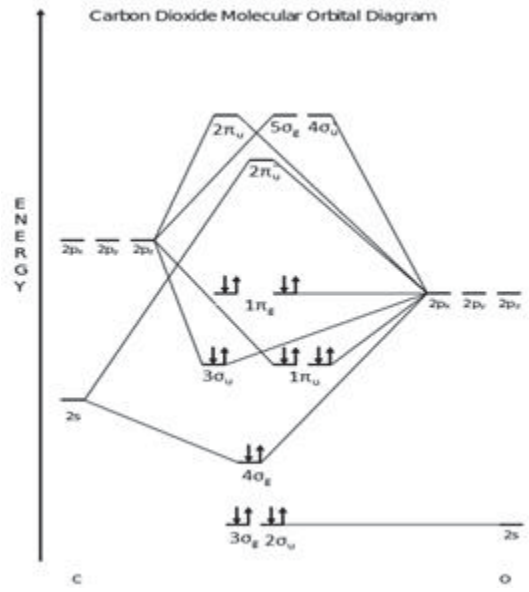

Figure 1.3 Molecular orbital diagram of CO_2.

1.6 Electrochemical reduction of CO_2

CO_2 is thermodynamically stable fully oxidized molecule. The process to convert CO_2 to reduced carbon species is kinetically very poor. Different methods such as thermochemical, photochemical, and electrochemical have been carried out for CO_2 reduction reaction (CO_2RR) [12]. Thermochemical process required high temperature and large amount of H_2. Photochemical process has very poor selectivity and low production rate. Numerous studies have revealed that the electrochemical reduction of carbon dioxide to valuable chemicals like CO, HCOOH, CH_3OH, C_2H_5OH, and ethylene is one of the attractive route. This is attributed to the simplicity, moderate efficiency, controllable selectivity, environmentally friendly, cost effectiveness. Moreover, this reaction can be carried out under ambient conditions in aqueous and non-aqueous electrolytes [13][14][15][16]. The major drawbacks are; the electrochemical reduction of CO_2 requires high overpotentials to

be reduced efficiently, hydrogen evolution reaction (HER) poses a main challenge as it competes with CO_2 reduction at the cathode surface and hence consumes the electrons. As a result, the faradaic efficiency of CO_2 conversion decreases. Up till now no economical and commercial process is available for the reduction of CO_2.

Therefore, an efficient electrocatalyst should be developed for the production of the selective desired product and the high faradic efficiency. Homogeneous and heterogeneous electrocatalysts have been widely used for CO_2 electroreduction. Homogeneous catalysts have some disadvantageous such as high cost and toxicity which hinder their application in industry. In contrast, heterogeneous catalysts have great potentiality for large-scale application due to their simple synthesis and environmentally friendly.

1.6.1 Reaction mechanism of CO_2 electroreduction

The electrochemical reduction of CO_2 takes place at the electrode-electrolyte interface. Reduction pathway proceeds usually in an aqueous electrolyte solution via multi-steps process involving number of electrons based on the product yielded. This catalysis process involves three major steps: i) adsorption of CO_2 on an electro-catalyst surface; ii) electron transfer and proton migration to form C-H bond; iii) desorption of the product from the electro-catalyst surface. The products generated as a result of CO_2 reduction are strongly dependent on different parameters such as, the nature of the electrode material, the applied potential and the electrolyte [17][18].

1.6.2 Electro-catalyst

Electro-catalyst should be designed as a highly selective cathode towards desired products and should suppress the hydrogen evolution side reaction. Metallic, non-metallic, and molecular are the most common electro-catalysts (Fig. 1.4). during the early stage, the electrochemical reduction of CO_2 studies have been based on several kinds of metallic electrodes such as; amalgamated copper, amalgamated zinc, lead, and mercury. Monometallic catalysts can be divided into subgroups based on the product selectivity: CO selective (e.g., Zn, Ag, and Au), formate selective (e.g., Fe, Ni, and Pt).

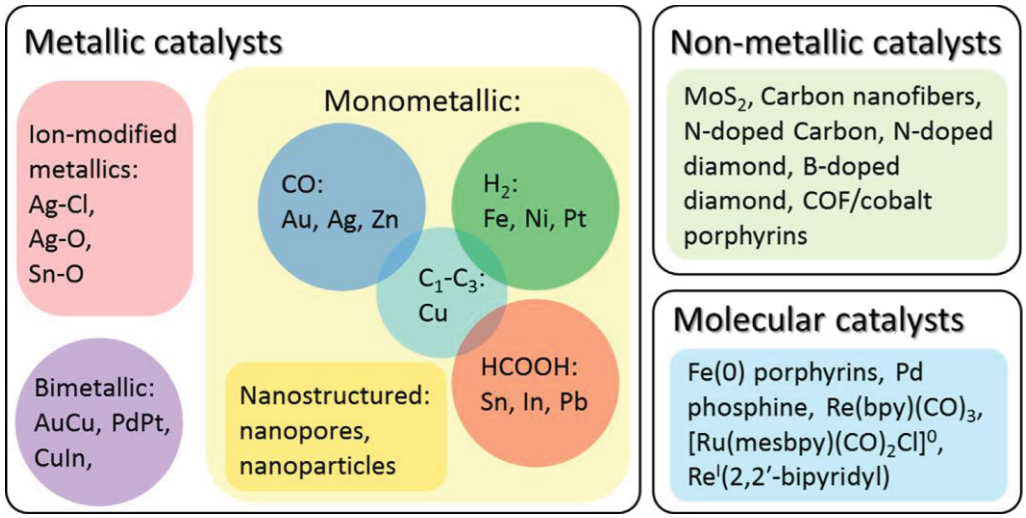

Figure 1.4 Different categories of electro-catalysts for CO_2 reduction [19].

Recently, Copper metallic electrode was found to exhibit higher catalytic activity to wide range of products like CO, formate, ethanol, and ethylene. Hori et al. have used metallic copper as an electro-catalyst for CO_2 reduction to hydrocarbons at high efficiencies. To date, various nanostructured catalysts have been used in aqueous solutions to reduce CO_2. Since nanostructured materials provide more surface active sites. Among these metals are Zn and Cu which has medium hydrogen overpotential characteristics [20][21]. Zn has weak CO binding energy while Cu has strong CO binding energy. As Cu-Zn catalysts have been demonstrated for CH_3OH production [22][23]. Figure 1.5 shows the pourbaix diagram for carbon dioxide reduction as a function of pH. Table 1.2 presents a wide range of CO_2 products as a result of the proton-assisted processes which makes the selectivity very challenging because of the similarity of all redox potentials for different reaction pathways.

However, most metals are expensive and not applicable for large scale applications. So, more efforts are needed to design an effective metal-free catalysts for CO_2 conversion with higher selectivity towards C-H and C-C bond-containing products. Cuprous oxide (Cu_2O) as a p-type semi-conductor with 2.14 eV bandgap has received high extensive investigation for electrochemical CO_2 reductions. Cu_2O was found to be the most active and selective electrode towards alcohols production from CO_2 reduction [24]. The oxygen species in Cu (I) increases the number of defect electrons so that CO_2 is easily adsorbed onto the surface of the catalyst which facilitates its reduction as well as conversion.

Table 1.2 Standard redox potentials for CO_2 electroreduction.

Reaction	E (V) vs. SHE
$2H^+ + 2e^- = H_2$	-0.41
$CO_2 + 2H^+ + 2e^- = HCOOH$	-0.61
$CO_2 + 2H+ + 2e- = CO + H_2O$	-0.53
$CO_2 + 4H^+ + 4e^- = C + 2H_2O$	-0.20
$CO_2 + 4H^+ + 4e^- = HCHO + H_2O$	-0.48
$CO_2 + 6H^+ + 6e^- = CH_3OH + H_2O$	-0.38
$CO_2 + 8H^+ + 8e^- = CH_4 + 2H_2O$	-0.24

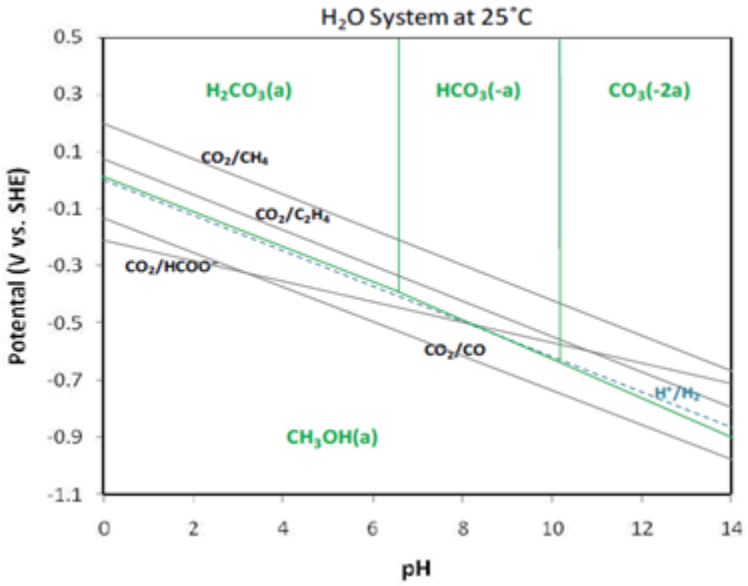

Figure 1.5 Pourbaix diagram for carbon dioxide reduction at 25 ºC.

Low selectivity, low products yield, large overpotential and low Faradic efficiency (FE) are the main problems associated to these systems. To overcome these drawbacks, metal and/or metal oxides dispersed on carbon materials supports which provide high surface area and more active sites have been used [25]. Graphene as a new carbon material has large specific surface area and excellent electron mobility over its surface which is expected to be a promising catalyst for CO_2 reduction process [26].

1.7 Statement of the problem

Carbon dioxide is a greenhouse gas which is produced from different resources around us and its atmospheric level increases rapidly. Capture and conversion of CO_2 to useful chemicals are the proper way to reduce the CO_2 level in the atmosphere. Methanol and ethanol have high energy density, easily stored, nontoxic and safe, and are considered as renewable energy sources need more attention to be produced form CO_2 reduction. The electrochemical reduction of CO_2 needs a high overpotential and is accompanied by many products such as CO. HCCOH, and CH_4. Besides the high potential and poor selectivity, hydrogen evolution reaction (HER) presents a big competition during the CO_2 reduction over the electrode surface. So, the electrochemical reduction of CO_2 requires an electro-catalyst which should be designed with high selectivity towards alcohols and to overcome the HER problem. Material properties and the catalyst behaviour such as the active sites, the geometries, the compositions, the substrate as well as the electron transfer mechanisms have to be thoroughly investigated. Also, the high product yield, the high Efficiency and the reproducibility are of great challenge.

1.8 Objectives of the study

Conversion of CO_2 to C_1 products (CO and formate) have been intensively studied. New trends lie in designing advanced cathode materials to convert CO_2 to more value-added C_2-C_4 products. Up to date, no electro-catalyst exhibited a good selectivity C_2-C_4 products. Many scientists have used carbon nanomaterials and developed an alternate conversion of CO_2 to useful chemicals. We expected by reviewing the literature of the past three decades that carbon nanomaterials/metal oxides would direct a new path in the electrochemical reduction of CO_2. High yield and high selectivity of the desired products are the main challenge. We expect that using bimetallic and/or carbon supported catalysts would be a new alternating direction for CO_2 reduction due to the synergy effect and the unique reaction sites arises from the new structure building and morphology. The main objectives proposed in this work are as follows:

1. Proper preparation of the copper surface through either Electro-polishing Cu foil, mechanical and chemical treatment.
2. The synthesis of Graphene oxide using Hummer method and its characterization via XRD and Raman spectroscopy.
3. The synthesis of graphene/metal oxides (Cu_2O, and ZnO) nanocomposites using co-precipitation method and characterize samples via different tools like, XRD, SEM, EDS, TEM, Raman, XPS, and Uv-vis Absorption.
4. Fabrication of the cathode material by depositing the as-synthesized graphene-based metal oxides on the copper surface and using three electrode cell for CO_2 reduction followed by product analysis using GC-MS

5. To design a suitable electrochemical cell of three electrodes for the CO_2 conversion and to enhance the efficiency of the electrochemical conversion of CO_2 to methanol or other hydrocarbons via studying the pH, electrolyte type and temperature parameters and electroreduction starting voltage range from -0.2 to -1.8 V vs Ag/AgCl.
6. Analysis of the liquid products generated as a result of the CO_2 reduction via either direct injection or head-space GCMS instrument
7. Calculation of the Faradaic efficiency for the products produced for each electrode material.

1.9 Overview

The main goal of this study is to fabricate an efficient graphene-based metal oxides electrodes for the electrochemical reduction of CO_2 to value-added products with high selectivity and yields.

Chapter 2 present several studies that have investigated the reduction of CO_2 electrochemically using various categories of monometallic, bimetallic, non-metallic, and molecular electro-catalysts. Also, this chapter introduces several parameters that affect the electrochemical reduction process such electrolyte type, temperature, pH, and carbon supporting materials which affect the selectivity, efficiency, and the product yields.

Chapter 3 focuses on the experimental details of the designing and compartments of the three electrodes electrochemical cell used. Also, this chapter describes the synthesis of graphene oxide precursor and the proceeding used for synthesis and the fabrication of graphene/Cu_2O, graphene/ZnO, and graphene/ZnO/Cu_2O electrodes. Characterization techniques used to confirm the synthesis of the desired catalysts have been investigated. Chapter 3 describes the electrochemical measurements for electro-catalytic activity evaluation of the fabricated electrodes and the calculation of Faradaic efficiency.

Chapter 4 presents the results and the discussion of the as-synthesized electro-catalysts performance for the electrochemical reduction of CO_2 at graphene/Cu_2O in comparison with Cu_2O. Also, the effect of incorporating Cu_2O into graphene/ZnO and its catalytic activity for the CO_2 electroreduction using GCMS analysis and the Faradaic efficiency calculations. Chapter 5 concludes the experimental and the results obtained in this study.

CHAPTER 2

LITERATURE REVIEW

2.1 Different pathways for CO_2 reduction

Scientists have investigated the different methods for CO_2 conversion to value-added products as a promising way to reduce CO_2 atmospheric level [27][28][29]. Hydrogenation and photochemical reduction pathways are the most common methods used before [30][31][32]. However, the high temperature and the large amounts of hydrogen used in hydrogenation process makes it less efficient. Also, the very limited product yields and the low efficiency are the most critical drawbacks of photochemical method. Recently, electrochemical conversion of CO_2 has been intensively studied and found to be more advantages over other methods due to its simplicity, low cost, and high efficiency and high product yields [33][34] [35][36][37][38]. In addition, the selectivity of the electrochemical method over different structure of electro-catalyst electrodes towards desired value products such as methanol [39], CO [40], formate [41][42][43][14], and ethanol [44].

2.1.1 Hydrogenation of CO_2

In the past century, the hydrogenation of carbon dioxide to fuels such as formic acid, methanol, and ethanol has been intensively investigated. The most common process is the formation of methanol from synthetic gas, which contains CO, H_2, and CO_2 mixtures. The process is carried out at high temperature (300-400 ^oC) and under high pressure (~ 300 atm). The methanol formation through catalytic hydrogenation is an exothermic process, and the reverse water gas shift (RWGS) plays a critical role to slow down the rate of formation. So, a proper catalyst for CO_2 hydrogenation should be designed to be able to overcome water intolerance as well as to improve the activity and selectivity. Metallic copper catalysts showed a good activity toward methanol formation, and is directly proportional with the surface area of copper. Later, Cu (I) showed high activity toward methanol production than the metallic form by an order of magnitude. This is related to the strong intermediates (carbonates, formate, and methoxy species) stabilization over Cu (I) active sites [45]. Also, Cu/Zn oxide showed a high activity and selectivity toward methanol formation than Cu alone. ZnO is a wurtzite, n-type semiconductor. Besides oxygen vacancies, ZnO contains an electron pair which may serve as an active site for methanol synthesis. The electron pair in Zn^+ may create cation and anion lattice vacancies which can improve the adsorption and transformation of the reactant, as well as enhance copper

dispersion forming Cu-Zn active sites [46]. The CO_2 hydrogenation process is high hydrogen energy consuming, more H_2 per consumption than hydrocarbon produced.

2.1.2 Photoelectrochemical CO_2 conversion

Photoelectrochemical CO_2 conversion is a process in which carbon dioxide is reduced in the presence of sun light by aids of semiconductor photocatalysts. The role of the photocatalyst is to absorb the light and create electrons and protons needed for the reduction of CO_2 (CO_2RR). Various photocatalysts such as WO_3, TiO_2, ZnO, CdS, GaP, and SiC have been investigated for the CO_2 reduction to produce organic useful chemicals like formaldehyde and methanol. The drawback of the photoelectrochemical process is the low efficiency. Thermodynamically, 228 kJ of energy is required to convert one mole of CO_2 to methanol. $H^{\bullet}$ and $^{\bullet}CO2^{-}$ are the two main radicals formed upon photon absorption having an energy equal to or greater than the band gap of the semiconductor. Several studies have been investigated to improve the efficiency of photoreduction of CO_2 by modifying the surface with metal [47]. The electron-positive hole recombination leading to limited product formation on the catalyst surface lowers the efficiencies of the photocatalysis process. As a result the product yield should be improved in order to upgrade the photocatalytic CO_2 reduction to an industrial scale. Therefore, another alternative proper method for CO_2RR is necessary.

2.1.3 Electrochemical reduction of CO_2

Electrochemistry studies the chemical reactions occurring at the interface of an electron conductor (the working electrode) and an ionic conductor (the electrolyte). Electrons are transferred between the electrode and the electrolyte in the solution. It is called an electrochemical reaction when an external voltage drives the reaction or a voltage is produced by a chemical reaction. The oxidation - reduction (redox) reaction occurs when electrons are transferred between oxidants and reductants. Electricity is required for the electrochemical reduction of carbon dioxide to yield hydrocarbons and alcohols. This electricity can be produced from renewable energy sources including hydro, solar, wind, geothermal, wave and tides for the generation of electrons. Theoretically, water is oxidized at the anode and releases electrons followed by reduction of carbon dioxide at the cathode to hydrocarbons and alcohols. Unfortunately, the reduction potential of carbon dioxide is very close to water reduction. We would like to utilize all the potential to achieve the highest yield; however, increasing the reduction rate of carbon dioxide may also lead to the reduction of water, which will result in hydrogen formation. To solve the problem, a stable catalyst that has a high overpotential is required for the reduction of hydrogen.

2.2 Factors affecting CO_2 electroreduction

2.2.1 Supporting electrolyte for CO_2 electroreduction

Bicarbonate with a pH value of 7 is commonly used as an electrolyte for CO_2 electroreduction. This is attributed to the fact that, bicarbonate acts as a buffer and as a proton source. In addition it is relatively cheap, easy to handle, and environmentally friendly. Ionic liquid based electrolytes are proper electrolytes for CO_2 reduction due to their higher CO_2 solubility and lower reduction overpotentials. Few studies have investigated the effect of the supporting electrolyte on the activity and selectivity of electrochemical reduction of CO_2. As reported before the H_2 evolution is suppressed in presence of halide anion and smaller cation facilitates a higher hydration and hence more reductive product rather than CO, HCHO, and HCOOH. M. Muruganathan et al [4] have studied the effect of the supporting electrolyte ($LiClO_4$) in cold methanol on CO_2 reduction over Cu wire cathode at different potentials that range from -3 to -4 V under high pressure and low temperature. HPLC and GC were used for the analysis of the liquids produced. As shown in table 2.1 methane, ethylene, CO , and methyl formate are the main products and methane production increases with high negative potential (-4 V). Also, Li^{+1} ion with smallest cation size favoured high reductive products rather than ethylene and methyl formate. In addition to the effect of the small cation size Li^{+1}, the high negative potential and the Cu electrode which favors high reductive products.

Table 2.1 Electrochemical reduction of CO_2 at Cu electrode in $LiClO_4$/Methanol [4].

Potential (V vs. Ag. QRE)	Faradaic efficiency (%)						
	CH_4	C_2H_4	CO	$HCOOCH_3$	H_2	CO_2 red.	Total
-3.00	19	0.56	48.3	7.2	29.9	75.1	105.0
-3.25	20.6	0.46	39.3	6.5	40.7	66.9	107.6
-3.50	26.4	0.69	33.5	6.5	45.4	67.1	112.5
-3.75	36.1	0.83	8.6	6.0	73.9	51.5	125.4
-4.00	37.5	0.93	22.7	6.5	60.2	67.6	127.8

Among the metals, Zinc is considered as a promising catalyst towards the electroreduction of CO_2 to CO in nonaqueous electrolyte solutions, however its catalytic activity diminishes in aqueous solution. F. Quan et al. [48] have enhanced the efficiency of nanoscale Zn in NaCl electrolyte solution for the conversion of CO_2 to CO. Nanoscale Zn synthesized after anodization of Zn foil, the electroreduction of ZnO nanoplate in NaCl solution for 30 min at -1.3 V. The study evaluated the electroreduction of CO_2 of ZnO foil and nanoscale Zn in $NaHCO_3$. It was observed that faradaic efficiency of CO production was significantly increased three times over nanoscale Zn than Zn foil at -1.6 V vs. SCE. Moreover, replacing the cathodic electrolyte of $NaHCO_3$ with NaCl, the faradaic efficiency of CO production over nanoscale Zn was 93% at -1.6 V vs. SCE (Fig. 2.1) even for long electrolysis (10 h). This explains the role of the electrolyte solution on the CO_2 conversion efficiency which can be explained by the adsorption strength of halide anion (Cl^-) on the surface of the metal electrode.

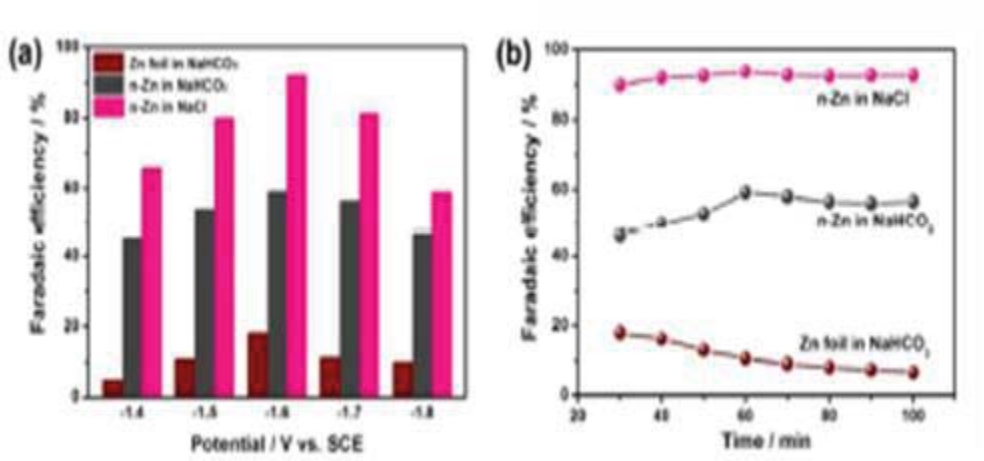

Figure 2.1 Comparison between Zn foil and n-Zn electrodes in CO_2 reduction. (a) FE_{CO} versus applied potential. (b) FE_{CO} versus electrolysis time at -1.6 V [48].

Copper is the most common and active electro-catalyst for the reduction of CO_2 despite the fact that the reaction proceeds at a high overpotential. The solubility of CO_2 is the main reason for this drawbacks. Many attempts are made to increase the CO_2 concentration in the electrolyte solution. Among them, one group reported the use of clathrate hydrate (ice-like substances) which has capability to capture large amounts of CO_2 on a copper foam which acts as a working electrode [49]. Moreover, the addition of tetrahydrofuran (THF) will enhance the clathrate hydrate formation at ambient pressure and a temperature of 0 ^oC allows vacancies for CO_2 enrichment. The electrolysis study (Fig. 2.2) showed the faradaic efficiencies of different gaseous and liquid products at different potentials -1, -1.3, and -1.7 V vs. Ag/AgCl. The results indicate the suppression of hydrogen evolution in presence of clathrate electrolyte solution. At a potential of -1.0 V the FE of CO reached up to 70% in presence of clathrate while the maximum FE of formic reached at -1.3 V with clathrate electrolyte. Also, FE all carbonaceous products reached 80% with clathrate compared to 20% without clathrate at -1.0 V vs. Ag/AgCl. Some hydrocarbons (C_2, C_3, and C_4) are formed and its FEs not significantly changes in presence or absence of clathrate. This scenario enhancement is attributed to the change in CO_2 concentration at Cu foam electrode surface in presence of clathrate electrolyte which facilitate the rate reaction of CO_2 reduction compared to HER rate.

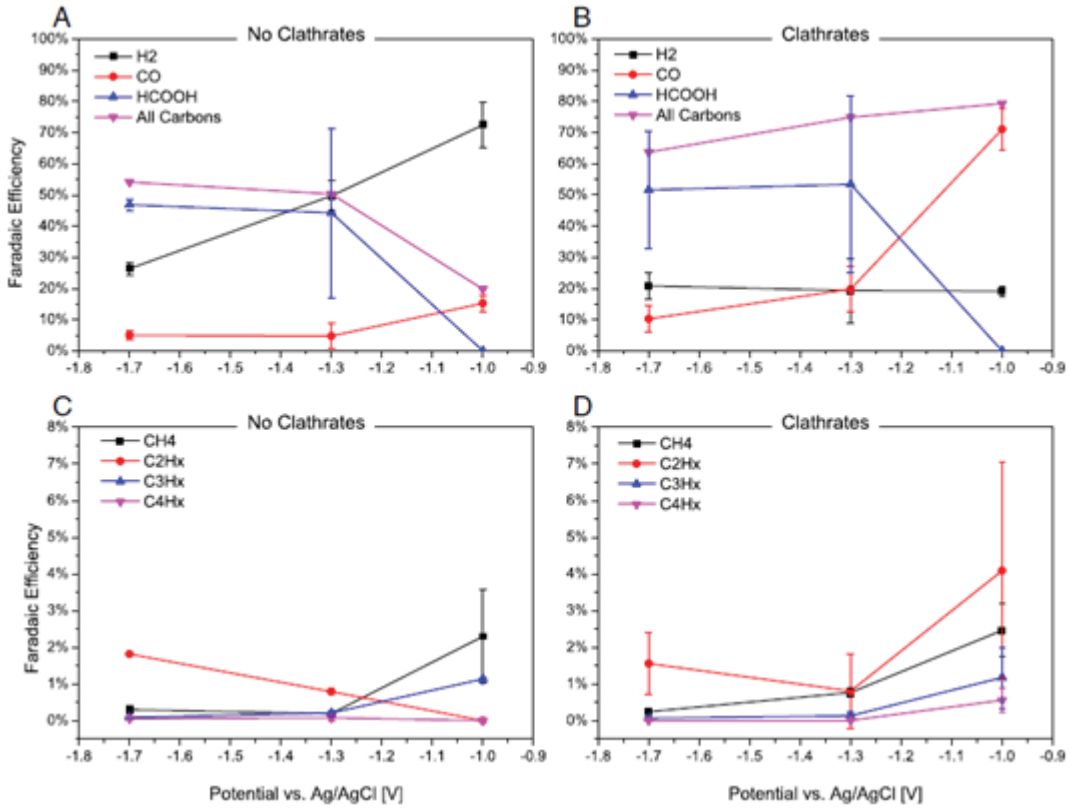

Figure 2.2 Faradaic efficiencies of the resulting products produced at copper-foam electrode in electrolytes without (A and C) and with (B and D) clathrates as a function of applied voltage.

The low solubility of CO_2 in aqueous solution is one of the main drawbacks of electrochemical reduction with low faradaic efficiency and hydrocarbons formation. S. Ohya et al. [50] have investigated the effect of electrochemical reduction of CO_2 in methanol-based electrolyte (methanol + KOH) with the aid of Zn pressed with and without presence of Cu or Cu_2O electrode. The results revealed that the current density decreases with the addition of copper oxide to Zn electrode. CO and H_2 were the only reduced products formed at Zn electrode. While in the presence of copper oxides, hydrocarbons are formed. Cu_2O/Zn electrode (Fig. 2.3) shows higher current efficiencies for hydrocarbons than CuO/Zn electrode. This study showed how much the formation efficiencies of methane and ethylene improved with Zn/Cu_2O electrode [2.5 wt. % Cu_2O content]. In addition, Cu_2O/Zn have performed low current density of hydrogen evolution at low temperature. They suggested a mechanism for the formation of hydrocarbons, as they are formed by the interaction between adsorbed CO and atomic hydrogen in the presence of copper oxide and zinc close together assist to prevent the evolution of CO and H_2.

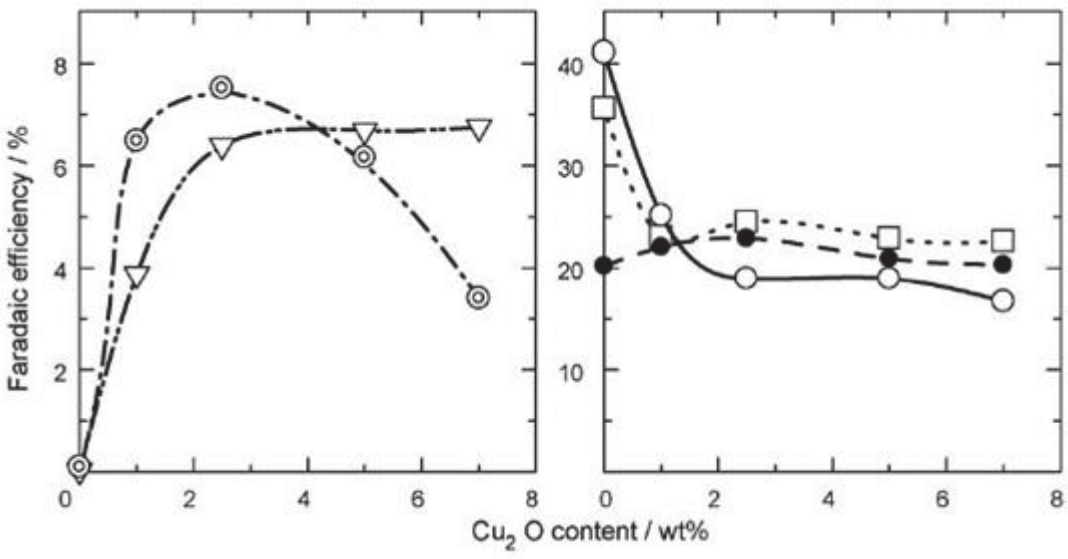

Figure 2.3 Effect of Cu_2O content on FE for the products produced at Cu_2O/ZnO powder-pressed electrode in KOH/methanol, ©CH_4, ▽ C_2H_4, °CO, □ HCOOH, ● H_2.

2.2.2 Nanostructured materials

Several studies have shown that the selectivity of Cu towards CO_2 reduction was dependent on the surface structure. J. Xie et al. [16] have studied the effect of the surface structure on CO_2 using Cu nanoflower compared to plycrsytalline Cu. Using two compartment cell separated by nafion membrane and 0.1 M $KHCO_3$ as an electrolyte, Pt and Ag/AgCl as a counter and a reference electrode, respectively at 10 ^oC. Copper foil ultrasonically treated with 2 M HCl and the electropolished in solution containing phosphoric acid 85%, sulphuric acid 95%, and water in a ratio of 13:4:2. Then electrochemical pulsed anodic oxidation (Chronoamperometry) for CuO NFs preparation. As shown in figure 2.4 Cu NFs has catalytic performance of CO_2 reduction higher than Cu foil, due to the large surface area of Cu NFs. In addition, the faradaic efficiency of H_2 evolution was 47% at Cu foil. However, a much lower Faradaic efficiency of 23% at Cu NFs which means that more H_2 suppression occurred at Cu NFs and more CO_2 reduction. Also, it was noted that Cu foil favours C_2H_4 production while Cu NFs favours CH_4 production. The above results are an evidence that the surface structure could alter the reaction pathways.

S. Sen et al. [51] have studied the difference between copper nanofoams and smooth copper in the electrochemical reduction of CO_2. The surface morphology of Cu NFs yields formic acid as a result of CO_2 reduction with faradaic efficiency 26% at -1.1 V which is higher than that obtained at a smooth copper (1% at -1.1 V). This improvement can be attributed to the high surface area, porosity, and the reactive species of Cu NFs which facilitate the reaction between hydrogen and adsorbed CO_2 to form high-order hydrocarbons.

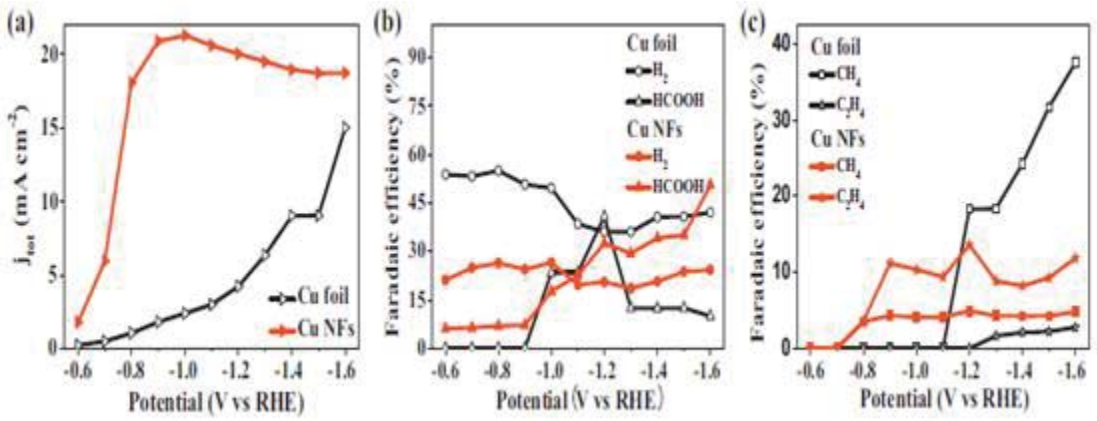

Figure 2.4 CO_2 reduction with Cu NFs and Cu foil at different potentials in 0.1 M $KHCO_3$. Total current densities (a), FEs for H_2 and HCOOH (b), and FEs for CH_4 and C_2H_4 (c) [16].

It is reported that the morphology, geometry, and roughness of copper surface has a big influence on the catalytic activity and products selectivity during CO_2 reduction. R. Reske et al. [52] have worked on the activity and the selectivity based on varying the size of the active species where they studied the catalytic activity of the Cu NPs from 2- 15 nm size range compared to bulk Cu. Airtight cell having three electrodes, Pt as a counter and Ag/AgCl as a reference electrode in 0.1 M $KHCO_3$ and CO_2 30 ml/min at pH 6.8 and potential range from + 0.22 to -1.1 V/RHE. As shown in figure 2.5, Cu bulk (foil) has the lowest catalytic activity as its current density was -23 mA/cm^2. In contrast Cu NPs show higher catalytic activity (high negative current density) towards the CO_2 reduction with decreasing size. The selectivity measurement showed that NPs below than 15 nm produced more H_2 and CO while hydrocarbons increased with increasing size. *Y. Chen et al.* [40] studied the reduction of CO_2 over Au nanoparticles compared to polycrystalline Au in 0.5 M $NaHCO_3$ at pH 7.2. It was found that Au NPs verified high current density and high faradaic efficiency of CO_2 reduction to CO at low overpotentials.

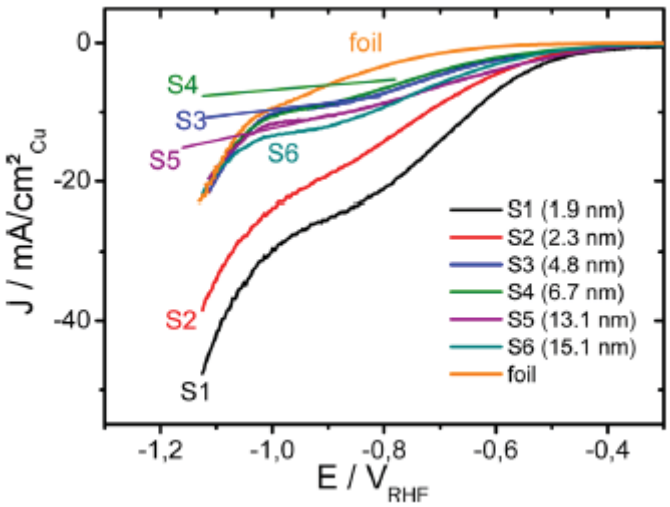

Figure 2.5 Linear sweep voltammetry of CO_2 reduction on Cu NP (S1-S6) with -5 mV/s scan rate [52].

E. Nursanto et al. [53] have studied the relation between Au morphologies and their activity towards the CO_2 reduction from nanoparticles to aggregates to layered Au. The electrochemical reduction process carried out in 0.5 M $KHCO_3$ and pH 7.03 after saturated with CO_2 for 30 min. As seen from figure 2.6, the current density of Au nanoparticles increases with a thickness increase of Au layer compared to bare carbon paper and Au foil. The Faradaic efficiency was investigated for each potential and the data shows that all Au NPs to layered Au were selective for CO formation from -0.59 to -0.79 V vs. RHE and decreased in lower and higher potential regions due to H_2 evolution. It was noted that as the size of Au decreases the selectivity to CO production decreases as well, which means that high thickness is required to be efficient for CO formation. The lowest selectivity of the smaller Au NPs size towards CO formation related to the active corner sites on Au NPs which selective for H_2 evolution and less edge sites which selective for CO.

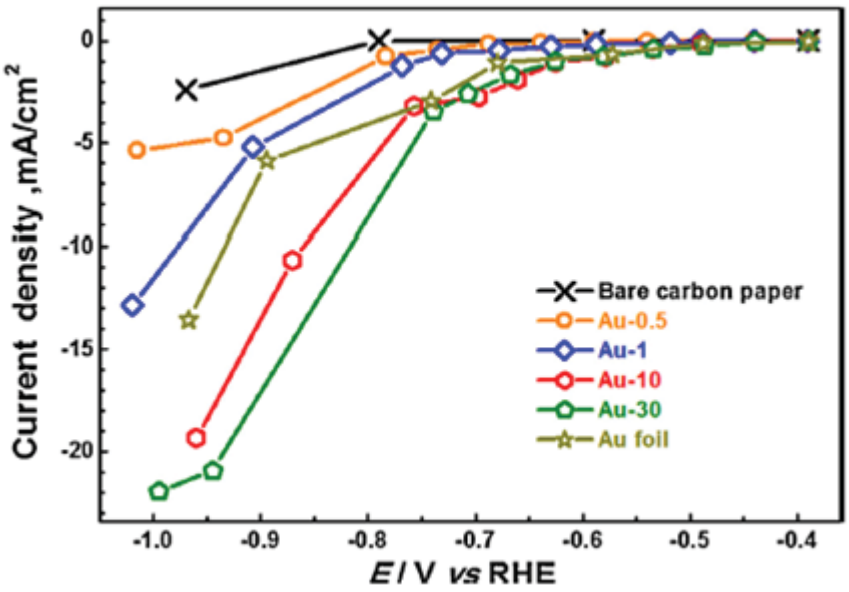

Figure 2.6 Total current densities of bare carbon paper, Au foil, and Au-T samples as a function of bias potential measured in 0.5 M $KHCO_3$ [53].

High overpotential and low faradic efficiency are the fundamental challenges of CO_2 reduction due to the competitive HER. But CO_2 adsorption, intermediate formation and product removal on the active sites are the key points to overcome these challenges. So, the relation between the activity and the selectivity towards CO_2 reduction and Pd particle sizes ranging from 2.4 to 10.3 nm based on the ratios of corner, edges, and terrace sites of Pd NPs has been studied [54]. The study shows that as the particle size of Pd NPs decreases the Faradaic efficiency of CO production increases along with increasing the current density, which varies from 5.8% at -0.89 V vs RHE over 10.3 nm particle size to 91.2% over 3.7 nm size (Fig. 2.7). DFT calculations indicate that this increase is due to the ratio of corner and edge sites of Pd NPs. Furthermore, corner and edge sites facilitate the CO_2 adsorption and COOH* intermediate formation compared to the terrace site.

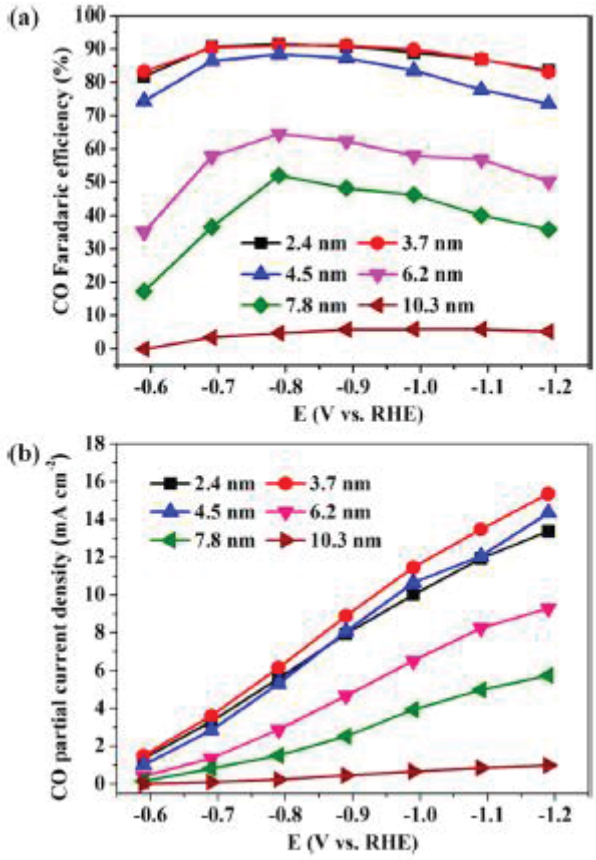

Figure 2.7 Applied potential dependence of (a) Faradaic efficiencies and (b) current densities for CO production at Pd NPs [54].

It was reported in the literature that the products depend on many factors such as the nature of the electrode material. Many studies are shown that Cu electrode modifications will enhance the activity and the selectivity of the CO_2 reduction. G. Keerthiga et al. [20] have studied the product selectivity for electrochemical reduction of CO_2 on pure Cu with (111) orientation and electrodeposited Cu (Cu/Cu) with (220) orientation. The product distributions showed that methane was the dominating product over the pure Cu electrode while ethane was the predominant product over the electrodeposited Cu electrode. At -1.0 V vs. RHE no products were detected other than methane and ethane with maximum faradaic efficiencies up to 6% and 18%, respectively. Figure 2.8 shows the value of the current densities with and without CO_2 saturation for different Cu forms. The products distribution of methane, ethane, and hydrogen over pure Cu and electrodeposited Cu (Cu/Cu-L, Cu/Cu-H) at different potentials. Cu/Cu-L with (220) orientations favors ethane production. The production of C_2 product also claimed by the role played by Cl^- ion which supress the proton adsorption and hence facilitate the C-C formation and so stabilizes the CH_2 intermediate which undergoes dimerization to C_2 formation.

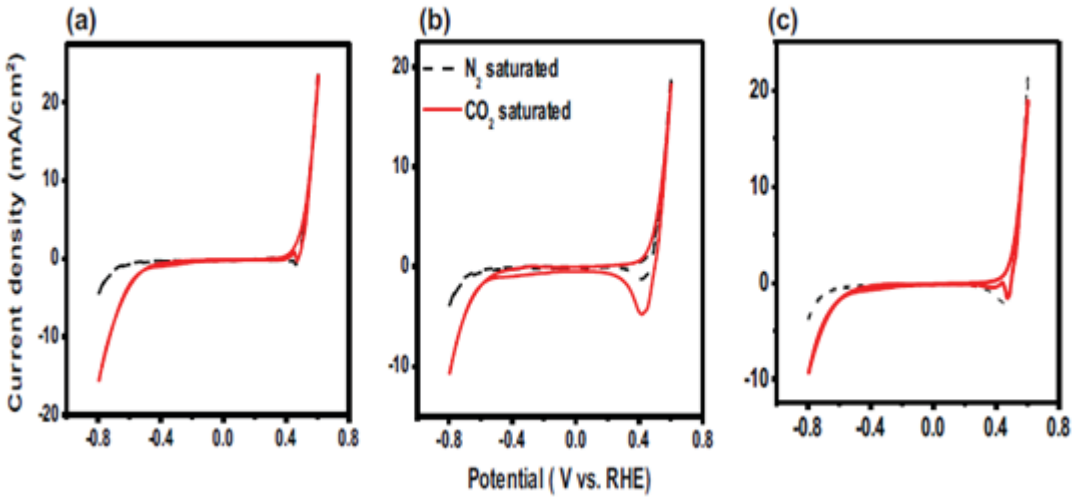

Figure 2.8 Cyclic voltammogram for (a) Cu, and electrodeposited (b) Cu/Cu-L, and (c) Cu/Cu-H [20].

TiO_2 is a well-known photo-catalyst for the CO_2 reduction. Here a number of scientists have studied the electro-catalytic activity of TiO_2 towards CO_2 reduction [55]. The study indicated that Ti^{3+} is the catalytic active sites formed on TiO_2 surface which is responsible for CO_2 reduction (scheme 2.1). The cyclic voltammetry indicated that the reduction of CO_2 on TiO_2 modified GCE can only be observed at a potential that is more negative than -1.3 V vs. Ag/AgCl.

$$(TiO_2)Ti^{4+} + e \rightarrow (TiO_2)Ti^{3+}$$

$$(TiO_2)Ti^{3+} + CO_2 \rightarrow (TiO_2)Ti^{4+} + CO_2^{-\cdot}$$

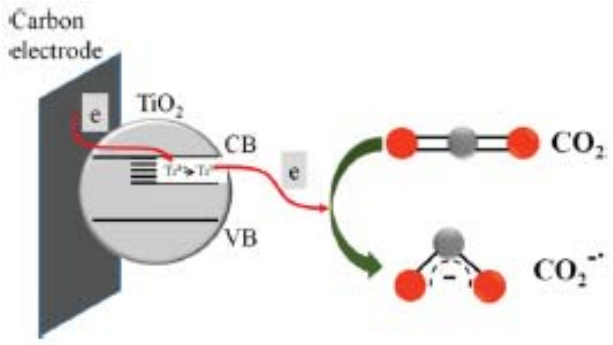

Scheme 2.1 Electrochemical conversion of Ti^{4+} to Ti^{3+} and electron transfer from Ti^{3+} to CO_2 [55].

The role of Ti^{3+} is confirmed by carrying out the electrochemical process in $LiClO_4$ where no CO_2 reduction was observed. This is due to Li^+ ions that have blocked the active sites of Ti^{3+}. In contrast, when reduction was carried out in TEAP solution which failed to block the Ti^{3+} active site and CO_2 reduction took place. GC-MS indicated that Methanol was the dominating product formed at TiO_2 electrode.

Due to the high surface area and the unique properties of the nanostructured materials, they have attracted much attention for the CO_2 reduction. The catalytic activity difference between nanostructured Zn (dendrites) and bulk Zn for electrochemical reduction of CO_2 to CO has been reported [21]. Electrochemical reduction studies of CO_2 in 0.5 M $NaHCO_3$ solution exhibited that the current density of Zn nanostructured is two times higher than that of bulk Zn (Fig. 2.9a). Also, its selectivity towards CO formation was enhanced three times higher than that of Zn bulk at a potential range from -0.9 to -1.1 V vs. RHE (Fig. 2.9b) in addition to the suppression of hydrogen evolution by Zn dendrites.

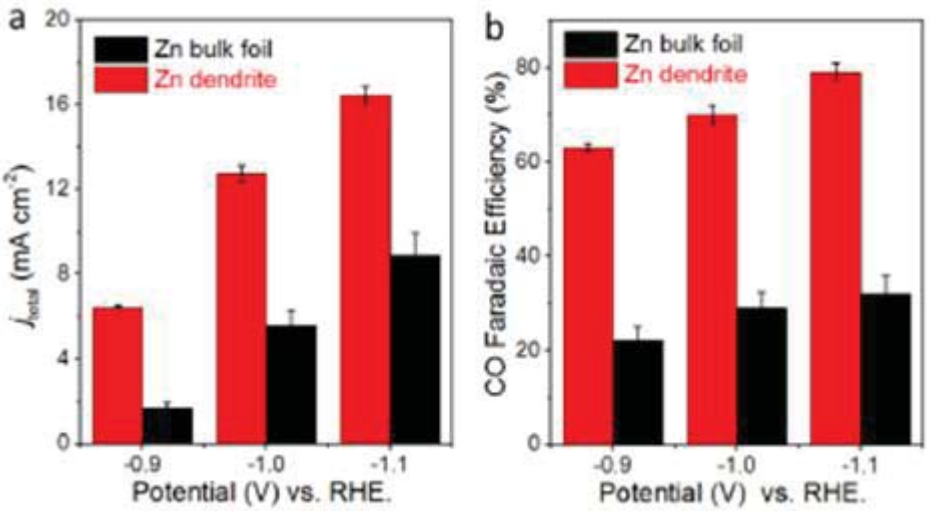

Figure 2.9 Comparison of (a) total current density, (b) CO Faradaic efficiency of bulk and dendritic Zn catalysts at -1.1 V vs RHE [21].

Among most metals, Au is the most selective catalyst for the reduction of CO_2 to CO, but it is not applicable for large scale application due to its high costs. Compared to Au metal electrode, silver is a promising selective catalyst for CO production from CO_2 electroreduction. Q. Lu et al. [56] have studied the activity and the selectivity difference between nanoporous Ag and polycrystalline Ag towards CO_2 reduction in 0.5 M $KHCO_3$ aqueous solution. Figure 2.10 shows that the total current density and clarify the current density enhancement at nanoporous Ag than polycrystalline Ag. Also, CO faradaic efficiency is significantly increased over np-Ag than Polycrystalline one. The study revealed that trace amount of formate was formed besides CO over np-Ag at a more negative potential than -0.8 V vs. RHE. The high activity and selectivity of np-Ag is attributed to the high surface area and intrinsic activity of nanoporous with curved internal surface and hence high density of step sites. So, np-Ag stabilize the CO_2^- intermediate adsorption on its surface followed by two protons and another electron reduction to form CO as explained by tafel analysis (Fig. 2.11).

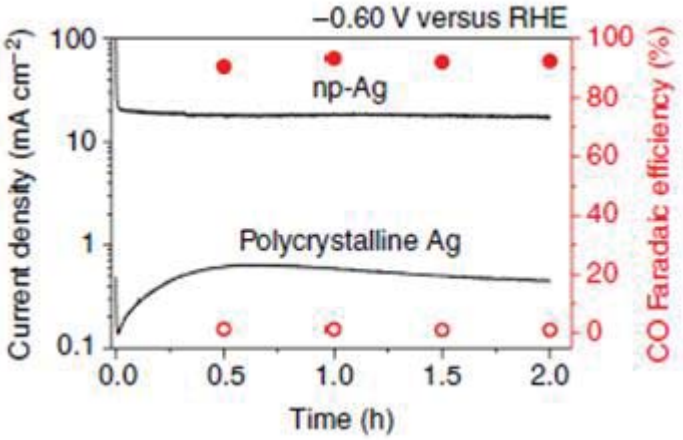

Figure 2.10 CO_2 reduction activity of np-Ag and polycrystalline Ag at -0.6 V vs RHE.

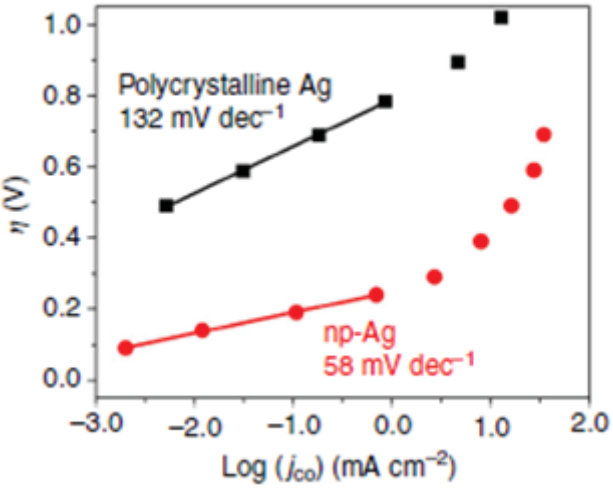

Figure 2.11 Overpotential vs CO production partial current density on polycrystalline Ag and np-Ag [56].

T.Y. Chang et al. [57] have studied the reduction of CO_2 in a cell of three electrodes using Cu_2O/ Carbon cloth as a working electrode and an alkaline electrolyte solution of 0.5 M NaOH. Cyclic voltammetry (Fig. 2.12) with a scan rate of 50 mV/s was selected, applying a potential range from 0.0 to -1.7 V for catalyzed and non-catalyzed carbon cloth electrodes. Solutions saturated with N_2 and CO_2 have shown that Cu_2O acts as a notable catalyst for the CO_2 reduction, The current response was -5.57 mA/cm^2 compared to other non-catalyzed carbon electrode (- 3.58 mA/cm^2). Also, the potentostatic measurement for both catalyzed and non-catalyzed electrodes with CO_2 saturated solution showed high current density with catalyzed one compared to the other electrode which shows the catalytic ability of Cu_2O catalyzed electrode. GC/FID analysis confirmed the methanol is the primary product for both electrodes.

Another study has been undertaken on polyaniline/Cu_2O based electrode by A. Nirmala et al. [3]. Cyclic voltammetry data showed a reduction peak at -0.1 V on polyaniline/Cu_2O electrode saturated with CO_2. The function of this electrode was confirmed by two cases, the first case by studying the current-potential curve from -0.2 to 0.4 V vs. SCE at a scan rate of 50 mV/s in the absence of CO_2. The second case, the same conditions were used in the presence of CO_2 on bare Pt loaded C electrode. In both cases, no reduction peaks were observed. This imply the catalytic activity of polyaniline/Cu_2O electrode towards CO_2 reduction. The electroreduction of CO_2 at different constant potentials showed that the higher current density was observed at -0.3 V chosen as the low overpotential for CO_2 reduction. The main products were acetic acid at a current efficiency of 63% and formic acid at 30.4% which were confirmed by GC-MS, ion chromatography and ^{1}H NMR.

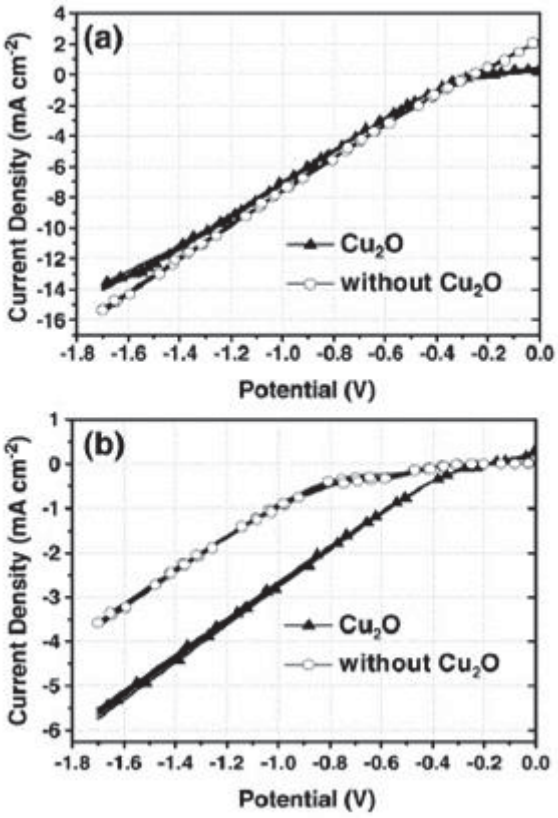

Figure 2.12 CV profiles for Cu_2O-catalyzed and non-catalyzed carbon clothes in (a) N_2-saturated and (b) CO_2-saturated electrolytes [57].

Formation of different products CO, HCOOH, and CH_3OH over Cu/CuO core/shell through electrochemical reduction of CO_2 investigated by Yangchun Lan et al. [58] using three electrode cell, Pt and Ag/AgCl as counter and reference electrodes, respectively in 0.1 M $KHCO_3$ electrolyte solution. Analysis of the products showed that CO produced with faradic efficiency 21.5 % at -1.73 V, HCCOH with faradaic efficiency 20.2% at -1.73 V and small amount of the desired methanol produced with a Faradic efficiency of 2.5% at -1.35V which is about ten times higher than that reported using Cu foil as a working electrode (0.2 % at -1.751 V vs Ag/AgCl) in 0.1 M $KHCO_3$. The high catalytic activity of Cu/CuO core/shell can be explained by the high promotion of Cu(I) produced from reduction of CuO. This result was confirmed by the XPS analysis which indicates the reduction of CuO to Cu(I) and then Cu(I) is reduced to Cu during the electrochemical reduction of CO_2. As mentioned before the CO_{ad} species can undergoes to form HCOOH or released to produce CO. Here, the CO_{ad} protonated on the surface to form CH_3O and the surface of Cu/CuO core shell promotes the addition of hydrogen to produce CH_3OH.

Unfortunately, the faradic efficiencies of alcohol formation from CO_2 reduction is very low. F. Jia et al. [59] have focused on the selectivity of the electrochemical reduction of CO_2 to alcohols using nanostructured Cu-Au alloys compared to nanostructured Cu. Although gold metal catalyzed CO_2 to CO only. The electrochemical reduction of CO_2 on Cu-Au alloy revealed the high cathodic current at more negative potential than -1 V vs. SCE than that recorded on nanostructured Cu electrode as shown in figure 2.13.The results showed that the $Cu_{63.9}Au_{36.1}$/ NCF electrode favors conversion of CO_2 and GC analysis of the reduction products indicate the formation of methanol (retention time 2.21 min) and ethanol (retention time 2.66 min) in addition the faradic efficiency of methanol on that

electrode was 15.9% (19 times that for pure Cu). The study claimed the effect of nanostructure and size on faradic conversion of alcohols.

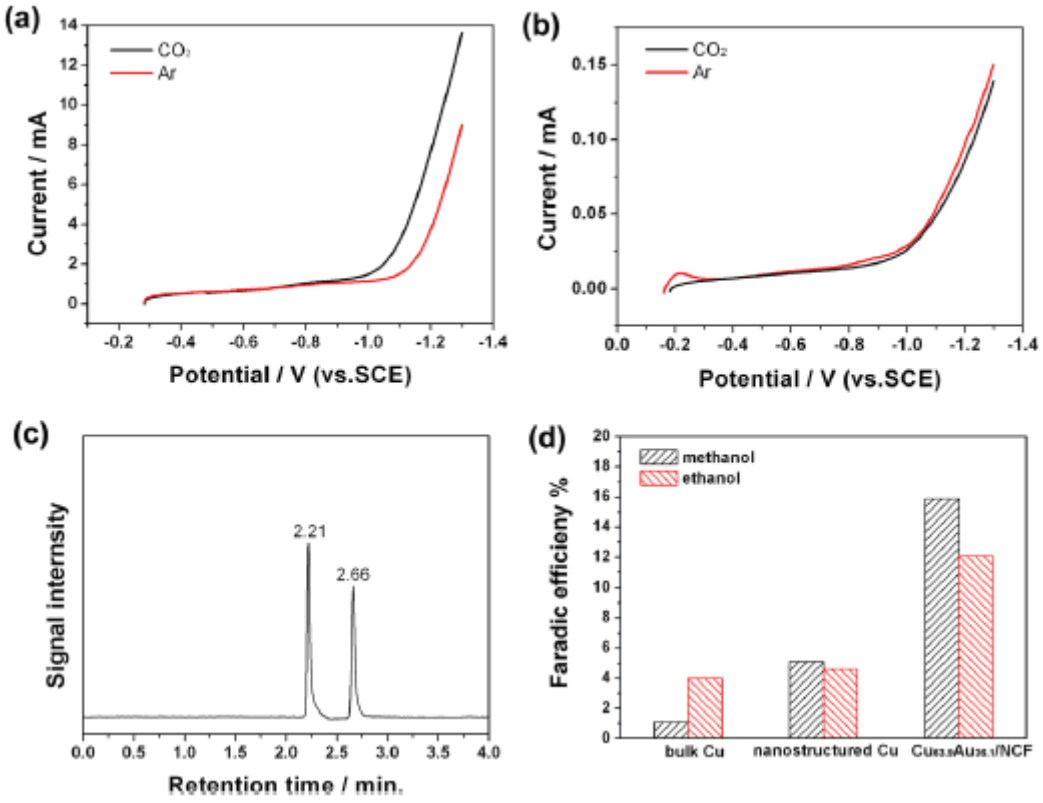

Figure 2.13 LSV curves of $Cu_{63.9}Au_{36.1}$/CNF (a) and Cu NPs (b) in 0.2 M PBS saturated with CO_2 (black line) and Ar (red line). (c) GC spectrum of liquid products produced on $Cu_{63.9}Au_{36.1}$/CNF. (d) FE of methanol and ethanol in 0.5 M $KHCO_3$ solution [59].

Another study have shown that the morphology effect of nanostructure materials on faradaic efficiency of CO_2 electroreduction have been investigated by J. Qu et al. [60]. The study evaluated the RuO_2/TiO_2 nanocomposites with two different morphologies modified Pt electrode, one as TiO_2 nanotubes and the other as TiO_2 nanoparticles. Cyclic voltammetry (CV) measurement showed better electrocatalytic activity towards CO_2 reduction in 0.5 M $NaHCO_3$ for RuO_2-TiO_2 nanotubes than the other with nanoparticles shape. Moreover, GC-MS result indicates the conversion of CO_2 to methanol with high faradic efficiency (60.5 %) at RuO_2/TiO_2 NTs compared to 40.2 % at RuO_2/TiO_2 NPs. This study have shown that the importance of nanostructures in CO_2 reduction to get high efficiency in addition to selectivity, belongs to high surface area which could create more active sites.

2.2.3 pH Effect

The pH value of the solution is a key factor for the electrochemical reduction of CO_2 due to the suppression of hydrogen evolution as an undesired side reaction. Copper electrode is one of the most promising metal electrode for the CO_2 reduction to hydrocarbons like methane and ethylene. To understand the mechanism of the reaction selectivity, many parameters should be considered, among these parameters the pH of the solution. As discussed before, methane formation is a pH dependent while ethylene formation does not depend on the pH value. Here, K. Schouten et al. [61] have studied the effect of the pH on CO_2 and CO reduction on Cu (111) and Cu (100). Cell of three electrodes system with a potential change from 0 to -1.5 V, in phosphoric acid (pH 1) and phosphate buffers (pH 7 and 12). Online electrochemical mass spectrometry (OLEMS) used to detect the gaseous products. During CO reduction it was clear that H_2, CH_4, and C_2H_4 are the three main products detected. For hydrogen, it started at -0.35 V and increasing with more negative potential. Methane has different characteristics between Cu (111) and Cu (100) at a pH 1 where it starts early at – 0.45 V on Cu (100). Ethylene starts early at -0.4 V at pH 7 and 12 on Cu (100) rather than Cu (111). For CO_2 reduction at pH 1, CH_4 forms at -0.55 V on Cu (100) while no CO_2 reduction on Cu (111). At pH 7, ethylene forms at lower potential than methane on Cu (100) while they have similar potential on Cu (111). It can be concluded that methane formation is a pH dependent and CHO adsorbed is the key intermediate. In contrast, ethylene formation is a pH independent and CO dimer is the key intermediate (Fig. 2.14).

Figure 2.14 Reaction mechanism for CO_2 reduction on Cu single crystal electrode.

2.2.4. Temperature Effect

The temperature effect on the electrochemical reduction of CO_2 to methane, ethylene, and ethane using Cu foil as a working electrode, $NaHCO_3$ as catholyte, $KHCO_3$ as anolyte, with a potential ranged from -1.6 to -2 V was investigated by S. Kaneco et al. [13]. They have reported that as the temperature is lowered the Faradic efficiencies (46 %) of methane increased (as shown in fig. 2.15) and below 273 K was selective for methane formation in addition hydrogen evolution was suppressed with lowering the temperature.

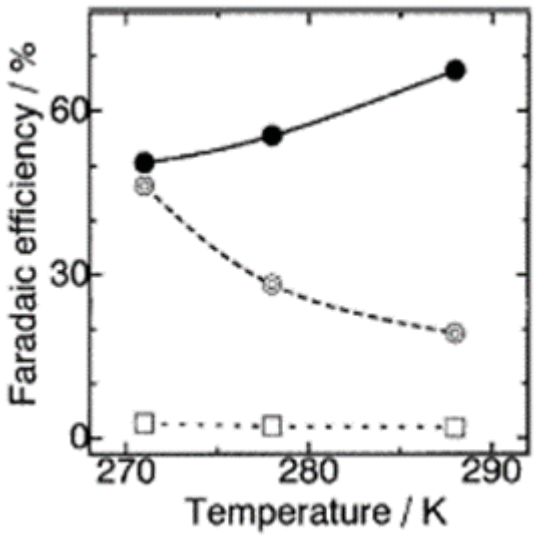

Figure 2.15 Temperature effect on FE of products at Cu electrode at -2 V. ⊚ CH_4, □ HCOOH, ● H_2 [13].

A. Naitoh et al. [62] have reported that the electrochemical reduction of CO_2 used H-type cell with copper as a cathode and platinum as an anode in methanol and in the presence of benzalkonium salt at two different temperature, 0 ^oC and -15 ^oC with potential range from -1.3 to -2.3 V vs SCE. The results showed that the main products of CO_2 reduction are CO, methane, and ethylene. The Faradic efficiencies of these products were found increase with decreasing the potential at both temperatures and the best potential was found to be -2.2 V. They have claimed that the best products faradaic efficiencies at low temperature results compared to those at ambient conditions related to the fact of better CO_2 solubility in methanol at low temperature. Also, the same group [36] have studied the electrochemical reduction of CO_2 at -30 ^oC using H-type cell, Cu foil ac cathode and Pt as anode, and SCE as reference electrode in benzalkonium and methanol electrolyte and a potential scan from -1.8 to -2 V. Methane, carbon monoxide, and ethylene were the products obtained from CO_2 reduction. The Faradaic efficiency of methane 52.5 % at -2 V at -30 ^oC compared to the previous study in addition to the depression of hydrogen evolution at the lower temperature.

2.3 Carbon-based electrode for CO_2 electroreduction

Carbon has different forms like carbon nanotube, graphene, and fullerene. These forms have conductivity properties which vary based on the carbon structure form. This conductivity can be a great support for CO_2 electroreduction by facilitating the electron transport. Some scientists have reported the effect of metal doped carbon/TiO_2 heterogeneous catalyst on the electroreduction of CO_2 [63]. The electrolysis of Pt/C-TiO_2 and Pt-Pd/C-TiO_2 loaded on glassy carbon RDE were performed in 0.2 M NaF/10 mM pyridine solution and potential range from -0.2 to -1 V vs. Ag/AgCl. Figure 2.16 shows the voltammogram of Pt/C-TiO_2 electrode with N_2 and CO_2 saturated NaF/pyridine solution and compared to Pt electrode. It is clear that the current density has significantly increased at s potential that is more negative than -0.9 V vs. Ag/AgCl in case of Pt/C-TiO_2 electrode surface. In addition to the role played by Pt and co-catalyst (pyridine) towards CO_2 reduction. The liquid products were analyzed by GC, reveals the methanol and isopropanol were the major products at Pt/C-TiO_2. While, at Pt foil only methanol product was observed (Fig. 2.17).

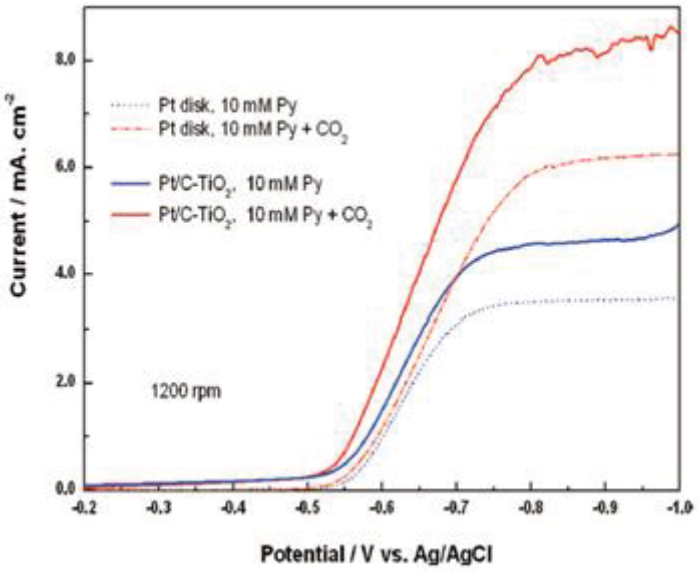

Figure 2.16 Comparison of hydrodynamic voltammogram for a Pt/C-TiO_2 RDE with a Pt RDE in PyH^+-loaded NaF saturated with N_2 and CO_2 [63].

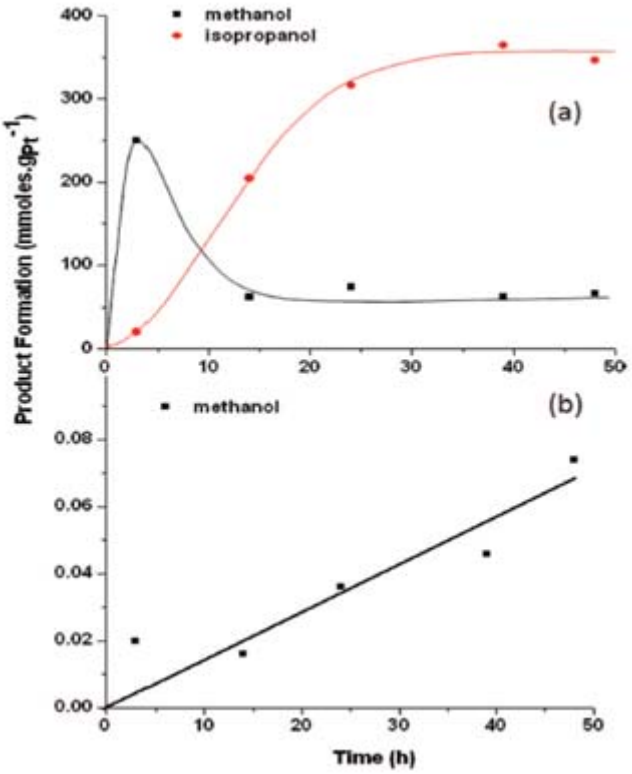

Figure 2.17 GC analyses as a function of time for constant current electrolysis using (a) Pt/C-TiO_2 and (b) Pt foil cathodes [63]

Carbon nanofibers, carbon nanocoils, and ordered mesoporous carbon present high efficient in CO_2 electroreduction varies significantly based on crystallinity, morphology, and porosity properties. In addition to selectivity enhancement, also high hydrocarbons C_1-C_9 and alcohols have been surprisingly produced. On the other hand, modified carbon materials with some metals like Pd take more attention due to the low hydrogen overpotential and its high capability to adsorb hydrogen on its surface, hence this paly a very important role for the intermediate formation to proceeds CO_2 reduction. Here, S. Perez-Rodriguez et al. [12] have demonstrated the effect of Pd catalyst modified carbon materials for electroreduction of CO_2. The 20% Pd/C electrocataylst synthesized and coated on glassy carbon with net material loading around 0.038 mg, carbon electrode was

used as counter and Ag/AgCl as reference electrodes in 0.1 M $NaHCO_3$. At the beginning the electrochemical studies of Pd/C electrocatalyst was recorded in the range from -0.8 to 0.9 V vs. Ag/AgCl with and without CO_2 saturated solution. It is clear from the measurements recorded that Pd/OMC and Pd/CNF favoured hydrogen evolution with the highest current density at -0.8 V.

Figure 2.18 shows the CVs of Pd/C catalysts studied in the range from -1.4 to 0.9 V vs. Ag/AgCl in Ar and CO_2 saturated solution. It is clear from figure 2.18 that a peak appeared at -1 V for all Pd/C catalyst is attributed to CO_2 reduction. More focus, Pd/OMC presented the high reduction peak compared to the others. At the same time it is mentioned that this catalyst has the highest tendency for hydrogen evolution. This results confirmed the role played by hydrogen adsorbed on Pd active site and hence interact with adsorbed CO_2 reduced species.

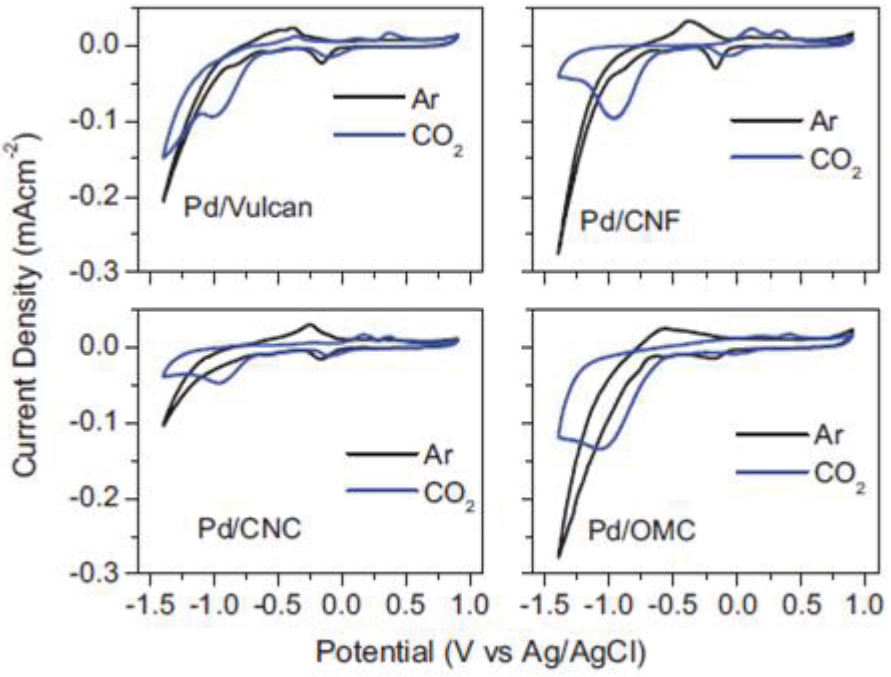

Figure 2.18 CVs of Pd/C catalyst in 0.1 M $NaHCO_3$ with and without CO_2 saturated solution [12].

By considering the comparison between CO and reduced CO_2 stripping (Fig. 2.19), the results have revealed that the oxidation of reduced species as a result of CO_2 reduction takes place at a potential lower than that of CO oxidation. Briefly, it is realized that at -1 V vs Ag/AgCl, CO_2 is not only reduced to CO but also $COOH_{ad}$, COH_{ad}, and CH_x. In addition, hydrogen blocking occurred over catalyst surface with the presence of these species which explains the role played by the absorbed hydrogen atoms over Pd surface enhanced the reactivity of electrochemical reduction of CO.

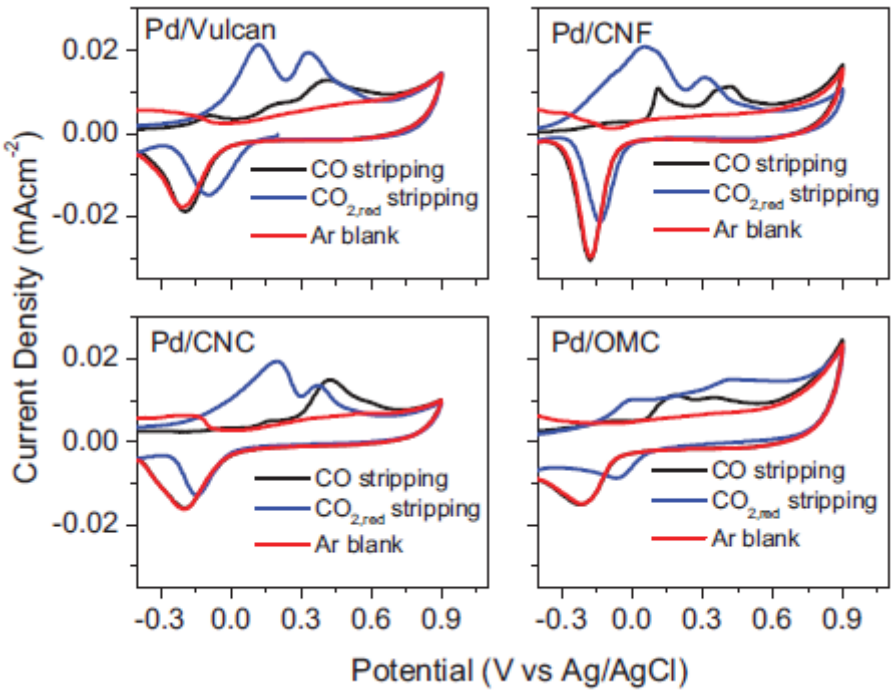

Figure 2.19 Comparison of CO and reduced CO_2 stripping voltammograms for Pd/C catalyst [12].

R. Zhang et al. [64] have studied the electrochemical reduction of CO_2 over SnO_2/N-MWCNTs composite modified GCE in 0.1 mol/L $KHCO_3$ aqueous solution. The cyclic voltammetry curves showed that SnO_2 will not be reduced to Sn^{+2} or Sn if the cathode potential higher than -1.3 V vs. Ag/AgCl. Also, the average current density of SnO_2/N-MWCNTs electrode is higher than that of N-MWCNTs as the potential decreases from -0.9 to -1.3 V which improved the enhancement of electrochemical reduction of highly conductive N-MWCNTs when decorated with n-type semiconductor SnO_2. In addition, SnO_2/N-MWCNTs produced formate more efficiently than N-MWCNTs only as faradic efficiency decreases from 46% to 9.4 % as potential decreases (Fig. 2.20 b). Ion chromatography using 30 mmol/L KOH as mobile phase were used for liquid product analysis.

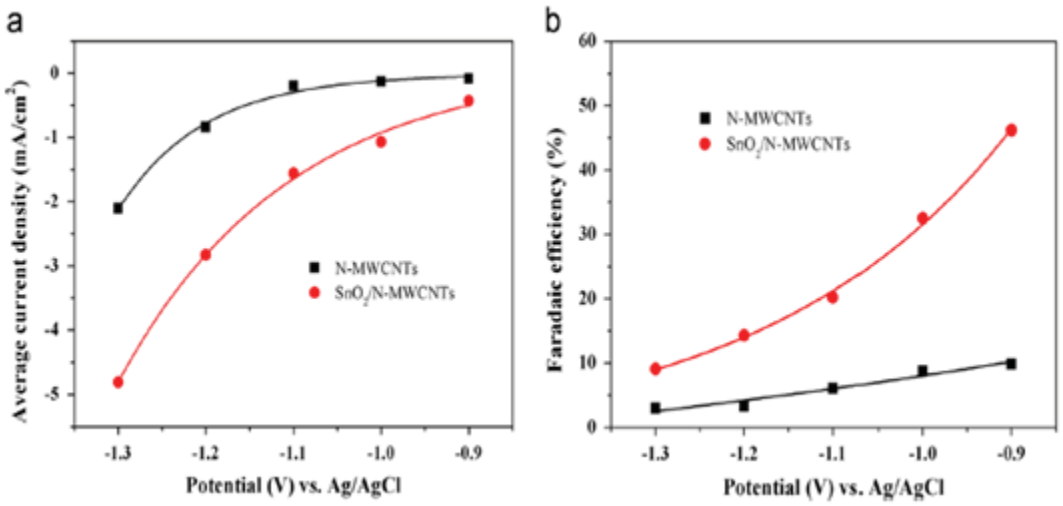

Figure 2.20 Average current densities (a) and FE for formate (b) of N-MWCNTs and SnO_2/N-MWCNTs at different potentials [64]

CHAPTER 3

EXPERIMENTAL SECTION

Through a very deeply study of literature, design of a suitable metal oxide catalyst with an excellent support particularly with large surface area, an excellent electron mobility, and high CO_2 adsorption will play a critical role in the electrochemical reduction of CO_2 in terms of selectivity and high product yield. So, we prepared a different metal oxides/graphene catalysts, have different morphologies to evaluate its performance for CO_2 reduction. In this experimental section, we will discuss a details of catalyst preparation, electrode fabrication, characterization, and electrochemical measurements as well as faradaic efficiency calculation of the product.

3.1 Materials

Graphite powder and sodium nitrate ($NaNO_3$, 98%) was obtained from Koch-Light Laboratories Ltd. Sulfuric acid (H_2SO_4 95–97%) and potassium permanganate ($KMnO_4$, 99.5%) and ethanol solution (99.9%) were purchased from Fluka. Hydrogen peroxide solution (30%, w/v), copper (II) chloride anhydrous, Zinc chloride, sodium dodecyl sulfate (SDS, 99 %), sodium hydroxide, and hydroxylamine hydrochloride ($NH_2OH.HCL$, ≥ 98.5%) were obtained from BDH Chemicals Ltd. Nafion perfluorinated ion-exchange resin (5 wt. %), dichloromethane (≥ 99.9 %, GC grade), acetone, and isopropanol were purchased from Sigma Aldrich. Carbon dioxide and nitrogen gas cylinders with purity of

99.99 % were purchased from SIGAS Company. All chemical were of analytical grade and used as received without any purification. All water used are ultrapure water.

3.2 Synthesis of Electro-catalysts

3.2.1 Synthesis of graphene Oxide (GO)

The graphene oxide (GO) synthesized using modified Hummers' methods as described previously [65]. A 2 g graphite powder and 1 g sodium nitrate were mixed with 46 ml H_2SO_4 in ice bath and stirred for 15 min, then 6 g potassium permanganate was added gradually to the above solution with continuous stirring and kept for 1 hour. After that, 92 ml of deionized water was added slowly with stirring for 15 minutes. The suspension solution was diluted by adding 280 ml of warm water. Followed by titrating with 10 ml hydrogen peroxide (30 %). The suspended solution was filtrated then washed with water several times. The solid precipitated was dried at 60 ^oC for 24 hours.

3.2.2 Synthesis of Cu_2O and graphene (GN)/Cu_2O

Cuprous oxide (Cu_2O) and GN/Cu_2O nanoparticles were synthesis according to the method described earlier [66]. A 1 mg/ ml GO solution was prepared and sonicated for 2 hr. 3 ml GO solution was dissolved in 15.1 ml ultrapure water then sonicated for 30 min. Then added the calculated amount of 0.1 M $CuCl_2$ to the above solution and 0.087 g sodium dodecyl sulfate (SDS), then left solution under stirring for 1 h to obtain various GN/Cu_2O weight ratios. After that 0.9 ml 1M NaOH was added to the mixture, followed by 4 ml

$NH_2OH.HCl$ was rapidly injected to the solution mixture. Stirring for 30 min for growth nanoparticles. Yellowish brown precipitate was observed, centrifuged and washing with ethanol and water several times to remove the desirable impurities and surfactant. Cu_2O was prepared by the same method without adding GO solution. Schematic 1 shows the procedure synthesis of GN/Cu_2O nanocomposite.

3.3.3 Synthesis of graphene (GN)/ZnO/Cu_2O composites

The graphene/ZnO/Cu_2O composites were synthesized via modified co-precipitation method as follows: 0.1 M $ZnCl_2$, 0.1 M $CuCl_2$, and 0.087 gm sodium dodecyl sulfate (SDS) were mixed with 1 mg/ ml GO solution under vigorous stirring for 2 h. 1 M NaOH and 1 M $NH_2OH.HCl$ were rapidly injected into the solution mixture and stirred for 30 min. Then, centrifuged and washed with ethanol and water repeatedly, and dried in vacuum at 40 ^oC for 18 h. The calculated amounts of $ZnCl_2$ and $CuCl_2$ were added to obtain various ZnO/Cu_2O weight ratios. Also, graphene/ZnO was synthesized using the same procedure.

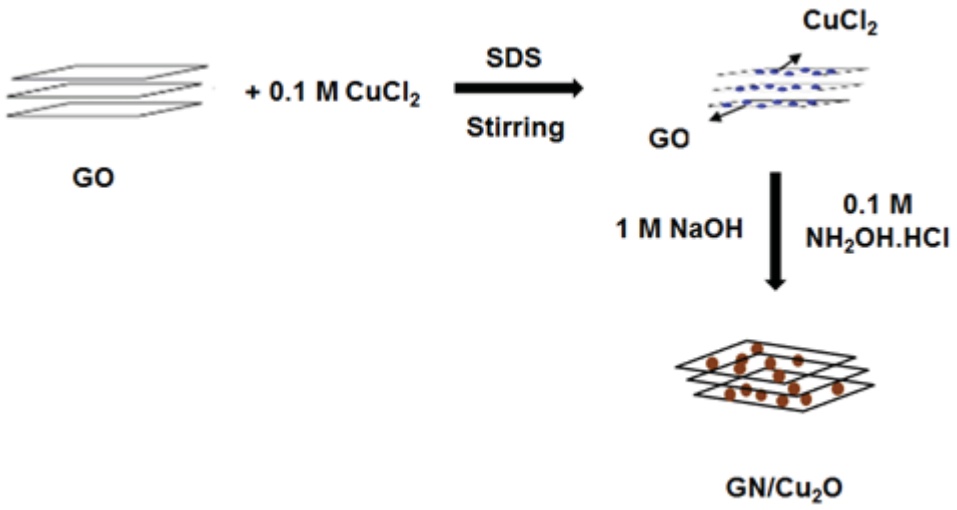

Scheme 3.1 Schematic show synthesis route of graphene/Cu_2O nanocomposite.

.

3.3 Characterization of the as-synthesized composites

X-ray diffraction (XRD) data were collected using Rigaku MiniFlexII X-ray diffractometer (Japan) to identify phases present in the synthesized samples in the range of 2 theta angle from 20^0 - 80^0, using Cu $K_{\alpha 1}$ radiation (g=0.15416 nm), accelerating voltage = 30 kV and tube current = 10 mA. Surface morphologies were examined under a field emission scanning electron microscope (FESEM, Lyra 3, Tescan, Czech Republic) using both secondary electron (SE) and back-scattered electron (BSE) detectors, with accelerating voltages of 20-30 kV in order to characterize grain morphologies, and an energy dispersive X-ray spectroscope (EDS, Oxford Inc., UK) was used for elemental analysis of the phases present. Raman spectroscopy (Raman) pattern were analyzed the D and G bands of graphene structure in the range from 500 to 200 cm^{-1}. A JEOL-2100F field emission transmittance electron microscope (FE-TEM) conducted at 200KV was used for TEM & HR-TEM particle size measurement. The oxidation state of elements were determined using X-ray photoelectron spectrometer (XPS, Thermo Scientific ESCALAB 250 Xi).

3.4 Electrode Fabrication

To fabricate the working electrodes, copper foil (fisher scientific company) was first cut into 1.3 cm x 1.3 cm dimensions as shown in figure 3.1, and polished using silicon carbide grain (150 mesh), and ultrasonically treated in diluted sulfuric acid (H_2SO_4). Then cleaned with acetone and dried under N_2 atmosphere. 1 mg prepared powder was dispersed in 60 µl nafion solution (5 wt. %) and 1 ml acetone and then ultrasonicated for 15 min. one

portion of the suspension ink (100 µl) was dropped on the copper foil and dried under hot incandescent lamp for 24 h.

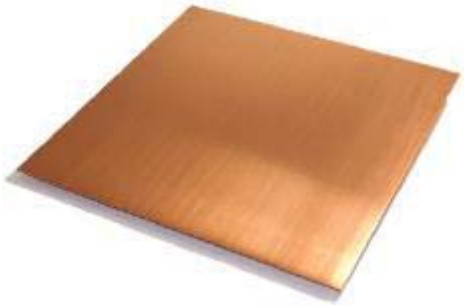

Figure 3.1 Copper foil electrode.

3.5 Electrochemical Cell

Electrodes can be assembled in one compartment, or in several. In many compartments we can avoid interactions between reaction and electrode interface, which have great importance to prevent adsorption of impurities on working electrode. In two electrode compartment, products formed at counter electrode do not go to block active sites on working electrode.

Electrochemical reduction of CO_2 was carried out in a three-electrode cell where a Pt and Ag/AgCl were used as the counter and reference electrodes, respectively. GNs/ Cu_2O electrode (3.38 cm^2) was used as working electrode. Divided two compartment electrochemical cell was connected with potentiostat (Gamry) for electrochemical measurements as shown in scheme 3.2. A 25 ml 0.5 M $NaHCO_3$ (pH= 7.25) used as

electrolyte. Working and reference electrodes were assembled in one side and the counter electrode was in the other side. The two compartments were filled with same 0.5 M $NaHCO_3$ solution as electrolyte. Before CO_2 reduction experiments, N_2 will pure into the cell to remove the dissolved oxygen in the cell. Potential was applied between working and reference electrodes, while the current was measured between working and counter electrodes. The two compartments were separated by fitted glass membrane.

3.6 Electrochemical measurements

LSV were scanned in the range from -0.2 to -1.8 V vs Ag/AgCl with scan rate 20mV/s. prior to measurement, High purity N_2 or CO_2 (99.99 %) saturated electrolyte solution were employed to evaluate the electrode behavior. Current response of electrode were measured at different potentials under CO_2-saturated solution via chronoamperometry process. All electrochemical measurements were carried out at room temperature. All potentials measurements in these experiments measured with respect to Ag/AgCl reference electrode.

3.6.1 Linear sweep voltammetry

To investigate the performance of our catalyst. Electro-catalyst electrode under different conditions of N_2 and CO_2 saturated in 0.5M $NaHCO_3$ and run the linear sweep voltammetry in potential range of -0.2 to -1.8 V vs. Ag/AgCl. After the inception of given potential, we recorded current vs voltage behavior and measured constructive results. In both cases, under N_2 and CO_2 purging, there was no physical change in working electrodes which

basically signify stability of our catalysts. Similarly in N_2 saturated electrolyte, whole current was due to hydrogen evolution reaction while in CO_2 saturated electrolyte we noticed two type of reactions, CO_2 reduction and hydrogen evolution. Both of these reactions competes each other's. Hydrogen evolution consumes electrons and lowers the CO_2 reduction.

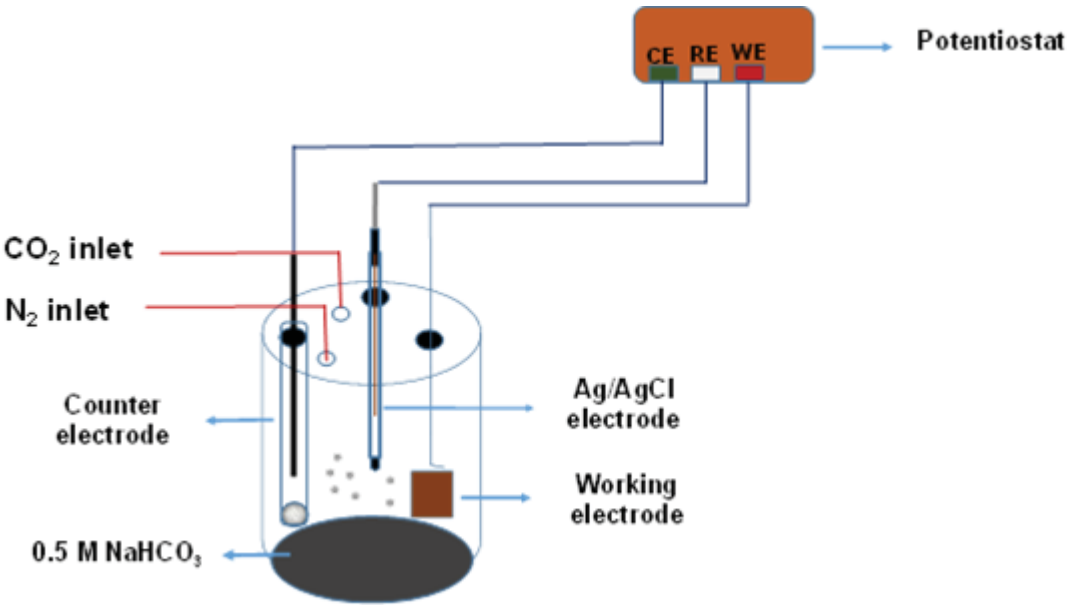

Figure 3.2 The electrochemical cell for CO_2 reduction.

3.6.2 Chronoamperometry

To investigate the stability of the catalyst, chronoamperometry was done for graphene-based electrodes. We conducted chronoamperometry test for fixed potential value. We measured the current or current density as a function of time. Actually, most of the surface modification electrodes presented a decreasing in current/current density with time. This is related to detachment of electrode surfaces. Sometimes some electrode will presents an increase in the current/current density as a function of time. This can be explained by the continuous reduction of the CO_2 molecules over electrode surface and no species as a result of CO_2 reduction adsorbed on the electrode surface.

3.7 GC-MS Analysis

Liquid product was analyzed by GC-MS (Agilent technologies). In our case, we used aqueous electrolyte solution which cannot be injected to the GC column. So, to avoid the damage of GC column, the CO_2 reduction product should be extracted from the aqueous solution. We used dichloromethane (≥ 99.9 %, GC grade, SIGMA ALDRICH) for organic product extraction. After that sample directly injected into GC-MS. Helium gas was used as carrier gas and 0.2 ul liquid samples was injected. Column temperature was held for 5 min at 40 ^oC and increased by 10 ^oC/min upto 200 ^oC and held for 10 min.

3.8 Calculation of Faradaic efficiency

Faradaic efficiency is describes the efficiency with which charge (electrons) are transferred in a system facilitating an electrochemical reaction. Based on number of electrons passed through the electrolyte solution to proceed the reaction. Also, Faradaic efficiency is expressed the selectivity of the electrochemical reaction for the production of desired product. Faradaic efficiency can be calculated via the following equation;

$$\mathbf{FE\ (\%) = (Z.N.F/q)\ x\ 100}$$

Where, Z is number of electrons, n is number of mole produced, and q is the total charge applied during the electrolysis process.

CHAPTER 4

RESULTS & DISCUSSION

4.1 Graphene oxide: XRD and Raman spectra

4.1.1 XRD structural of graphene oxide

First, we starting our procedure with synthesis of graphene oxide using using modified Hummers, methods. Then, the as-synthesized graphene oxide used as a precursor for graphene/Cu_2O catalyst synthesis. Graphene nanosheet (GN), which is a two-dimensional (2D) carbon material serve as a support because of its unique properties such as; high conductivity (10^3-10^4 S/m) and surface area (2630 m^2/g). We expect that these unique structure make graphene a promising component for the electrochemical reduction of CO_2. Figure 4.1 shows the X-ray diffraction (XRD) patterns of graphene oxide and graphite powder. Clearly, it was observed the characteristic peak (002) of graphene oxide centered at 2 theta 11° which corresponding to the interlayer d-spacing of 0.784 nm compared to that of graphite powder at around 2 theta 26°. XRD result reveals that the graphite powder was oxidized to graphene oxide using the strong oxidizing agent ($KMnO_4$). This explained by the attaching of oxygenated functional groups such as hydroxyl (–OH), carboxyl (–COOH) and carbonyl (–C=O) groups on both sides of carbon sheets [67].

4.1.2 Raman spectra

Raman scattering is a well-known as an essential technique for carbonaceous materials characterization. Fig. 4.2 shows the Raman spectra of GO. The two obvious peaks at around 1330 cm^{-1} and 1589 cm^{-1} were related to the D and G bands, respectively. G band is characteristic of graphitic sheets and D band is characteristic of defects within the hexagonal graphitic structure. XRD and Raman spectra results confirms the sp^2 carbon structure of graphene oxide [68].

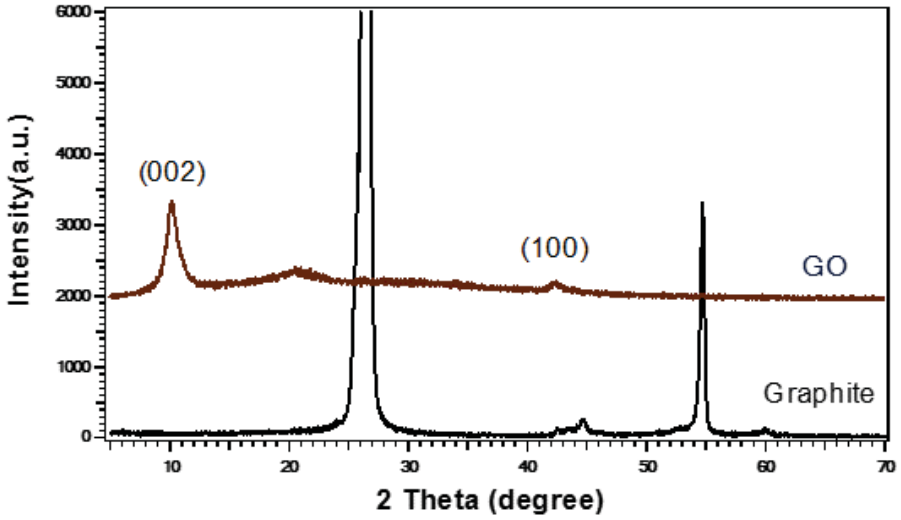

Figure 4.1 XRD patterns of graphite and graphene oxide (GO).

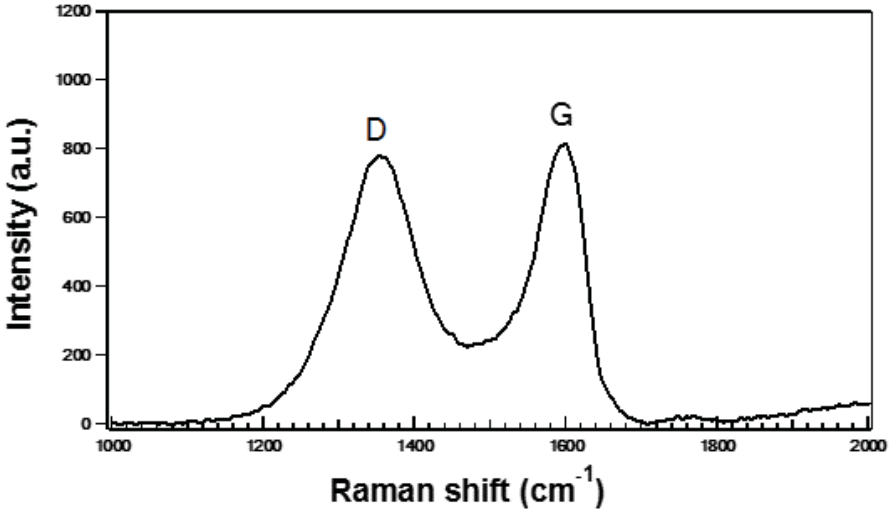

Figure 4.2 Raman spectra of GO showing the D & G bands.

The main target is to synthesis and fabricate graphene as supporting high-conductivity material for Cu_2O and ZnO catalysts for the electrochemical reduction of CO_2. The electrochemical reduction of CO_2 is a process involving electrons and protons transfer. The CO_2RR is very complex process because of the insufficient knowledge of surface-mediated electrochemical reaction pathways. The wide variety of products ranging from C_1-C_3 as well as number of electrons transferred ranging from CO (2e), CH_3OH (6e) and CH_3CH_2OH (12e) up to $CH_3CH_2CH_2OH$ (18e) during the CO_2 reduction demonstrates big challenges in understanding the reaction mechanisms. The choice of the desired CO_2 reduction products is still very critical, since CO_2 reduction process has different pathways. Table 4.1 shows the estimates costs for different CO_2 reduction products. As seen from table 4.1, it is not economically to convert CO_2 to methane, methanol, ethanol, or ethylene. In contrast, CO, formic acid, formaldehyde, and propanol have high market values. Designing an active, selective, and stable electro-catalyst for CO_2 reduction still need more efforts. Many studies have been investigated the reduction of CO_2 to C_1 products. Moreover, the design of advanced catalyst to convert CO_2 to more value-added products such as C_2-C_4 through C-C coupling reaction is very challenging task. There are no appreciable catalysts able to achieve this task since the CO_2 reduction reaction mechanism is still unclear. Bimetallic and carbon supported metal/metal oxide catalysts may presents some opportunities due to their synergic effect. The structure control and morphology which arises active reaction sites should be investigated.

Table 4.1 The estimated costs for major CO_2 reduction products assuming electricity at a price of $0.07 per KWh, a cell potential of 2V [19].

Product	# of electrons per product molecule	Market price[a]	Estimated cost[a]	Best known catalyst
Syngas	2	25–90	376	Au, Ag, Zn
Carbon monoxide	2	600	271	Au (95%), Ag (92%)
Formic acid	2	1200–1600 (90%)	163	Sn (80%)
Formaldehyde	4	3500	501	B-doped diamond (74%)
Methanol	6	350	705	Cu (< 5%)
Methane	8	150–250	1880	Cu (55%)
Ethanol	12	700–1000	981	Cu (< 5%)
Ethylene	12	950–1200	1611	Cu (< 5%)
Propanol	18	1800	1128	Cu (< 5%)

[a] Unit: USD per metric ton; the values are extracted from multiple sources in the internet.

4.2 Graphene/Cu_2O electrode for the electrochemical reduction of CO_2 to ethanol

4.2.1 A brief overview

Electrochemical reduction of CO_2 occurs at large negative overpotentials and is limited by hydrogen evolution as a competitive reaction in an aqueous electrolyte. Hence, an efficient catalyst should be designed to overcome these limitations. Furthermore, the product formed as a result of CO_2 reduction depends on nature of electrode material, pH, and electrolyte [17][18][69]. To date, copper/copper oxides catalysts were extensively investigated for electrochemical reduction of CO_2 [24][70][61][71][72]. Oxygen species in copper (I) increase the number of defect electrons so that CO_2 was easily adsorbed onto the catalyst surface; however, CO_2 reduction at relatively high overpotentials and poor selectivity towards alcohols over Cu_2O catalyst are the major obstacles. Therefore, surface modifications are highly desired [16].

In this study, we evaluate the role of graphene as supporting catalyst for the electrochemical reduction of CO_2 in aqueous solution. Graphene provide large surface area for the Cu_2O active sites, subsequently enhance the electron mobility which can promote the CO_2 adsorption and reduction activity as well [26]. The as-synthesized graphene/Cu_2O catalyst not only exhibited high performance for CO_2 reduction compared to Cu_2O, but also showed good selectivity towards ethanol production. The product yield as well as the Faradaic efficiency (FE) have been investigated.

4.2.2 XRD analysis of Graphene (GN) / Cu_2O NPs

The reaction of graphene oxide with $CuCl_2$ in alkaline medium and in the presence of $NH_2OH.HCl$ as reducing agent was carried out to synthesis graphene (GN)/Cu_2O nanocomposite. To demonstrate the successful synthesis of Cu_2O and GN/Cu_2O catalysts, various analytical techniques were employed. The crystal structure of the as-synthesized catalysts were analysed by XRD technique and their patterns are given in figure 4.3. It was observed that characteristic peaks appeared at 2 theta angles 36.4^o, 42.3^o, 61.3^o, and 73.5^o which can be assigned to reflections (111), (200), (220), and (311) cubic crystal structure of Cu_2O planes, respectively. These results are agreed with JCPDS card no. 87-2076 [57,66]. XRD data revealed that crystalline size of Cu_2O in the range from 40-60 nm. According to XRD pattern there are no impurities detected indicating the purity and crystallinity of Cu_2O. Also, it was found the difference between unsupported Cu_2O and GN/Cu_2O composite, as the peaks of pure Cu_2O are sharper and narrower than those of GN/Cu_2O which is related to the role of graphene in controlling the size of nanoparticles/cubes.

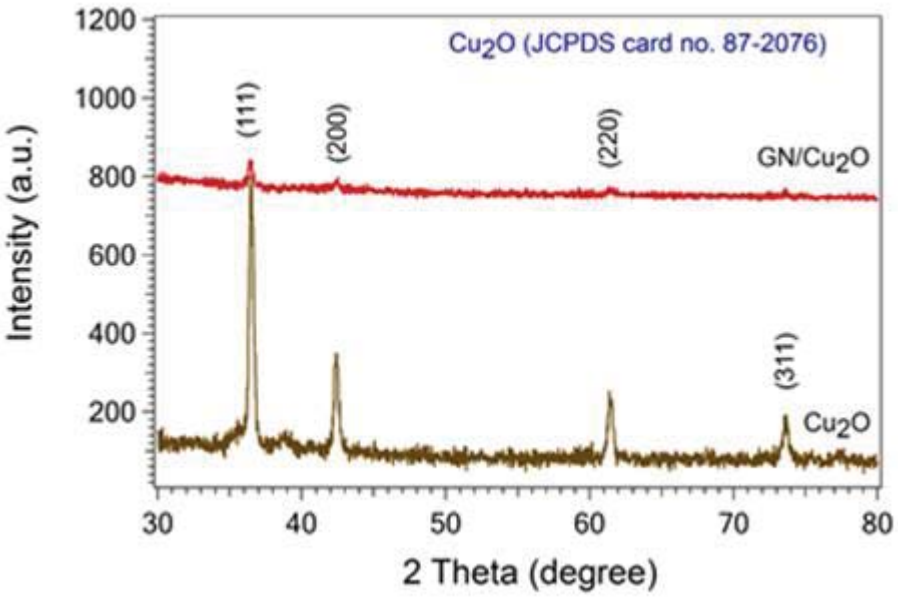

Figure 4.3 XRD patterns of Cu_2O and graphene (GN)/Cu_2O composite.

4.2.3 FE-SEM & TEM analysis

The surface morphology of Cu_2O and GN/Cu_2O NPs was investigated with FE-SEM as shown in figure 4.4 the SEM images clearly indicates the surface morphology and size of Cu_2O nanoparticles, it can be seen from (fig. 4.4 a) the cubic structure of Cu_2O is a cluster of particles agglomeration and the cubic edge length varying from 200- 500 nm. On the other side as we can observe from the difference between unsupported Cu_2O and GN/ Cu_2O NPs. Graphene wrapped Cu_2O very well and keeping the cubic structure shape of Cu_2O as shown in figure 4.4 (b and c). The size of Cu_2O dispersed onto graphene was reduced to around 200 nm smaller than that unsupported Cu_2O, Which strongly confirmed the enhancement of nanoparticles size due to graphene addition. This is result are compatible with the results obtained by XRD. As shown in figure 4.5, Cu, O, and C peaks are clearly observed by EDS analysis which in good agreement with XRD results. Al and Mg peaks appeared in EDS spectra are coming from the sample holder.

The TEM image of GN/Cu_2O revealed that the graphene layers were wrapped the Cu_2O nanoparticles with an average size of 20-50 nm as shown in figure 4.6 (a). HRTEM image exhibited a lattice fringe spacing of 0.213 nm in several orientation regions, corresponding to (200) crystal plane of Cu_2O as shown in figure 4.6 (b). These results are in good agreement with the results obtained from XRD.

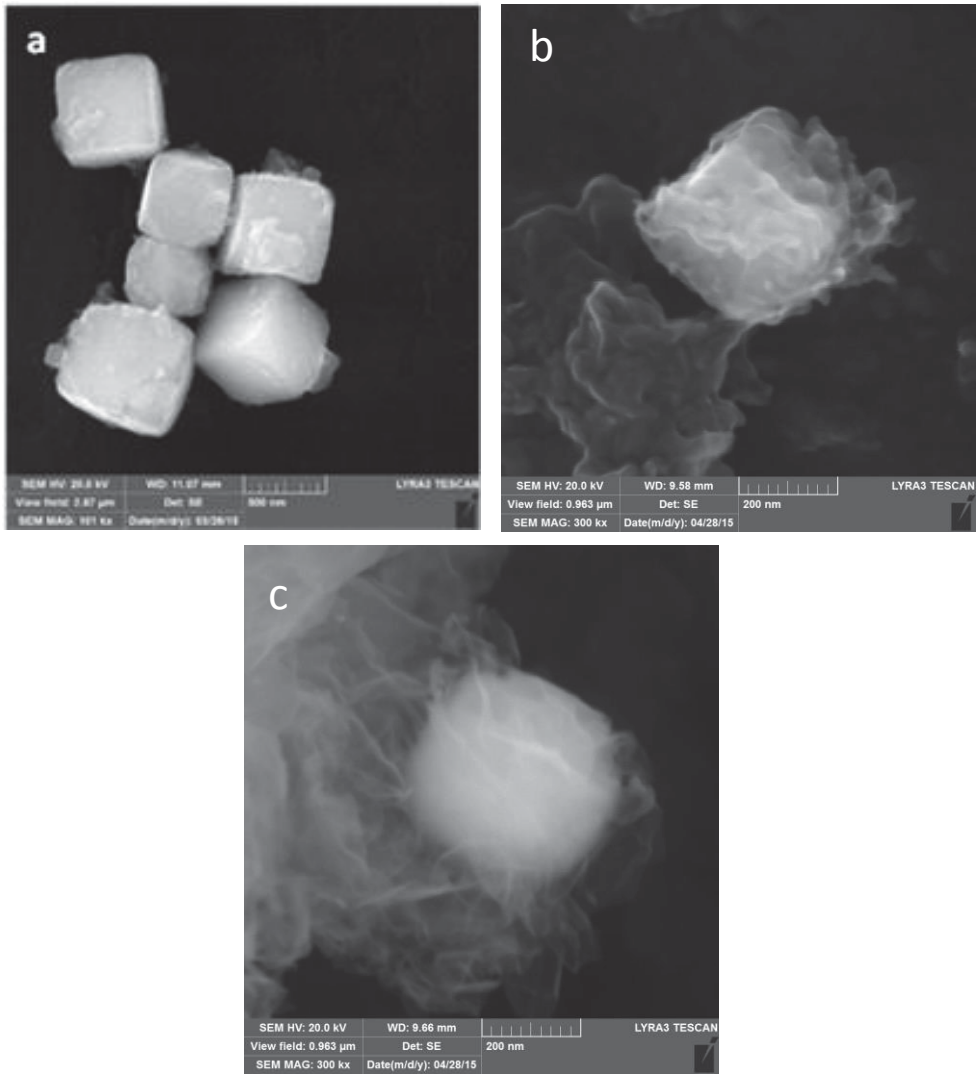

Figure 4.4 FE-SEM images of (a) Cu_2O and (b,c) GN/Cu_2O composite.

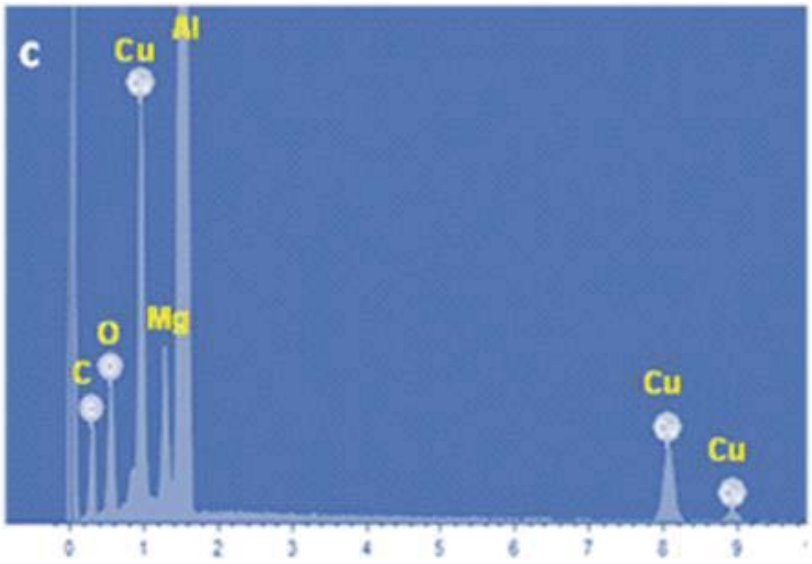

Figure 4.5 EDS spectra of GN/Cu_2O composite.

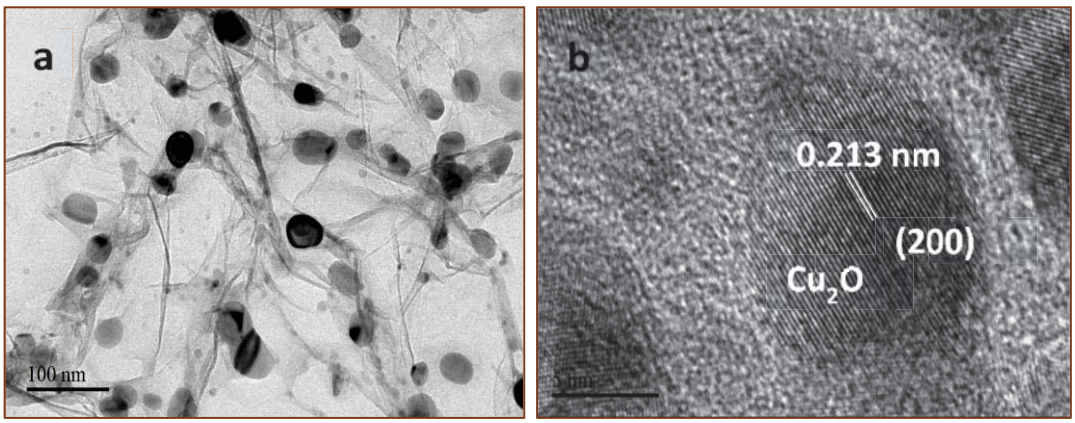

Figure 4.6 TEM image (a) and HRTEM (b) of GN/Cu_2O composite.

4.2.4 Raman Spectroscopy

Raman scattering is a well-known as an essential technique used for characterize the carbonaceous materials. Raman spectra shows two obvious broad G and D bands appeared at 1586 cm^{-1} and 1350 cm^{-1}, respectively for graphene oxide (GO) and GN/Cu_2O samples as shown in figure 4.7. Further observation showed that I_D/I_G ratio for GN/Cu_2O composite larger than that of GO, confirming the removal of oxygen functional groups in GO during the reduction process [73].

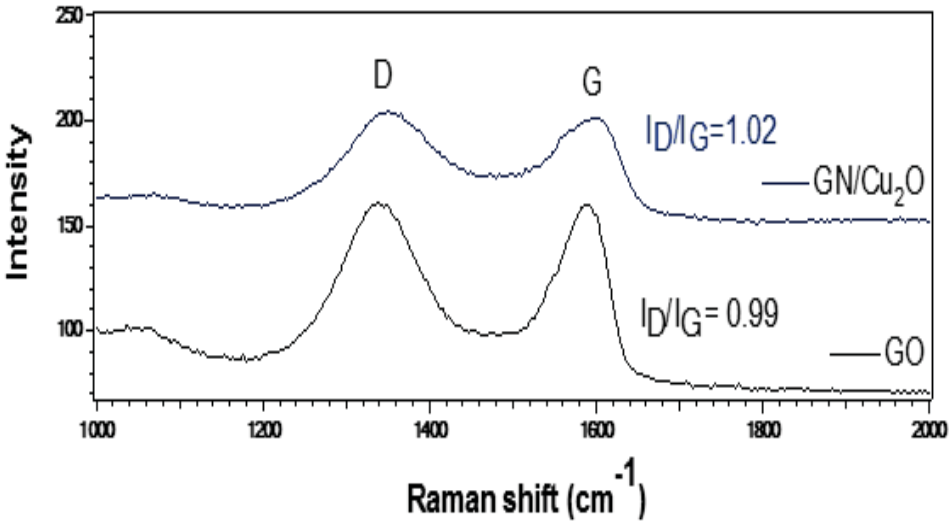

Figure 4.7 Raman spectra of GO and GN/Cu_2O showing the intensity ratio of D/G bands.

4.2.5 Electrochemical tests

4.2.5.1 Linear Sweep Voltammetry measurement

The voltammetric behavior of the copper modified with Cu_2O and GN/Cu_2O electrodes compared with copper foil, in aqueous 0.5 M $NaHCO_3$ (Sigma Aldrich) electrolytes saturated with CO_2 (99.99%) were investigated by studying the linear sweep voltammetry (LSV) measurements ranging from -0.2 to -1.8 V versus Ag/AgCl scanned at a sweep rate of 20 mV/s. Figure 4.8 demonstrates the linear sweep voltammetry curves of bare Cu foil, Cu_2O, and GN/Cu_2O electrodes under N_2 saturation to clarify the influence of hydrogen evolution. The current density gradually increased with increasingly the negative potential applied to the cathode as shown in figure 4.8. Under N_2 saturation, the recorded currents were mainly related to hydrogen evolution reaction. There is an obvious reduction peak at -1.3 V, while the solution remained clear. This peak is related to the reduction of Cu^{+1} to Cu^0 (metallic form) on the electrode surface. As seen from this figure, copper modified electrodes (Cu_2O and/or GN/Cu_2O) exhibited higher current densities values than copper foil (bare electrode). Briefly, GN/Cu_2O electrode performed the highest current density value compared to the other electrodes, revealing the graphene contribution. Figure 4.9 illustrates the LSV measurements curves of the electrodes in CO_2 saturated 0.5 M $NaHCO_3$ solution. There is no significant change in the voltammograms shape between the electrodes, moreover the onset potentials depends on pH and adsorption/desorption mode at electrode surface. However, the highest current density value has been recorded over GN/Cu_2O compared to Cu_2O modified electrodes. Based on 0.1 mg of loaded material, the current density values at -1.7 V over GN/Cu_2O and Cu_2O were 12.2 and 8.4 mA/cm^2,

respectively. Graphene has high electrical conductivity and high surface area properties leads to increases the available surface area of the catalyst. Therefore, the higher current density value for GN/Cu_2O electrode is indicative of the graphene enhancement of this electrocatalytic effect. Comparing with some previous reports over copper based electrodes, the measured current at GN/Cu_2O electrode is a promising [57][74][75][59]. GN/Cu_2O electrode performed higher cathodic current values in the N_2 saturated than in the CO_2 saturated electrolyte (inset fig. 4.9). The exact nature of this behavior may associated with the reduction of CO_2 on GN/Cu_2O surface and resulting in adsorption of some species [57][74]. These results concluded that graphene may be a promising support for Cu_2O active sites in catalytic activity toward CO_2 reduction.

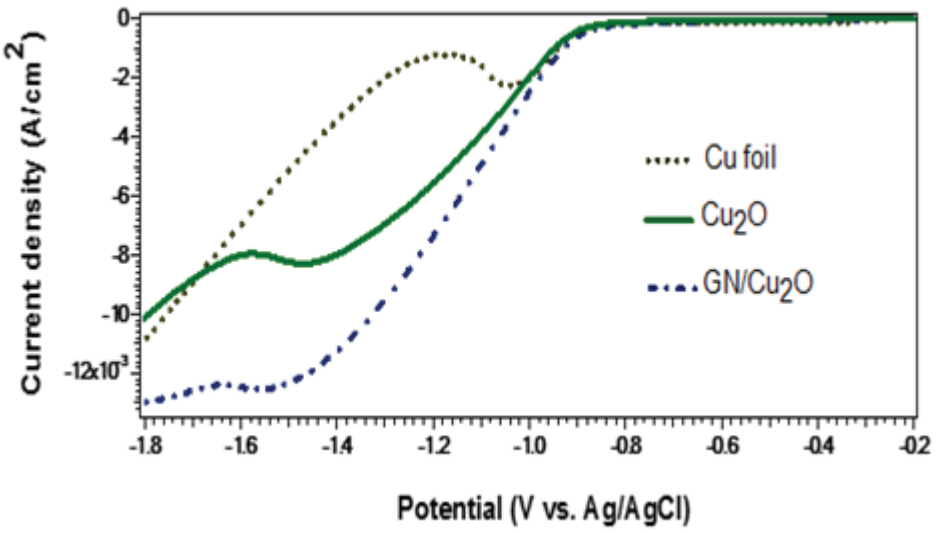

Figure 4.8 Linear sweep voltammetry curves over Cu, Cu_2O, and GN/Cu_2O saturated with N_2 in 0.5 M $NaHCO_3$ at scan rate of 20 mV/s.

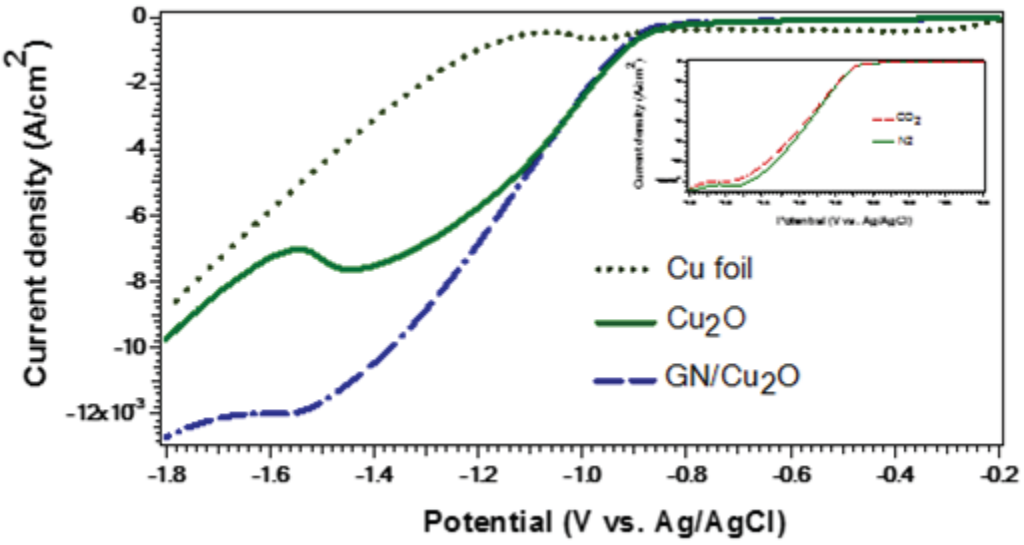

Figure 4.9 Linear sweep voltammetry curves over Cu, Cu_2O, and GN/Cu_2O saturated with CO_2 in 0.5 M $NaHCO_3$ at scan rate of 20mV/s. Inset is LSV over GN/Cu_2O under N_2 (dashed line) and CO_2 (straight line) saturated electrolytes.

4.2.5.2 Chronoamperometry

To evaluate the electrochemical activity of electrode surface towards CO_2 reduction, electrolysis was carried out at fixed electrode potential for 20 min reduction. Figure 4.10 demonstrate the current responses for GN/Cu_2O at -0.9 and -1.3 V *vs.* Ag/AgCl. The current started at high value and decreased gradually with time. At -0.9 V, the electrode possess high current started approximately at -10 mA and declined slowly to -0.5 mA. Also, at -1.3 V, GN/Cu_2O electrode exhibited an initial current value of -31 mA and decreased rapidly to -4 mA after 20 s of electrolysis, then it goes constantly for the remaining time as shown in figure 4.10. The degradation nature of the high recorded current explained by the detachment of the oxide surface [74][76] [77].

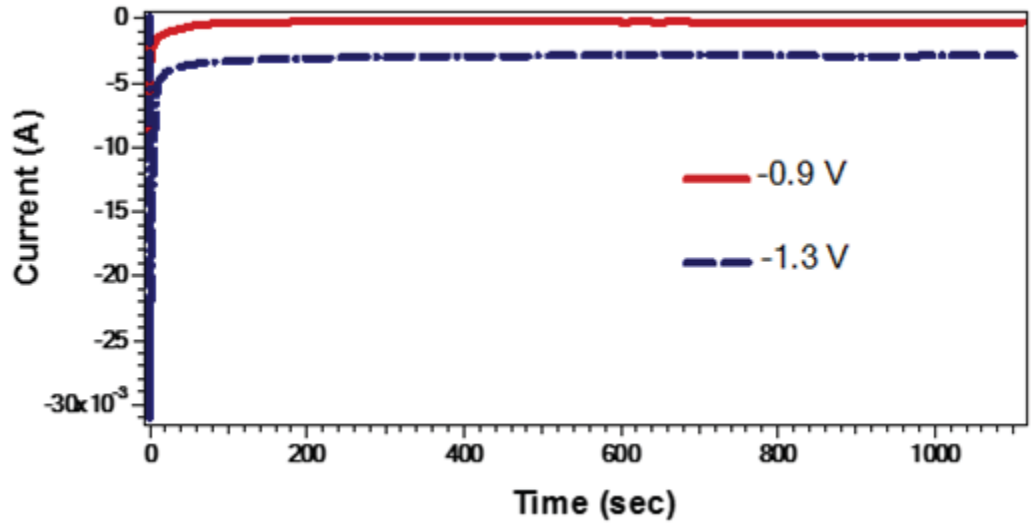

Figure 4.10 Current responses at different potentials over GN/Cu_2O with CO_2 staurted 0.5 M $NaHCO_3$ electrolyte.

4.2.6 GC-MS analysis & Faradaic Efficiency

After the electrolysis processes and CO_2 reduction at GN/Cu_2O electrode surface, the liquid product was analyzed by GC-MS, varying fixed potentials have been tested. Ethanol was found to be the predominant product produced as a result of CO_2 reduction at a retention time of 1.66 minute as shown in figure 4.11. Furthermore, the produced ethanol is highly dependent on the electrode potential. The faradaic efficiencies of ethanol is up to 9.93 % and 6.75 % at -0.9 and -1.3 V, respectively as shown in table 4.2. FE is calculated based on 12 electrons are required to convert CO_2 to ethyl alcohol. The decreasing of faradaic efficiency is associated with the reduction of Cu_2O to Cu^0 at -1.3 V as investigated from figure 4.8. Consequently, it can be seen that GN/Cu_2O electrode seems to be highly selective towards ethanol production. In comparison, no liquid products were detected at -0.9 V over Cu_2O-based electrode under the same reaction conditions. Other products may have formed as well, but in much smaller quantities. For comparison with analyte samples, standard ethanol solutions were injected. The maximum Faradaic efficiency was obtained at -0.9 V and decreased with increasing the applied potential up to -1.3 V as can be seen in figure 4.12. The decrease of FE % value is associated with the partial reduction of Cu (I) and the increasing of the hydrogen evolution rate.

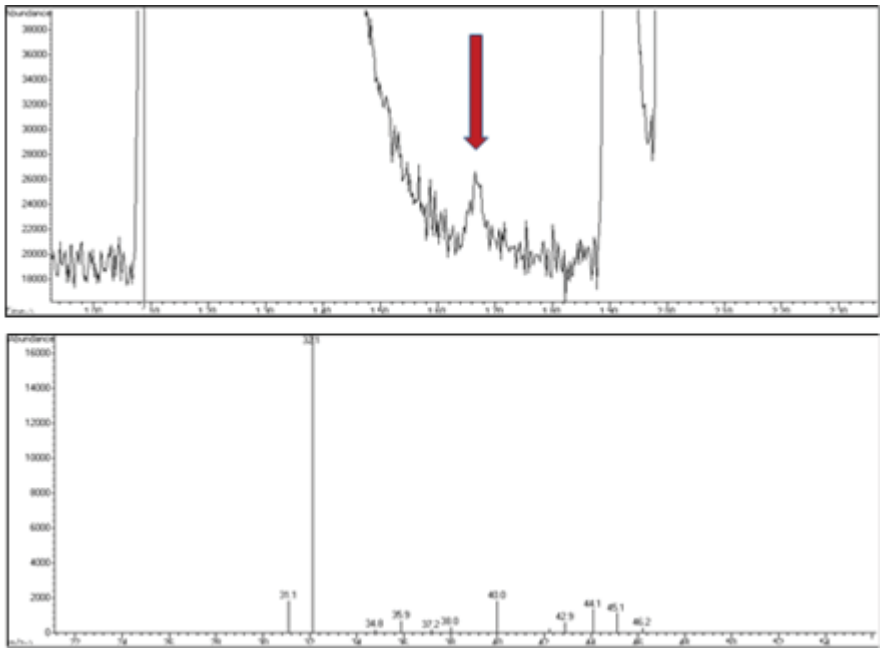

Figure 4.11 GC-MS chromatogram (top) shows ethanol peak at RT=1.66 min produced over GN/Cu_2O at -1.3 V vs. Ag/AgCl for 20 min reduction. Mass spectra (bottom) shows defragments of ethanol.

Table 4.2 Faradaic efficiency of ethanol produced over 0.1 mg GN/Cu_2O weight loading at different potentials.

Electrode potential (vs. Ag/AgCl)	Current density (mA/cm^2)	charge (C)	Ethanol conc. (ppm)	FE (%)
-0.9	0.5257	2.1324	0.3369	9.93
-1.3	2.754	11.1708	1.2	6.75

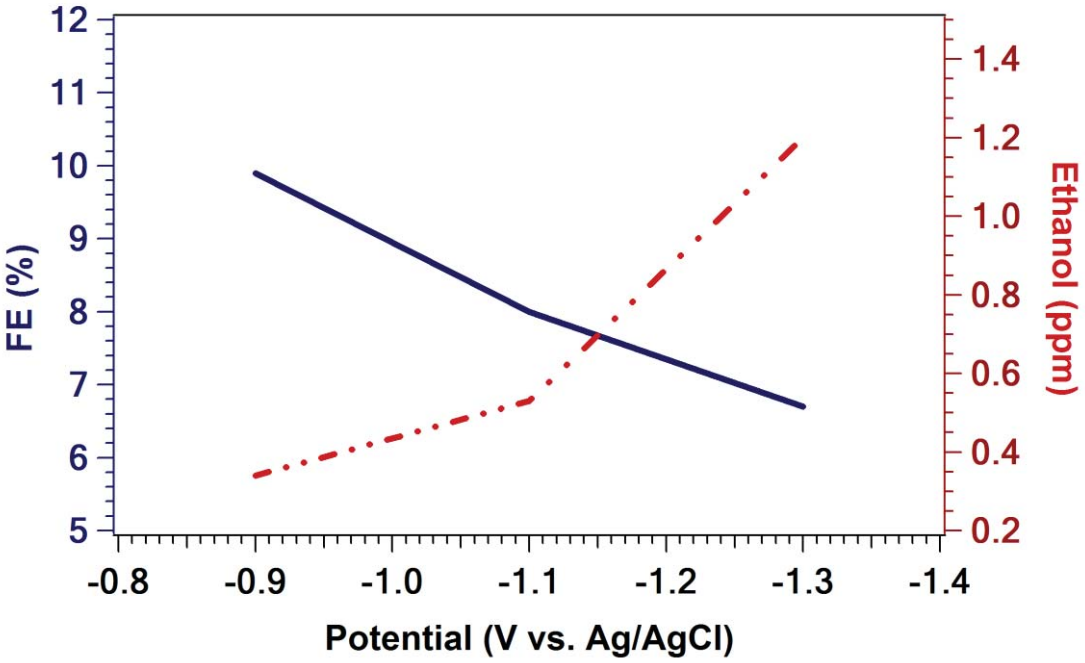

Figure 4.12 Faradaic efficiency and ethanol concentration (ppm-dashed line) produced using GN/Cu_2O surface at different applied potentials.

4.2.7 Summary

In summary, the electrochemical reduction of CO_2 was performed using copper modified graphene/Cu_2O electrode revealed that the current density was improved due to graphene contribution. Based on 0.1 mg of GN/Cu_2O catalyst loading, LSV measurements resulted in a high current density value of 12.2 mA/cm^2 at -1.7 V versus Ag/AgCl. Ethanol was found to be the predominant liquid reduction product at -0.9 V under ambient conditions. No liquid products other than ethanol were detected, implying the selectivity towards C_2 products. These results suggest that graphene-based catalyst can be efficiently used for electrochemical reduction of CO_2.

Table 4.3 Comparison of Faradaic efficiency for ethanol production on different copper based electrodes.

Electrode	Electrolyte/Condition	Ethanol (FE %)	Ref.
Cu_2O (1 mg cm^{-2})	0.5 M $KHCO_3$ / -1.39 V vs. Ag/AgCl	10.1	[71]
HKUST-1[a] (1 mg cm^{-2})	0.5 M $KHCO_3$/ -0.9 V vs. Ag/AgCl	10.3	[72]
Electropolished Cu	0.1 M $KHCO_3$/ -0.99 V vs. RHE	N.D. (not detectable)	[78]
0.1 μm Cu_2O	0.1 M $KHCO_3$/ -0.99 V vs. RHE	6	
3.6 μm Cu_2O	0.1 M $KHCO_3$/ -0.99 V vs. RHE	16.37	
Polycrystalline Cu	0.1 M $KHCO_3$/ -5 mA/cm^2	6.9	[35]
Electrodeposited Cu_2O	0.5 M $KHCO_3$/ -1.82 V vs. Ag/AgCl	N.R. (not reported)	[79]
Cu (100)	0.1 M $KHCO_3$/ -5 mA/cm^2	9.7	[80]
GN/Cu_2O (0.1 mg material loading)	0.5 M $NaHCO_3$/ -0.9 V vs. Ag/AgCl	9.93	This work

[a] Cu-based MOF supported on gas diffusion electrode.

4.3 Graphene/ZnO/Cu_2O electrocatalyst for highly selective CO_2 conversion into n-propanol

4.3.1 A brief overview

Recently, various metallic electrodes have been used for the electrochemical reduction of CO_2 [20][21][49]. Based on the product selectivity, these metallic catalysts can be divided into groups. Au, Ag, and Zn metals are exhibits CO_2 electroreduction selectivity towards CO, while Fe, Ni, and Pt are hydrogen selective metals [19]. However, most of these metals are not applicable for large-scale applications due to their high cost. Therefore, more efforts are needed to design highly active and selective electro-catalysts for the electrochemical reduction of CO_2 to products containing C-H and C-C bonds. In recent years, copper have been widely used as an active cathode for converting CO_2 into high-value products [76][24]. Cu exhibits catalytic activity to reduce CO_2 to C_1-C_2 products [19]. Note in this regard that ZnO has been reported to stabilize Cu atoms and to strengthen Cu-CO^- links, and thus result in increased the activity and selectivity towards alcohol production [81][23].

Here, we fabricated graphene/ZnO/Cu_2O as an electrocatalyst for CO_2 reduction. Graphene has a large surface area and an excellent electron mobility properties which considered to be a promising support for CO_2 reduction [82]. The linear sweep voltammetry of 0.2 mg catalyst loading was carried out for GN/ZnO and GN/ZnO/Cu_2O. In CO_2 saturated electrolytes, the cathodic current of the catalyst containing Cu_2O showed significant increase from 4 to 8 mA/cm^2 at -1.8 V vs. Ag/AgCl, and the largest current density value was obtained for a Cu_2O/ZnO weight ratio of 2:1 on graphene. The process mainly produced n-propanol using GN/ZnO/Cu_2O-based electrodes The Faradaic efficiency for

CO_2 conversion to n-propanol was 22% and 30% for GN/ZnO/Cu_2O (with a Cu_2O/ZnO weight ratios of 2:1 and 1:2) at an applied potential of -1.2 and -0.9 V vs. Ag/AgCl, respectively. In contrast, no alcohol was detected using GN/ZnO under all of the conditions tested.

4.3.2 Graphene (GN)/ZnO/Cu_2O structure

We used the following procedure for synthesis of graphene (GN)/ZnO/Cu_2O as a binary and tertiary composites as follow: 3 ml of 1 mg/ ml GO solution was added to 180 ml ultrapure water and sonicated for 30 min. Then, calculated amount of 0.1 M $ZnCl_2$, 0.1 M $CuCl_2$, and 0.087 gm sodium dodecyl sulfate (SDS) were mixed with GO solution under vigorous stirring for another 2 h at 34 ^oC. After that,1 M NaOH and 1 M $NH_2OH.HCl$ were rapidly injected into the solution mixture and stirred for 30 min. Then, centrifuged and washed with ethanol and water repeatedly, and dried in vacuum at 40 ^oC for 18 h. A two tertiary composites with different ZnO/Cu_2O weight ratios were prepared. Sample S1 assigned to composite with ZnO/Cu_2O weight ratios of 2:1, while S2 sample assigned to composite with ZnO/Cu_2O weight ratios of 1:2. Figure 4.13 shows the XRD patterns of as-synthesized composites. XRD patterns of GN/ZnO show diffraction peaks at 31.7^o, 34.3^o, 36.2^o, 47.4^o, 56.5^o, 62.7^o, and 67.8^o with crystal orientations (100), (200), (101), (102), (110). (103), (112), and (201) Planes which compatible with hexagonal wurtzite crystal structure of ZnO JCPDS card no. (01-075-1526), respectively [83][84].

And those peaks appeared at 2 theta angles 36.4°, 42.3°, 61.3°, and 73.5° which can be assigned to reflections (111), (200), (220), and (311) are consistent with the cubic crystal structure of Cu_2O planes (JCPDS card no. 087-2076) [66]. Pure ZnO and Cu_2O were prepared using the same procedure for comparison as shown in figure 4.13. The intensive and clear peaks reveal the well and highly crystalline ZnO synthesized particles. The broadening of GN/ZnO peaks than those of ZnO peaks implying the effect of graphene incorporation into ZnO.

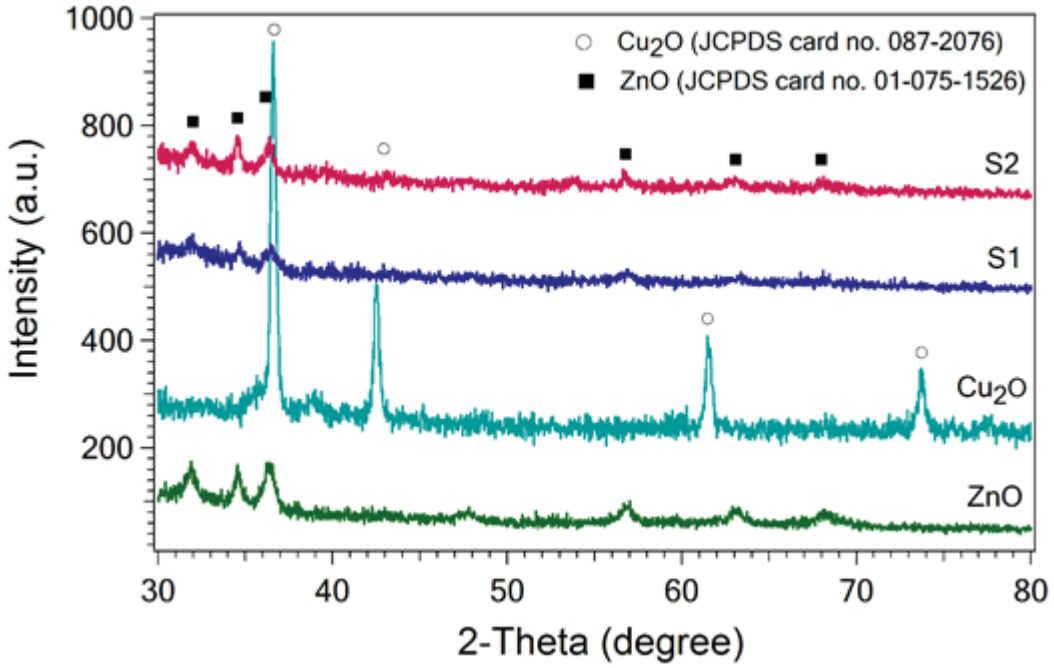

Figure 4.13 Powder XRD patterns of as-prepared Cu_2O, ZnO, and GN/ZnO/Cu_2O catalysts.

4.3.3 FE-SEM & TEM images of composites

The morphology and microstructure of the as-synthesized ZnO, GN/ZnO, and GN/ZnO/Cu_2O composites were characterized using FE-SEM as shown in Figure 4.14. The ZnO deposits as look like rods morphology have an average particle size around 500 nm as shown in figure 4.14 (A). This reflects the successful synthesis of well crystalline ZnO nanoparticles at very low temperature using $NH_2OH.HCl$ in alkaline media. Graphene incorporation into ZnO is clear appear as transparent layer graphene wrapped ZnO particles on both sides forming GN/ZnO hybrid structure as shown in figure 4.14 (B). Figure 4.14 (C-D) show the structure morphology of GN/ZnO/Cu_2O with different ZnO/Cu_2O weight ratios, i.e., S1 and S2 nanocomposites. Here, the morphology of tertiary composite is differ than that of GN/ZnO coincide the incorporation of Cu_2O. It is clear that ZnO dendrites decorated with small spherical particles. EDS of S2 and S1 (not shown here) samples exhibits the presence of Zn and Cu peaks in the material composition as shown in figure 4.15, which compatible with the XRD results. In addition, the EDS elemental mapping of the as-synthesized GN/ZnO/Cu_2O composite (S1) shown in figure 4.16. The elemental mapping confirms the presence and the well distribution of C, O, Cu, and Zn elements. These results are in a good agreement with the XRD results. A transparent graphene sheet decorated with Cu_2O particles and long leaf-like shapes of ZnO were observed in the HR-TEM image as shown in figure 4.17.

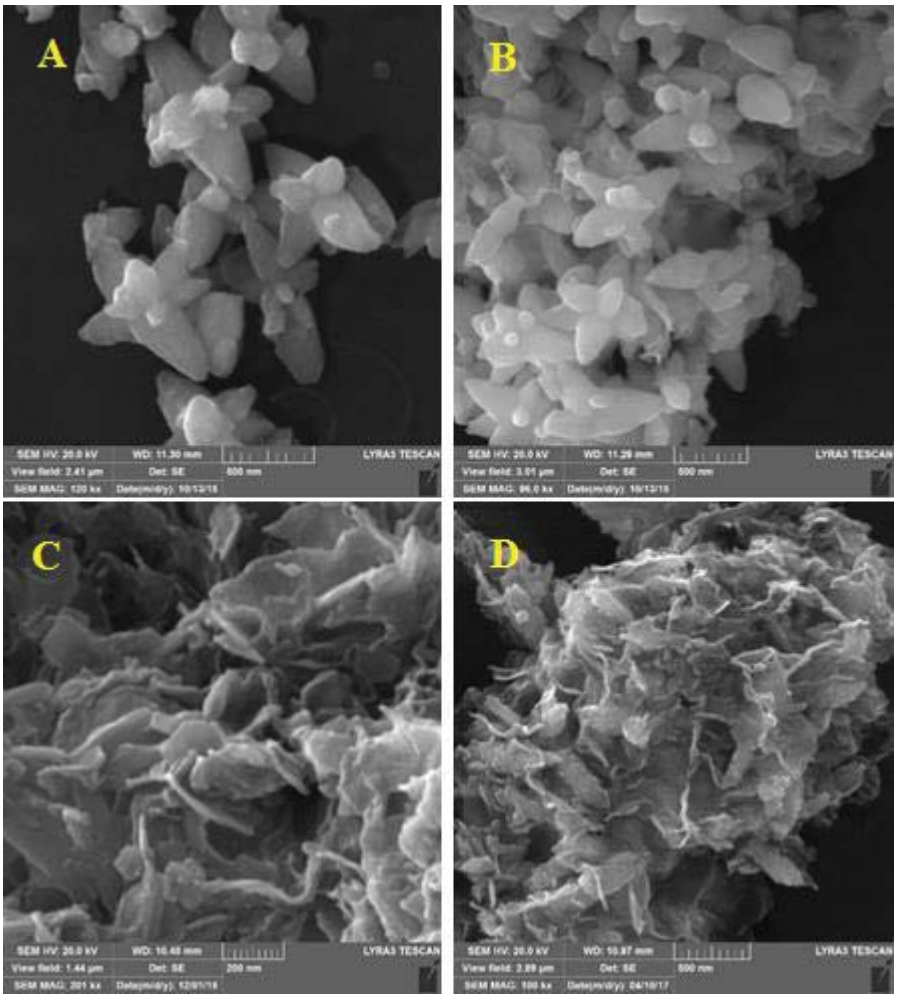

Figure 4.14 FE-SEM images of as-prepared (A) ZnO, (B) GN/ZnO, (C) GN/ZnO/Cu_2O (S1) , and (D) GN/ZnO/Cu_2O (S2) composites.

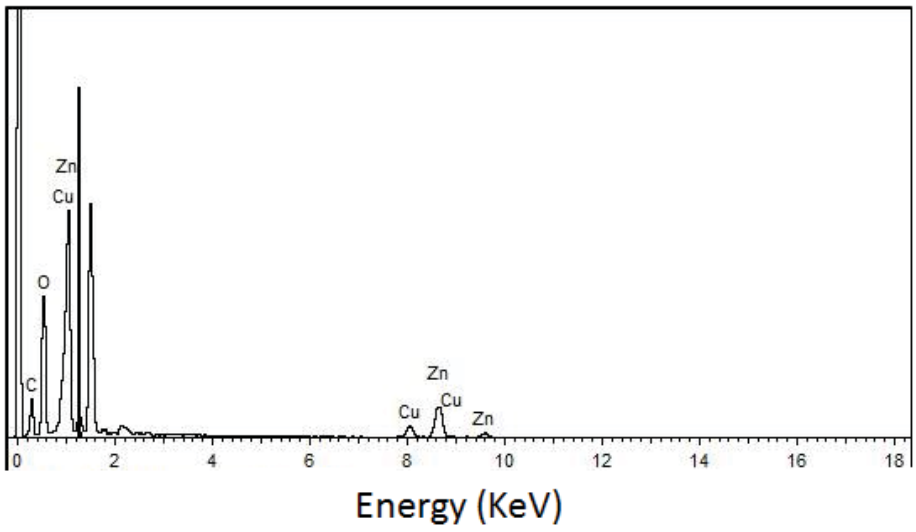

Figure 4.15 EDS analysis of GN/ZnO/Cu_2O (Cu_2O/ZnO weight ratio of 2:1) catalyst indicates the presence of Zn and Cu elements.

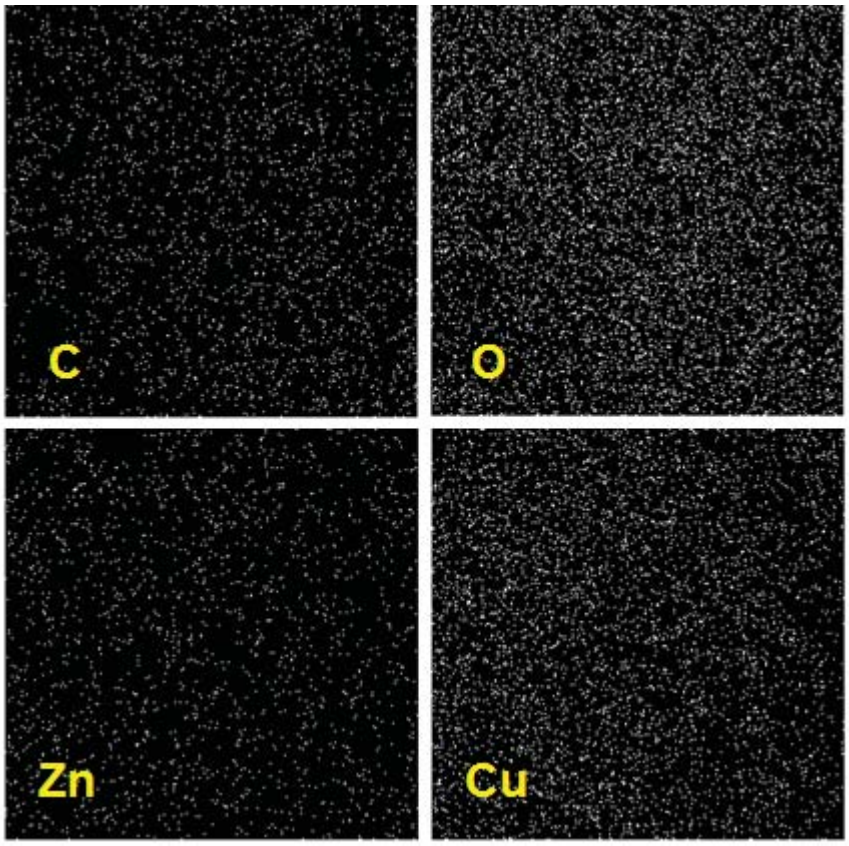

Figure 4.16 EDS elemental mapping of GN/ZnO/Cu_2O (Cu_2O/ZnO weight ratio of 2:1) composite.

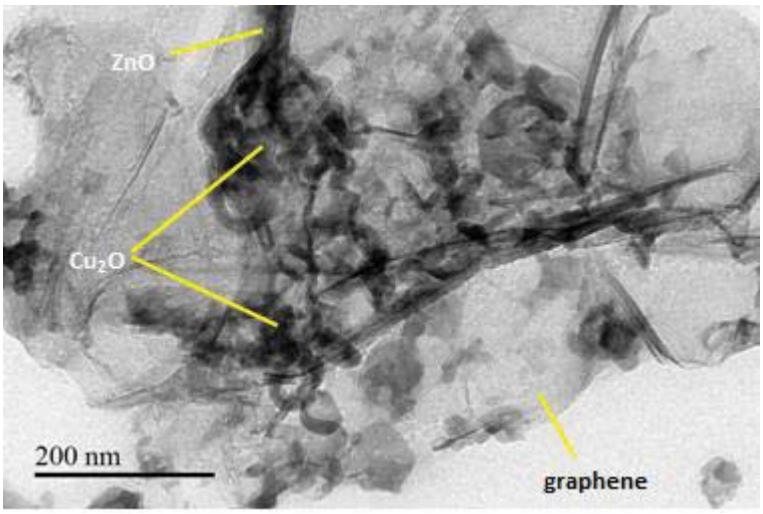

Figure 4.17 HR-TEM image of the as-synthesized GN/ZnO/Cu_2O (Cu_2O/ZnO weight ratio of 2:1) composite.

4.3.4 Raman Spectra

Figure 4.18 shows the Raman spectra for GO and GN/ZnO/Cu_2O composites. The G and D bands of graphene structure appeared at 1586 cm^{-1} and 1350 cm^{-1}, respectively as shown in figure 4.18. As can be seen, the D/G intensity ratio in case of S1 or S2 is larger than that of GO (inset fig. 4.18), indicating the removal of the oxygen functional group in GO and hence the reduction of graphene oxide to graphene [83].

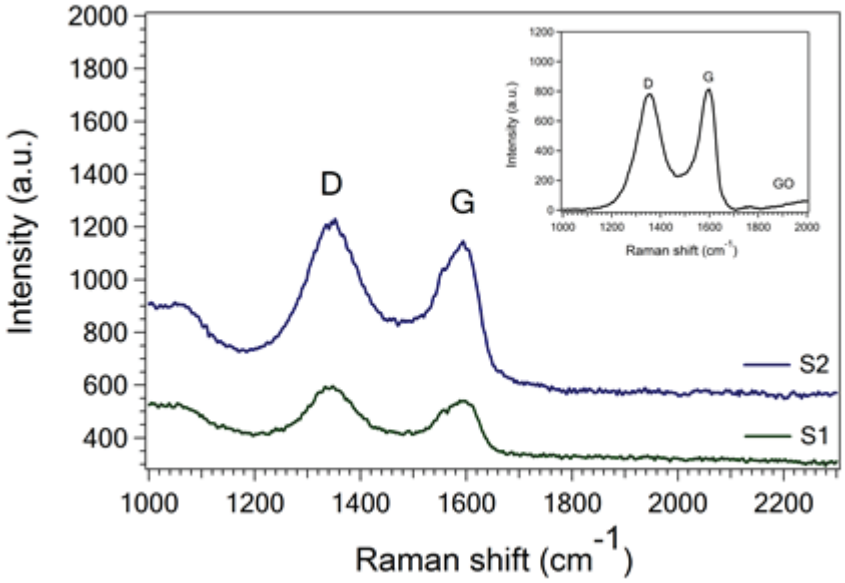

Figure 4.18 Raman spectra of GN/ZnO/Cu_2O (S1 and S2) composites. Inset is Raman spectra of GO.

4.3.5 UV-vis absorption spectra

To further demonstrate the successful synthesis of GN/ZnO/Cu_2O composites, various analytical techniques are employed. Figure 4.19 shows the absorption edge of ZnO NPs which is located at 360 nm. It is obvious that, the ZnO absorption edge was shifted to the lower wavelength at 220 nm with graphene contribution in GN/ZnO sample (synthesized via the same procedure for comparison). This is related to the decrease in ZnO band gap [85]. Cu_2O has high and intense absorbance than ZnO, therefore, the effect of introducing Cu_2O into GN/ZnO appeared as broadening peak covers the range from 200 to 300 nm as seen in S1 sample. There is a big remarkable change occurred with increasing the Cu_2O weight ratio as detected in S2 sample [86].

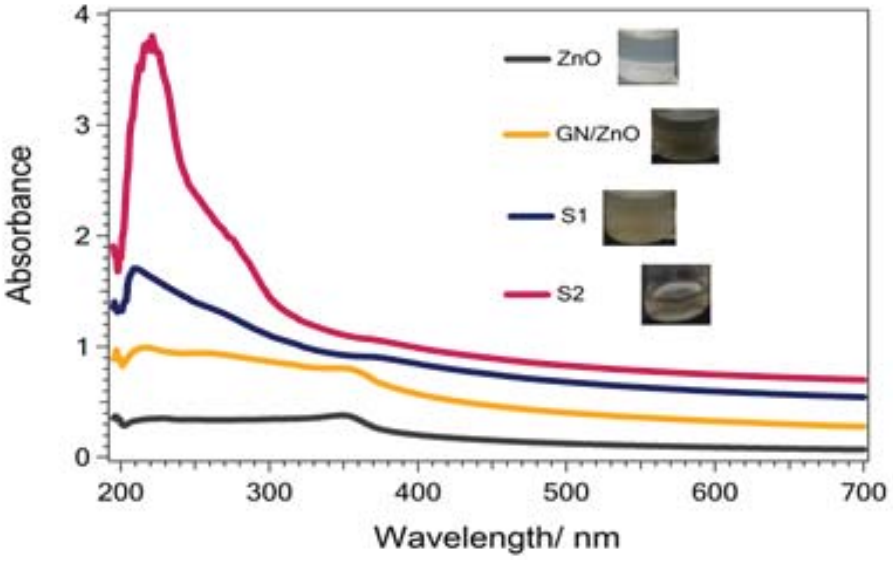

Figure 4.19 UV-vis absorption spectra of the as-synthesized ZnO, GN/ZnO, and GN/ZnO/Cu_2O composites.

4.3.6 XPS spectral characterization

To investigate the composition and the oxidation states of the elements, XPS for S2 sample was employed. Figure 4.20a shows the binding energies peaks of C 1s at 284.2, 286.6, and 288.4 eV, which were attributed to C-C, C-O, and C=O bands, respectively [87]. The O 1s binding energies at 529.6, 531.9, and 534.8 eV (Fig. 4.20b), peaks characteristic of Zn-O, OH, and C-O bands, respectively [88]. Figure 4.20c revealed that peaks at 1022.2 and 1045.6 eV were assigned to Zn 2p3/2 and Zn 2p1/2, respectively which agree with the Zn (II) oxidation state for ZnO [89]. Moreover, a peak characteristic of Cu 2p3/2 of the Cu (I) oxidation state at 932.2 eV also appeared as shown in figure 4.20d. The Cu 2p1/2 peak at 652.6 eV corresponds to Cu (II) oxidation state. However, no CuO peaks were detected by XRD analysis indicates a very trace amount of CuO in the synthesized composites. These results are consistent with XRD data, which confirm the presence of Cu (I) and Zn (II).

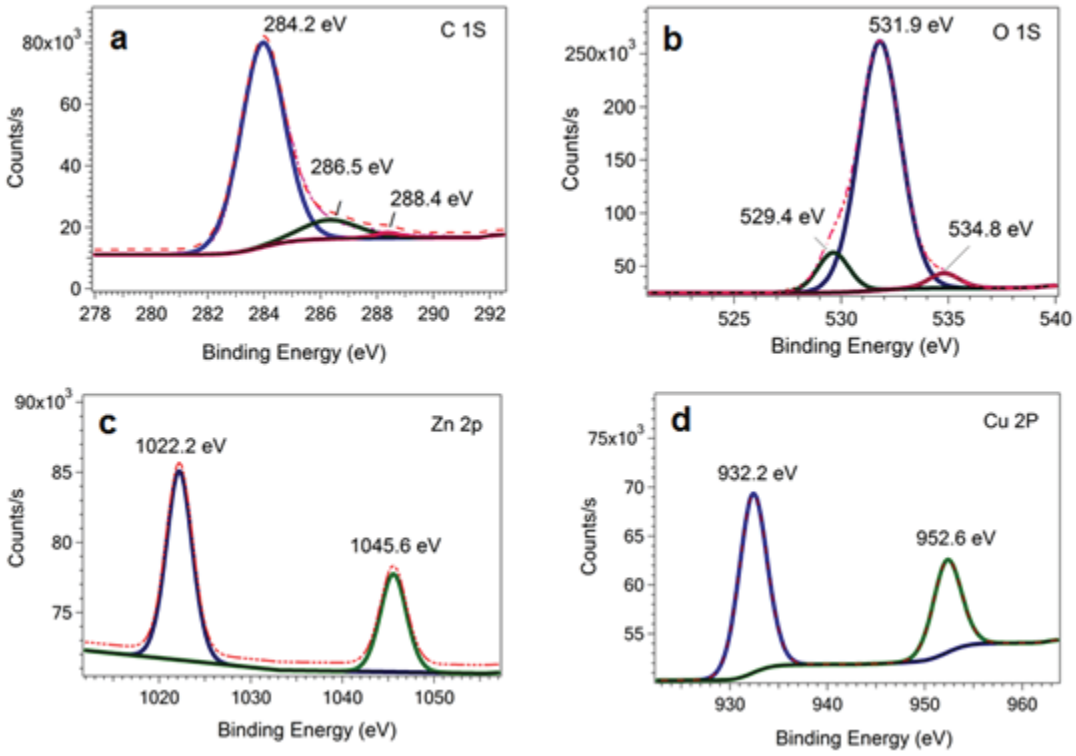

Figure 4.20 XPS spectra of GN/ZnO/Cu_2O (S2) composite: (a) C 1s scan, (b) O 1s scan, (c) Zn 2p scan, (d) Cu 2p scan after 90 sec etching.

4.3.7 Electrochemical tests

4.3.7.1 Linear sweep voltammetry

The electrochemical behavior of GN/ZnO, S1 and S2-based electrodes under N_2 saturation was investigated via the linear sweep voltammetry measurement (LSV) as shown in figure 4.21. As can be seen, the recorded currents were mainly attributed to the hydrogen evolution reaction (HER). Obviously, two reduction peaks at -1.0 and -1.3 V versus Ag/AgCl were attributed to the reduction of ZnO and Cu_2O, respectively. GN/ZnO exhibited the highest current density under N_2 saturated electrolyte, indicate the increasing rate of hydrogen evolution above electrode surface. The electrochemical reduction activity of CO_2 was measured by linear sweep voltammetry in the potential range of -0.2 to -1.8 V *vs.* Ag/AgCl at a scan rate of 20 mV S^{-1} as shown in figure 4.22. Under CO_2 saturation, GN/ZnO/Cu_2O (S2) electrode performed the highest current, i.e., as the Cu_2O/ZnO weight ratio was decreased, the current density decreased denoting the synergic effect of the both oxides (fig. 4.22). GN/ZnO/Cu_2O (S1) electrode exhibits high current density under CO_2 than N_2 saturation. In contrast, the current density value at GN/ZnO/Cu_2O (S2) electrode under CO_2 saturated electrolyte was found to be reduced than that under N_2 saturation, indicate the suppression of hydrogen evolution reaction at S2 electrode surface coincides with CO_2 reduction. T.Y. Chang et al. observed that Cu_2O-catalyzed carbon cloth exhibited lower current value under CO_2 saturated electrolyte compared to that under N_2 saturation [57]. Consequently, the LSV profiles revealed that the GN/ZnO/Cu_2O (S1 and S2) electrodes can efficiently promote the reduction of CO_2.

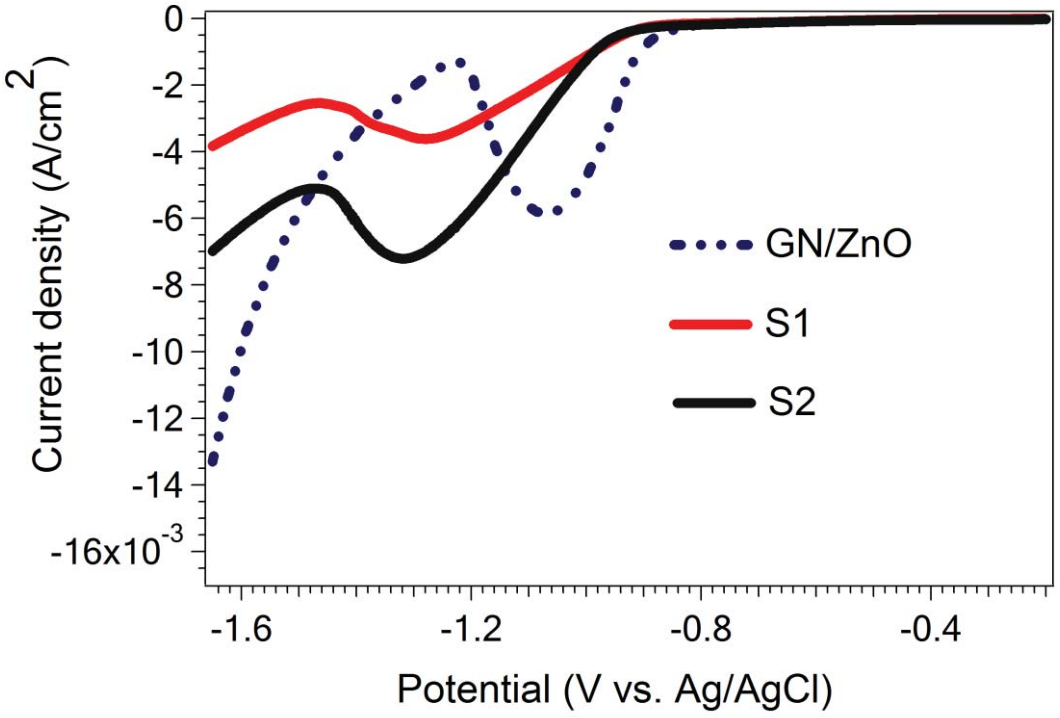

Figure 4.21 Linear sweep voltammograms of GN/ZnO (dotted line), S1 and S2-based electrodes in N_2 saturated 0.5 M $NaHCO_3$ solution at scan rate of 20 mV/s.

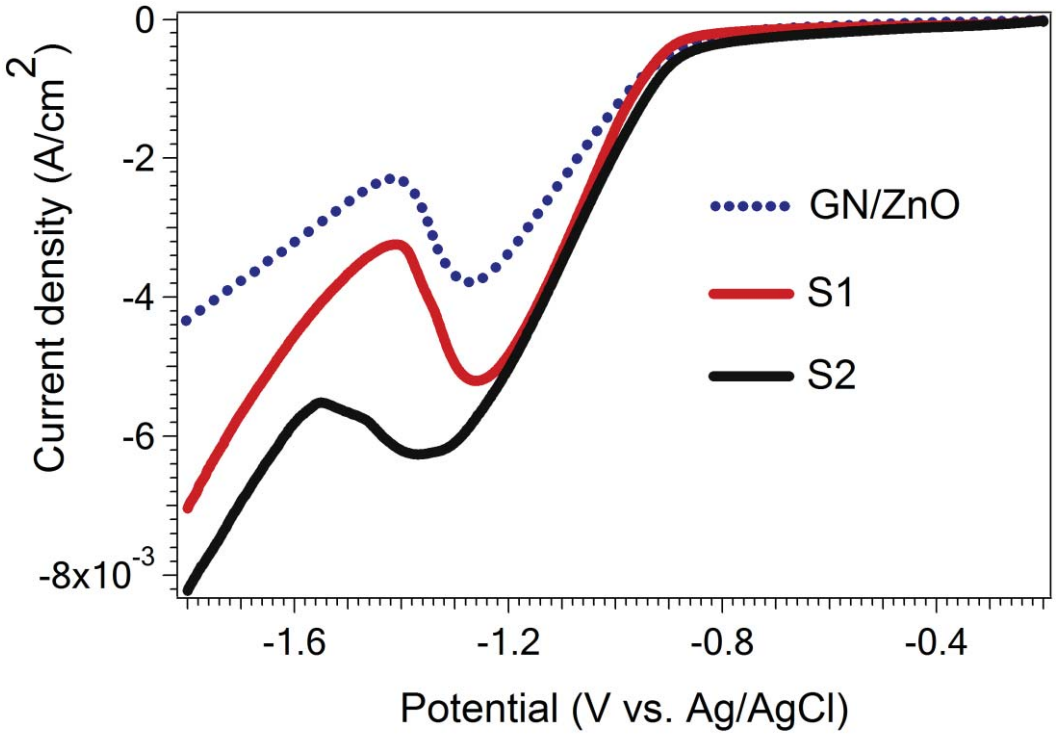

Figure 4.22 Linear sweep voltammograms of GN/ZnO (dotted line), S1 and S2-based electrodes in CO_2 saturated 0.5 M $NaHCO_3$ solution at scan rate of 20 mV/s.

4.3.7.2 Chronoamperometry

The electro-catalytic activity of GN/ZnO, GN/ZnO/Cu_2O (S1 and S2) electrodes towards CO_2 reduction was carried out at fixed potentials ranging from -0.8 to -1.8 V *vs.* Ag/AgCl at a sweep rate of 20 mV/s as shown in figure 4.23. After one hour of CO_2 bubbling and 20 min of CO_2 reduction, all electrodes showed the following feature: the current value was very high for the first 15 s and then decreased gradually. Then, current goes constantly during the remaining period. GN/ZnO, S1, and S2-based electrodes were tested at different fixed potentials to evaluate their catalytic activity towards CO_2 electroreduction.

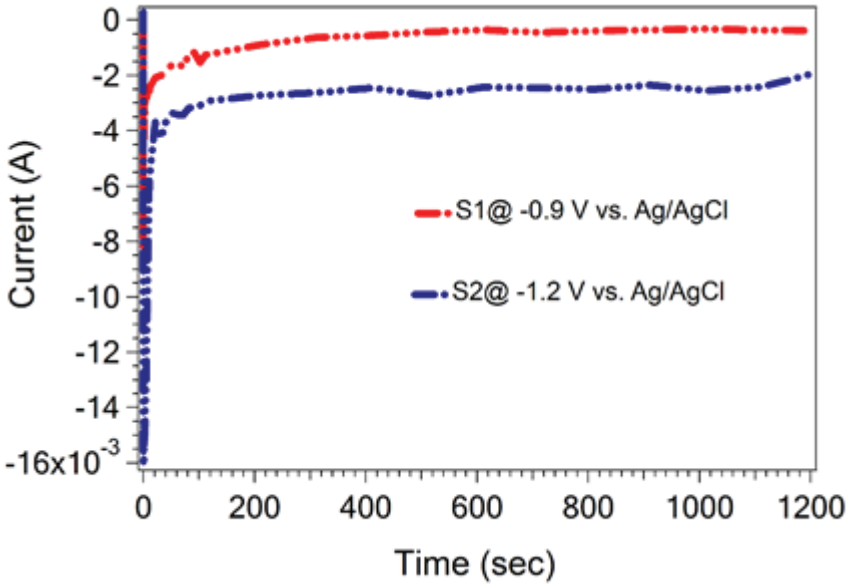

Figure 4.23 Current responses for GN/ZnO/Cu_2O (S1 and S2)-based electrodes in CO_2-saturated electrolyte.

4.3.8 GC-MS analysis & Faradaic efficiency

The liquid samples after CO_2 reduction were analyzed by a headspace gas chromatograph (Agilent technologies-7890A GC system) equipped with mass spectrometer (Inert MSD-with triple axis detector). Compounds were separated on a HP-5, 30 m x 0.32 mm x 0.25 µm GC column, with an injection and detector temperature of 220 and 250 ^{o}C, respectively. Helium was used as a carrier gas with a flow rate of 50 ml/min. N-propanol was found to be the predominant product over GN/ZnO/Cu_2O (S1 and S2) electrodes at -0.9 and -1.2 V, respectively after a 20 min reduction. In contrast, no liquid products have been detected at GN/ZnO electrode under the same conditions. It was identified by co-injection with standard samples and their quantifications were accomplished by integrating peak areas using calibration curves as depicted in figure 4.24. The GC peaks of real and propanol standard samples appear at approximately 1.37 min retention time. No other liquid products were detected, suggesting that n-propanol is the only liquid product produced. Table 4.4 shows the Faradaic efficiency for n-propanol produced using GN/ZnO/Cu_2O electrodes. FE is calculated based on 18 electrons are required to convert CO_2 to n-propanol. Also, this study did not investigate the gaseous products. Figure 4.25 shows the Faradaic efficiency for n-propanol as a function of applied potentials over S1 and S2 surfaces. The maximum Faradaic efficiency (30%) was obtained at -0.9 V using S1 surface, suggesting the strong stabilization of Cu(I) by ZnO. It can be seen that the FE decreased with increasing the applied overpotential at S1 surface, this may be due to the change of the product selectivity of the reaction coincide with the partial reduction of Zn(II). On the other hand, S2 performed high FE of 22% at -1.2 V. The increasing of FE with increasing the applied potential (starting from -0.9 to -1.2 V) at S2 surface might be related to the effect of the

high content of the Cu_2O active site. Table 4.5 shows the maximum Faradaic efficiency for n-propanol produced using GN/ZnO/Cu_2O-based electrodes comparing with some recent reports.

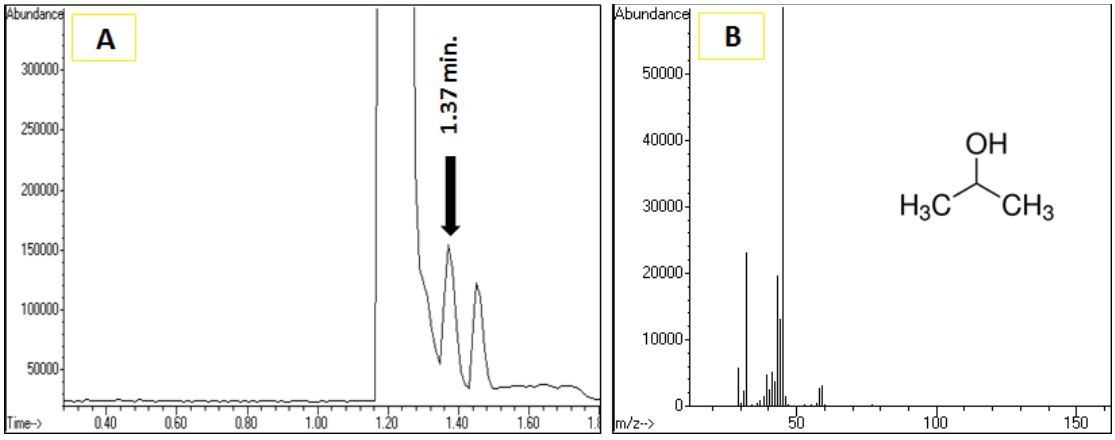

Figure 4.24 (a) GC-MS chromatogram shows n-propanol Peak (Black arrow) at RT= 1.37 min produced using GN/ZnO/Cu_2O surfaces. (b) Mass spectra show defragments of alcohol.

Table 4.4 Faradaic efficiency and n-propanol concentration obtained by CO_2 electroreduction using GN/ZnO/Cu_2O (S1 and S2) electrodes.

Electrode	E vs. Ag/AgCl	j (A/cm^2)	n-propanol (ppm)	FE (%)
GN/ZnO/Cu_2O (S1: ZnO/Cu_2O weight ratio of 2:1)	-0.9	6.34×10^{-4}	1.335	30
GN/ZnO/Cu_2O (S2: ZnO/Cu_2O weight ratio of 1:2)	-1.2	2.364×10^{-3}	3.68	22

Table 4.5 Comparison of Faradaic efficiency for n-propanol produced by CO_2 electroreduction using GN/ZnO/Cu_2O (S1 and S2) electrodes comparing with some related reports.

Electrode	**E and/or *j***	**FE (%)**	**Ref.**
Cu nanocrystal	-0.95 V vs. RHE	10.6	[12]
Cu (100)	-5 mA/cm^2	1.5	[14]
Cu(S)-[4 (100) × (111)]	-0.23 mA/cm^2 *	4.6	
Cu nanoparticles	-0.4 V vs. RHE	10	[15]
Cu_2O	1.39 V vs. Ag/AgCl	2.4	[16]
GN/ZnO/Cu_2O (S1: ZnO/Cu_2O weight ratio of 2:1)	-0.9 V vs. Ag/AgCl	30	This work
GN/ZnO/Cu_2O (S2: ZnO/Cu_2O weight ratio of 1:2)	-1.2 V vs. Ag/AgCl	22	

* Current density of n-propanol production

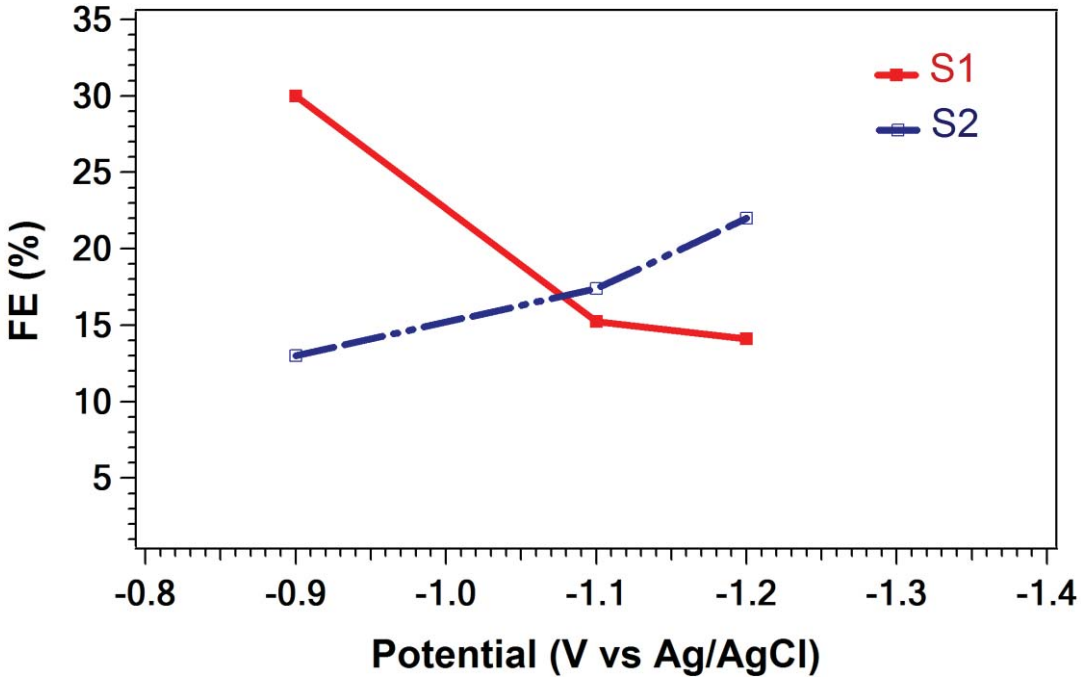

Figure 4.25 Faradaic efficiency for n-propanol produced over S1 and S2 (dashed line) surfaces at different applied potentials.

4.3.9 Summary

In summary, graphene/ZnO/Cu_2O binary and tertiary composite were synthesized via simple procedure with varying Cu_2O/ZnO weight ratios at very low temperature. The linear sweep voltammetry indicates that, the current increase upon increasing Cu_2O/ZnO weight ratio. Graphene/ZnO/Cu_2O (different Cu_2O/ZnO weight ratios) electrodes showed excellent catalytic activity and selectivity towards CO_2 electroreduction to isopropyl alcohol in 0.5 M $NaHCO_3$ aqueous solution and under ambient conditions. The high selectivity toward C_3 product stems from graphene contribution as well as stabilization of Cu (I) by ZnO. In addition, these results clearly shows the synergic effect of ZnO/Cu_2O weight ratio. We can concluded that graphene acting well as supporting high-conductivity material for ZnO/Cu_2O in the electrochemical reduction of CO_2.

CHAPTER 5

MECHANISM PATHWAY

5.1 Proposed mechanism at graphene/Cu_2O surface

As discussed in chapter 4 the electroreduction of CO_2 over graphene/Cu_2O surface produce ethanol. The GN/Cu_2O electrode seems to be highly selective towards ethanol as indicated at different potential. The electroreduction of CO_2 over various copper-based electrodes have been deeply studied [76][90]. However, the catalytic mechanisms proposed are still controversial. We suggest the mechanistic pathways for the electrochemical reduction of CO_2 to ethanol as described earlier [78]. It is well known, the adsorbate *CO species is the first intermediate formed during electrochemical CO_2 reduction at relatively high negative potentials [12][91][92]. In a recent electrokinetic study, *CH_xO intermediate is favored C-C coupling reaction rather than *CO intermediate [93]. Moreover, graphene enhances the electron transfer mobility over Cu_2O surface. As a result, *CO adsorbed species can further easily reduced to *$C_2H_xO_2$ intermediate through dimerization and hydrogenation reactions [70][78]. In addition, the critical role played by the edges formed as Cu^+ reduced to Cu during CO_2 reduction to coverage the surface of *CH_xO reactive species and facilitate their dimerization to *$C_2H_xO_2$ intermediate. Subsequently, *$C_2H_xO_2$ intermediate undergoes reduction to ethanol. Table 4.3 (chapter 4) shows comparison of faradaic efficiency for ethanol production over different copper-based electrodes. The Faradaic efficiency of

ethanol is mostly depend on the thickness of catalyst and the applied potential [78]. Therefore, from the results presented in table 4.3 (chapter 4) this likely reveal the graphene role in improvement the selectivity toward C_2 product using 0.1 mg GN/Cu_2O catalyst at -0.9 V (vs. Ag/AgCl). Figure 5.1 illustrated the proposed mechanism for ethanol production (C_2 product) as a result of the electrochemical reduction of CO_2 at graphene/Cu_2O surface.

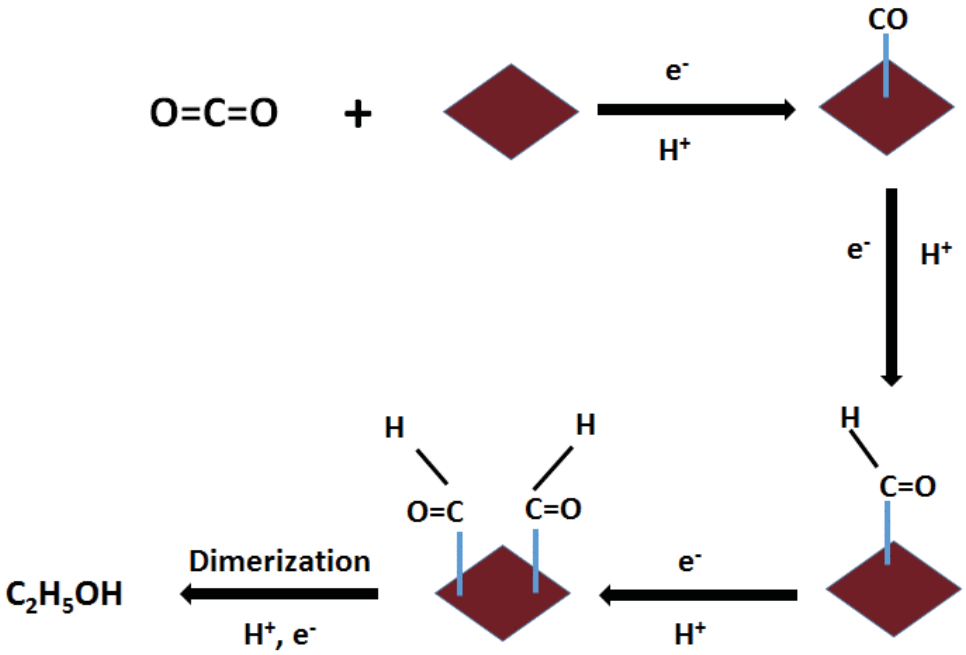

Figure 5.1 Proposed mechanism for the electroreduction of CO_2 to ethanol at GN/Cu_2O surface.

5.2 Proposed mechanism at graphene/ZnO/Cu_2O surface

Graphene/ZnO/Cu_2O based electrodes showed high selectivity toward n-propanol production as discussed in chapter 4. Up to now, there is no suggested mechanism for the conversion of CO_2 to C_3 product. In contrast, the electrochemical reduction of CO_2 to C_1 products has been extensively studied over different electrodes surfaces. However, the reaction mechanisms of CO_2 converting to C_1 or C_2 products have been proposed, the exact mechanism for CO_2 electroreduction is still unclear. It is reported that, Cu (I) stabilized by ZnO and a strengthening the link between active sites and CO^-, and thus result in increased alcohol production selectivity [81]. Propanol is produced in very trace levels as a result of CO_2 reduction using various surfaces [94][95]. E. Andrews et al. claimed that selectivity toward n-propanol production is improved over Cu/ZnO surface rather than Cu surface [95]. However, n-propanol has been produced as a result of CO_2 reduction over Cu surface at more negative potential (-1.1 V vs. RHE) and proposed by repeated dihydroxylation of enol-like surface intermediates [94]. On the other hand, J. Albo et al. have been evaluated the performance of Cu_2O/ZnO at different weight ratios for CO_2 reduction into methanol and traces of ethanol and propanol. This finding suggested that Cu_2O is supposed to be the active site for alcohol formation since the alcohol production was decreased with increasing ZnO loading [74]. The study claimed that the lower catalytic activity of Cu_2O/ZnO surfaces related to the coverage of the small Cu_2O particle size by large ZnO particle size. As well as, ZnO was fabricated without copper oxide for only HCOOH and CO formation [23][50]. In the present study, SEM and XPS results confirmed the deposition of Cu_2O over ZnO particles. Therefore, these results interpret the higher catalytic activity of GN/ZnO/Cu_2O (S1 and S2)-based electrodes as shown in figure 4.22

(chapter 4). Thus, step sites of Cu (I) with Zn decoration contains Cu-ZnO_x special active sites that make significant contributions to the activity toward n-propanol production. In addition, graphene does more than the high surface area, but also enhance the electron mobility causing more reduction of CO^- adsorbed species, leads to high molecular products. Graphene/Cu_2O was performed for efficient and high selectivity of CO_2 reduction to ethanol [96]. Graphene as non-metallic supporting high conductive material showed a critical role in stabilizing the adsorbed species and coupling of two C_1 to C_2 product. Also, some earlier studies indicated the formation of large hydrocarbons C_1-C_9 over carbon-based electrodes [12][63]. This is explain the suggested mechanism over GN/ZnO/Cu_2O (S1 and S2) surface as a highly selective electro-catalyst towards CO_2 reduction to n-propanol. Figure 5.2 illustrated the proposed mechanism for n-propanol production (C_3 product) as a result of the electrochemical reduction of CO_2 at graphene/ZnO/Cu_2O surface.

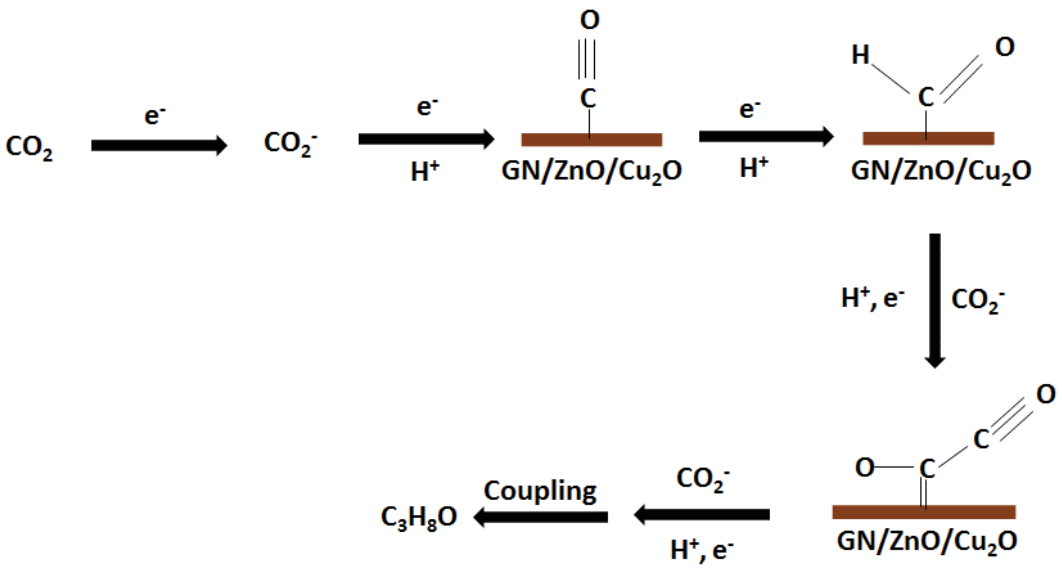

Figure 5.2 Proposed mechanism for the electroreduction of CO_2 into n-propanol at GN/ZnO/Cu_2O surface.

CHAPTER 6

CONCLUSIONS & RECOMMENDATIONS

6.1 Conclusions

Graphene/Cu_2O and graphene/ZnO/Cu_2O were successfully synthesized at very low temperature at 34 ^oC using simple wet chemical approach and fabricated as cathodes for CO_2 electroreduction in aqueous electrolyte solution.

The electrochemical reduction of CO_2 was performed using copper modified graphene/Cu_2O electrode revealed that the current density was improved due to graphene contribution. Based on 0.1 mg of GN/Cu_2O catalyst loading, LSV measurements resulted in a high current density value of 12.2 mA/cm^2 at -1.7 V versus Ag/AgCl. Ethanol was found to be the predominant liquid reduction product at -0.9 V under ambient conditions. No liquid products other than ethanol were detected, implying the selectivity towards C_2 products. These results suggest that graphene-based catalyst can be efficiently used for electrochemical reduction of CO_2.

Graphene/ZnO/Cu_2O binary and tertiary composites were synthesized via simple procedure with varying Cu_2O/ZnO weight ratios at very low temperature. The linear sweep voltammetry indicates that, the current increase upon increasing Cu_2O/ZnO weight ratio. Graphene/ZnO/Cu_2O (different Cu_2O/ZnO weight ratios) electrodes showed excellent catalytic activity and selectivity towards CO_2 electroreduction to n-propanol in 0.5 M $NaHCO_3$ aqueous solution and under ambient conditions. The high selectivity stems from

graphene contribution as well as stabilization of Cu (I) by ZnO. In addition, these results clearly shows the synergic effect of ZnO/Cu_2O weight ratio. The Faradaic efficiency for CO_2 conversion to n-propanol was 22% and 30% for $GN/ZnO/Cu_2O$ (with a Cu_2O/ZnO weight ratios of 2:1 and 1:2) at an applied potential of -1.2 and -0.9 V vs. Ag/AgCl, respectively. In contrast, no alcohol was detected using GN/ZnO under all of the conditions tested. We can concluded that graphene act well as supporting high-conductivity material for ZnO/Cu_2O in the electrochemical reduction of CO_2.

6.2 Recommendations for future work

Based on the difficulties encountered in this work such as the reduction of the metal oxides under applied potential and for better understanding of the reaction mechanism pathways, the following has been suggested for further analyses in the future:

1- Study the pulse-electrolysis approach to refresh the oxide phase of the electrode surfaces for more catalysts stability enhancing.
2- Some functionalization of graphene surface may enhance the performance of the electro-catalysts.
3- Fabrication and evaluation of electro-catalysts-based MOF for the electrochemical conversion of CO_2.
4- In this work, the results showed some synergic effect of ZnO/Cu_2O catalysts for conversion of CO_2 into n-propanol, we believe that more study are necessary for better understanding this synergic effect of both oxides.

References

[1] M.F. Baruch, J.E.P. Iii, J.L. White, A.B. Bocarsly, Mechanistic Insights into the Reduction of CO_2 on Tin Electrodes using in Situ ATR-IR Spectroscopy, ACS Catal. 5 (2015) 3148–3156. doi:10.1021/acscatal.5b00402.

[2] Z. Huo, M. Hu, X. Zeng, J. Yun, F. Jin, Catalytic reduction of carbon dioxide into methanol over copper under hydrothermal conditions, Catal. Today. 194 (2012) 25–29. doi:10.1016/j.cattod.2012.06.013.

[3] A. Nirmala, S. Yi, M. Vinoba, M. Bhagiyalakshmi, D. Hyun, Y. Yoon, S. Chan, S. Kwan, Electrochemical reduction of carbon dioxide at low overpotential on a polyaniline/Cu_2O nanocomposite based electrode, Appl. Energy. 120 (2014) 85–94. doi:10.1016/j.apenergy.2014.01.022.

[4] M. Murugananthan, M. Kumaravel, H. Katsumata, Electrochemical reduction of CO_2 using Cu electrode in methanol/$LiClO_4$ electrolyte, Int. J. Hydrogen Energy. 40 (2015) 6740–6744. doi:10.1016/j.ijhydene.2015.04.006.

[5] Q. Guo, Q. Zhang, H. Wang, Z. Liu, Z. Zhao, Core-shell structured ZnO @ Cu-Zn – Al layered double hydroxides with enhanced photocatalytic efficiency for CO_2 reduction, Catal. Commun. 77 (2016) 118–122. doi:10.1016/j.catcom.2016.01.019.

[6] G.A. Olah, G.K.S. Prakash, A. Goeppert, Anthropogenic Chemical Carbon Cycle for a Sustainable Future, J. Am. Chem. Soc. 133 (2011) 12881–12898.

[7] G. Centi, S. Perathoner, Opportunities and prospects in the chemical recycling of

carbon dioxide to fuels, Catal. Today. 148 (2009) 191–205. doi:10.1016/j.cattod.2009.07.075.

[8] K.P. Kuhl, T. Hatsukade, E.R. Cave, D.N. Abram, J. Kibsgaard, T.F. Jaramillo, Electrocatalytic Conversion of Carbon Dioxide to Methane and Methanol on Transition Metal Surfaces, J. Am. Chem. Soc. 136 (2014) 14107–14113.

[9] T.H. Shin, J. Myung, K.M. Naeem, C. Savaniu, J.T.S. Irvine, $Ce(Mn,Fe)O_2$–$(La,Sr)(Fe,Mn)O_3$ composite as an active cathode for electrochemical reduction of CO_2 in proton conducting solid oxide cells, Solid State Ionics. 275 (2015) 106–109. doi:10.1016/j.ssi.2015.03.015.

[10] S.M.A. Kriescher, K. Kugler, S.S. Hosseiny, Y. Gendel, M. Wessling, A membrane electrode assembly for the electrochemical synthesis of hydrocarbons from CO_2(g) and H_2O(g), Electrochem. Commun. 50 (2015) 64–68. doi:10.1016/j.elecom.2014.11.014.

[11] A. Behr, Carbon dioxide as an alternative C1-building block: activation by transition metal complexes, Angew. Chem. 100 (1988) 681–689.

[12] S. Pérez-rodríguez, N. Rillo, M.J. Lázaro, E. Pastor, Pd catalysts supported onto nanostructured carbon materials for CO_2 valorization by electrochemical reduction, Appl. Catal. B Environ. 163 (2015) 83–95. doi:10.1016/j.apcatb.2014.07.031.

[13] S. Kaneco, N. Hiei, Y. Xing, H. Katsumata, H. Ohnishi, T. Suzuki, K. Ohta, Electrochemical conversion of carbon dioxide to methane in aqueous $NaHCO_3$ solution at less than 273 K, Electrochim. Acta. 48 (2002) 51–55.

[14] H. Kim, I. Choi, S. Hyun, S. Jun, S. Jong, J. Han, J. Kim, H. Park, J. Hyun, S. Kim, Analysis on the effect of operating conditions on electrochemical conversion of carbon dioxide to formic acid, Int. J. Hydrogen Energy. 39 (2014) 16506–16512. doi:10.1016/j.ijhydene.2014.03.145.

[15] H.M. Jhong, S. Ma, P.J.A. Kenis, Electrochemical conversion of CO_2 to useful chemicals : current status , remaining challenges , and future opportunities, Curr. Opin. Chem. Eng. 2 (2013) 191–199. doi:10.1016/j.coche.2013.03.005.

[16] J. Xie, Y. Huang, W. Li, X. Song, L. Xiong, H. Yu, Efficient electrochemical CO_2 reduction on a unique chrysanthemum-like Cu nanoflower electrode and direct observation of carbon deposite, Electrochim. Acta. 139 (2014) 137–144. doi:10.1016/j.electacta.2014.06.034.

[17] N. Ullah, I. Ali, S. Omanovic, Electrochemical Reduction of CO_2 in an Aqueous Electrolyte Employing an Iridium/Ruthenium-Oxide Electrode, Can. J. Chem. Eng. 93 (2015) 55–62. doi:10.1002/cjce.22110.

[18] N. Spataru, K. Tokuhiro, C. Terashima, T.N. Rao, A. Fujishima, Electrochemical reduction of carbon dioxide at ruthenium dioxide deposited on boron-doped diamond, J. Appl. Electrochem. 33 (2003) 1205–1210.

[19] Q. Lu, F. Jiao, Electrochemical CO_2 reduction: Electrocatalyst , reaction mechanism , and process engineering, Nano Energy. 29 (2016) 439–456. doi:10.1016/j.nanoen.2016.04.009.

[20] G. Keerthiga, B. Viswanathan, R. Chetty, Electrochemical reduction of CO_2 on

electrodeposited Cu electrodes crystalline phase sensitivity on selectivity, Catal. Today. 245 (2015) 68–73. doi:10.1016/j.cattod.2014.08.008.

[21] J. Rosen, G.S. Hutchings, Q. Lu, R. V Forest, A. Moore, F. Jiao, Electrodeposited Zn Dendrites with Enhanced CO Selectivity for Electrocatalytic CO_2 Reduction, ACS Catal. 5 (2015) 4586–4591. doi:10.1021/acscatal.5b00922.

[22] Y. Kim, T. Si, B. Trung, S. Yang, S. Kim, H. Lee, Mechanism of the Surface Hydrogen Induced Conversion of CO_2 to Methanol at Cu (111) Step Sites, ACS Catal. 6 (2016) 1037–1044. doi:10.1021/acscatal.5b02083.

[23] Y. Hori, H. Konishi, T. Futamura, A. Murata, O. Koga, H. Sakurai, K. Oguma, Deactivation of copper electrode in electrochemical reduction of CO_2, Electochimica Acta. 50 (2005) 5354–5369. doi:10.1016/j.electacta.2005.03.015.

[24] X. Nie, G.L. Griffin, M.J. Janik, A. Asthagiri, Surface phases of Cu_2O (111) under CO_2 electrochemical reduction conditions, Catal. Commun. 52 (2014) 88–91. doi:10.1016/j.catcom.2014.02.022.

[25] Y. Yang, C. Han, B. Jiang, J. Iocozzia, C. He, D. Shi, T. Jiang, Z. Lin, Graphene-based materials with tailored nanostructures for energy conversion and storage, Mater. Sci. Eng. R. 102 (2016) 1–72. doi:10.1016/j.mser.2015.12.003.

[26] A.T. Najafabadi, Emerging applications of graphene and its derivatives in carbon capture and conversion: Current status and future prospects, Renew. Sustain. Energy Rev. 41 (2015) 1515–1545. doi:10.1016/j.rser.2014.09.022.

[27] G.A. Olah, A. Goeppert, G.K.S. Prakash, Chemical Recycling of Carbon Dioxide to

Methanol and Dimethyl Ether : From Greenhouse Gas to Renewable, Environmentally Carbon Neutral Fuels and Synthetic Hydrocarbons, J. Org. Chem. 74 (2009) 487–498.

[28] E. V Kondratenko, G. Mul, J. Baltrusaitis, G.O. Larrazabal, J. Perez-Ramirez, Status and perspectives of CO_2 conversion into fuels and chemicals by catalytic, photocatalytic and electrocatalytic processes, Energy Environ. Sci. 6 (2013) 3112–3135. doi:10.1039/c3ee41272e.

[29] M. Aresta, A. Dibenedetto, A. Angelini, Catalysis for the Valorization of Exhaust Carbon : from CO_2 to Chemicals , Materials , and Fuels. Technological Use of CO 2, Chem. Rev. 114 (2014) 1709–1742.

[30] L.I. Hardy, R.W. Gillham, Formation of Hydrocarbons from the Reduction of Aqueous CO_2 by Zero-Valent Iron, Environ. Sci. Technol. 30 (1996) 57–65.

[31] O.K. Varghese, M. Paulose, T.J. Latempa, C.A. Grimes, S.U. V, U. V Park, V. Pennsyl, High-Rate Solar Photocatalytic Conversion of CO_2 and Water Vapor to Hydrocarbon Fuels, Nano Lett. 9 (2009) 731–737.

[32] M.S. Hamdy, R. Amrollahi, I. Sinev, B. Mei, G. Mul, Strategies to Design Efficient Silica-Supported Photocatalysts for Reduction of CO_2, J. Am. Chem. Soc. 136 (2014) 594–597.

[33] A.P. Abbott, C.A. Eardley, Electrochemical Reduction of CO_2 in a Mixed Supercritical Fluid, J. Phys. Chem. B. 104 (2000) 775–779.

[34] Y. Hori, H.H.I. Wakebe, T. Tsukamoto, O. Koga, Electrocatalytic Process of CO

Selectivity in Electrochemical Reduction of CO_2 at Metal Electrodes in Aqueous Media, Electrochim. Acta. 39 (1994) 1833–1839.

[35] Y. Hori, R. Takahashi, Formation of Hydrocarbons in the Electrochemical Reduction of Carbon Dioxide at a Copper Electrode in Aqueous Solution, J. Chem. Soc., Faraday Trans. 85 (1989) 2309–2326.

[36] T. Mizuno, A. Naitoh, K. Ohta, Electrochemical reduction o f CO_2 in methanol at -30 oC, J. Electroanal. Chem. 391 (1995) 199–201.

[37] C. Finn, S. Schnittger, J. Yellowlees, J.B. Love, Molecular approaches to the electrochemical reduction of carbon dioxide, Chem. Commun. 48 (2012) 1392–1399. doi:10.1039/c1cc15393e.

[38] N.S. Spinner, J.A. Vega, W.E. Mustain, Recent progress in the electrochemical conversion and utilization of CO_2, Catal. Sci. Technol. 2 (2012) 19–28. doi:10.1039/c1cy00314c.

[39] S. Kuwabata, R. Tsuda, H. Yoneyama, Electrochemical Conversion of Carbon Dioxide to Methanol with the Assistance of Formate Dehydrogenase and Methanol Dehydrogenase as Biocat aly sts, J. Am. Chem. Soc. 116 (1994) 5437–5443.

[40] Y. Chen, C.W. Li, M.W. Kanan, Aqueous CO_2 Reduction at Very Low Overpotential on Oxide-Derived Au Nanoparticles, J. Am. Chem. Soc. 134 (2012) 19969–19972.

[41] B. Innocent, D. Pasquier, F. Ropital, F. Hahn, J.. Leger, K.. Kokoh, FTIR spectroscopy study of the reduction of carbon dioxide on lead electrode in aqueous

medium, Appl. Catal. B Environ. 94 (2010) 219–224. doi:10.1016/j.apcatb.2009.10.027.

[42] M. Alvarez-guerra, S. Quintanilla, A. Irabien, Conversion of carbon dioxide into formate using a continuous electrochemical reduction process in a lead cathode, Chem. Eng. J. 207–208 (2012) 278–284. doi:10.1016/j.cej.2012.06.099.

[43] P. Kang, C. Cheng, Z. Chen, C.K. Schauer, T.J. Meyer, M. Brookhart, Selective Electrocatalytic Reduction of CO_2 to Formate by Water- Stable Iridium Dihydride Pincer Complexes, J. Am. Chem. Soc. 134 (2012) 5500–5503.

[44] A. Goeppert, M. Czaun, J.-P. Jones, G.K.S. Prakash, G.A. Olah, Recycling of carbon dioxide to methanol and derived products-closing the loop, Chem. Soc. Rev. 43 (2014) 7995–8048. doi:10.1039/C4CS00122B.

[45] S. Bailey, G.F. Froment, J.W. Snoeck, K.C. Waugh, A DRIFTS study of the morphology and surface adsorbate composition of an operating methanol synthesis catalyst, Catal. Letters. 30 (1995) 99–111.

[46] J. Nakamura, T. Uchijima, Y. Kanai, T. Fujitani, The role of ZnO in Cu/ZnO methanol synthesis catalysts, Catal. Today. 28 (1996) 223–230.

[47] K. Hirano, K. Inoue, T. Yatsu, Photocatalysed reduction of CO_2 in aqueous TiO_2 suspension mixed with copper powder, J. Photochem. Photobiol. A Chem. 64 (1992) 255–258.

[48] F. Quan, D. Zhong, H. Song, F. Jia, L. Zhang, A highly efficient zinc catalyst for selective electroreduction of carbon dioxide in aqueous NaCl solution, J. Mater.

Chem. A Mater. Energy Sustain. 3 (2015) 16409–16413. doi:10.1039/C5TA04102C.

[49] D. Deciccio, S.T. Ahn, S. Sen, F. Schunk, G.T.R. Palmore, C. Rose-petruck, Electrochemical reduction of CO_2 with clathrate hydrate electrolytes and copper foam electrodes, Electrochem. Commun. 52 (2015) 13–16. doi:10.1016/j.elecom.2015.01.006.

[50] S. Ohya, S. Kaneco, H. Katsumata, T. Suzuki, K. Ohta, Electrochemical reduction of CO_2 in methanol with aid of CuO and Cu_2O, Catal. Today. 148 (2009) 329–334. doi:10.1016/j.cattod.2009.07.077.

[51] S. Sen, D. Liu, G.T.R. Palmore, Electrochemical Reduction of CO_2 at Copper Nanofoams, ACS Catal. 4 (2014) 3091–3095.

[52] R. Reske, H. Mistry, F. Behafarid, B.R. Cuenya, P. Strasser, Particle Size Effects in the Catalytic Electroreduction of CO_2 on Cu Nanoparticles, J. Am. Chem. Soc. 136 (2014) 6978–6986.

[53] E. Nursanto, H. Jeon, C. Kim, M. Jee, J. Koh, Y. Hwang, B. Min, Gold catalyst reactivity for CO_2 electro-reduction: From nano particle to layer, Catal. Today. 260 (2016) 107–111. doi:10.1016/j.cattod.2015.05.017.

[54] D. Gao, H. Zhou, J. Wang, S. Miao, F. Yang, G. Wang, J. Wang, X. Bao, Size-Dependent Electrocatalytic Reduction of CO_2 over Pd Nanoparticles, J. Am. Chem. Soc. 137 (2015) 4288–4291. doi:10.1021/jacs.5b00046.

[55] G.K. Ramesha, J.F. Brennecke, P. V Kamat, Origin of Catalytic Effect in the

Reduction of CO_2 at Nanostructured TiO_2 Films, ACS Catal. 4 (2014) 3249–3254.

[56] Q. Lu, J. Rosen, Y. Zhou, G.S. Hutchings, Y.C. Kimmel, J.G. Chen, F. Jiao, A selective and efficient electrocatalyst for carbon dioxide reduction, Nat. Commun. (2014) 1–6. doi:10.1038/ncomms4242.

[57] T. Chang, R. Liang, P. Wu, J. Chen, Y. Hsieh, Electrochemical reduction of CO_2 by Cu_2O-catalyzed carbon clothes, Mater. Lett. 63 (2009) 1001–1003. doi:10.1016/j.matlet.2009.01.067.

[58] Y. Lan, S. Ma, J. Lu, P.J.A. Kenis, Investigation of a Cu (core)/ CuO (shell) Catalyst for Electrochemical Reduction of CO_2 in Aqueous Soultion, Int. J. Electrochem. Sci. 9 (2014) 7300–7308.

[59] F. Jia, X. Yu, L. Zhang, Enhanced selectivity for the electrochemical reduction of CO_2 to alcohols in aqueous solution with nanostructured Cu-Au alloy as catalyst, J. Power Sources. 252 (2014) 85–89. doi:10.1016/j.jpowsour.2013.12.002.

[60] J. Qu, X. Zhang, Y. Wang, C. Xie, Electrochemical reduction of CO_2 on RuO_2 / TiO_2 nanotubes composite modified Pt electrode, Electrochim. Acta. 50 (2005) 3576–3580. doi:10.1016/j.electacta.2004.11.061.

[61] K.J.P. Schouten, E.P. Gallent, M.T.M. Koper, The influence of pH on the reduction of CO and CO_2 to hydrocarbons on copper electrodes, J. Electroanal. Chem. 716 (2014) 53–57. doi:10.1016/j.jelechem.2013.08.033.

[62] A. Naitoh, K. Ohta, T. Mizuno, H. Yoshida, M. Sakai, H. Nodat, Electrochemical reduction of carbon dioxide in methanol at low temperature, Electochimica Acta. 38

(1993) 2177–2179.

[63] N.R. De Tacconi, W. Chanmanee, B.H. Dennis, F.M. Macdonnell, D.J. Boston, K. Rajeshwar, Electrocatalytic Reduction of Carbon Dioxide Using Pt/C-TiO_2 Nanocomposite Cathode, Electrochem. Solid-State Lett. 15 (2012) B5–B8. doi:10.1149/2.008201esl.

[64] R. Zhang, W. Lv, G. Li, L. Lei, Electrochemical reduction of CO_2 on SnO_2/nitrogen-doped multiwalled carbon nanotubes composites in $KHCO_3$ aqueous solution, Mater. Lett. 141 (2015) 63–66. doi:10.1016/j.matlet.2014.11.040.

[65] A.A. Ismail, R.A. Geioushy, H. Bouzid, S.A. Al-sayari, A. Al-hajry, D.W. Bahnemann, TiO_2 decoration of graphene layers for highly efficient photocatalyst : Impact of calcination at different gas atmosphere on photocatalytic efficiency, Appl. Catal. B Environ. 129 (2013) 62–70. doi:10.1016/j.apcatb.2012.09.024.

[66] M. Liu, R. Liu, W. Chen, Graphene wrapped Cu_2O nanocubes : Non-enzymatic electrochemical sensors for the detection of glucose and hydrogen peroxide with enhanced stability, Biosens. Bioelectron. 45 (2013) 206–212. doi:10.1016/j.bios.2013.02.010.

[67] Y. Qian, F. Ye, J. Xu, Z. Le, Synthesis of Cuprous Oxide (Cu_2O) Nanoparticles/Graphene Composite with an Excellent Electrocatalytic Activity Towards Glucose, Int. J. Electrochem. Sci. 7 (2012) 10063–10073.

[68] S. Stankovich, D.A. Dikin, R.D. Piner, K.A. Kohlhaas, A. Kleinhammes, Y. Jia, Y. Wu, Synthesis of graphene-based nanosheets via chemical reduction of exfoliated

graphite oxide, Carbon N. Y. 45 (2007) 1558–1565. doi:10.1016/j.carbon.2007.02.034.

[69] J. Albo, P. Castaño, A. Irabien, Towards the electrochemical conversion of carbon dioxide into methanol, Green Chem. 17 (2015) 2304–2324. doi:10.1039/c4gc02453b.

[70] K.P. Kuhl, E.R. Cave, D.N. Abram, T.F. Jaramillo, New insights into the electrochemical reduction of carbon dioxide on metallic copper surfaces, Energy Environ. Sci. 5 (2012) 7050–7059. doi:10.1039/c2ee21234j.

[71] J. Albo, A. Irabien, Cu_2O-loaded gas diffusion electrodes for the continuous electrochemical reduction of CO_2 to methanol, J. Catal. 343 (2016) 232–239. doi:10.1016/j.jcat.2015.11.014.

[72] J. Albo, D. Vallejo, G. Beobide, O. Castillo, P. Castaço, Copper-Based Metal–Organic Porous Materials for CO_2 Electrocatalytic Reduction to Alcohols, ChemSusChem. 9 (2016) 1–11. doi:10.1002/cssc.201600693.

[73] Z. Zhang, L. Ren, W. Han, L. Meng, X. Wei, X. Qi, J. Zhong, One-pot electrodeposition synthesis of ZnO/graphene composite and its use as binder-free electrode for supercapacitor, Ceram. Int. 41 (2015) 4374–4380. doi:10.1016/j.ceramint.2014.11.127.

[74] J. Albo, A. Sáez, J. Solla-gullón, V. Montiel, A. Irabien, Production of methanol from CO_2 electroreduction at Cu_2O and Cu_2O/ZnO-based electrodes in aqueous solution, Appl. Catal. B Environ. 176–177 (2015) 709–717.

doi:10.1016/j.apcatb.2015.04.055.

[75] Y. Lan, C. Gai, P.J.A. Kenis, J. Lu, Electrochemical Reduction of Carbon Dioxide on Cu/CuO Core/Shell Catalysts, ChemElectroChem. 1 (2014) 1577–1582. doi:10.1002/celc.201402182.

[76] M. Le, M. Ren, Z. Zhang, P.T. Sprunger, R.L. Kurtz, J.C. Flake, Electrochemical Reduction of CO_2 to CH_3OH at Copper Oxide Surfaces, J. Electrochem. Soc. 158 (2011) E45–E49. doi:10.1149/1.3561636.

[77] L.M. Aeshala, R.G. Uppaluri, A. Verma, Effect of cationic and anionic solid polymer electrolyte on direct electrochemical reduction of gaseous CO_2 to fuel, J. CO_2 Util. 3–4 (2013) 49–55. doi:10.1016/j.jcou.2013.09.004.

[78] D. Ren, Y. Deng, A.D. Handoko, C.S. Chen, S. Malkhandi, Selective Electrochemical Reduction of Carbon Dioxide to Ethylene and Ethanol on Copper (I) Oxide Catalysts, ACS Catal. 5 (2015) 2814–2821. doi:10.1021/cs502128q.

[79] D. Kim, S. Lee, J.D. Ocon, B. Jeong, J. Kwang, J. Lee, Insights into an autonomously formed oxygen-evacuated Cu_2O electrode for the selective production of C_2H_4 from CO_2, Phys. Chem. Chem. Phys. 17 (2014) 824–830. doi:10.1039/C4CP03172E.

[80] Y. Hori, I. Takahashi, O. Koga, N. Hoshi, Electrochemical reduction of carbon dioxide at various series of copper single crystal electrodes, J. Mol. Catal. A Chem. 199 (2003) 39–47. doi:10.1016/S1381-1169(03)00016-5.

[81] Y. Kim, T. Si, B. Trung, S. Yang, S. Kim, H. Lee, Mechanism of the Surface

Hydrogen Induced Conversion of CO_2 to Methanol at Cu(111) Step Sites, ACS Catal. 6 (2016) 1037–1044. doi:10.1021/acscatal.5b02083.

[82] J. Yu, J. Jin, M. Jaroniec, A noble metal-free reduced graphene oxide–CdS nanorod composite for the enhanced visible-light photocatalytic reduction of CO_2 to solar fuel, J. Mater. Chem. A. 2 (2014) 3407–3416. doi:10.1039/c3ta14493c.

[83] Z. Zhang, L. Ren, W. Han, L. Meng, X. Wei, X. Qi, J. Zhong, One-pot electrodeposition synthesis of ZnO/graphene composite and its use as binder-free electrode for supercapacitor, Ceram. Int. 41 (2014) 4374–4380. doi:10.1016/j.ceramint.2014.11.127.

[84] C. Hsieh, C. Lin, Y. Chen, J. Lin, Synthesis of ZnO@Graphene composites as anode materials for lithium ion batteries, Electrochim. Acta. 111 (2013) 359–365. doi:10.1016/j.electacta.2013.07.197.

[85] A.A. Ashkarran, B. Mohammadi, ZnO nanoparticles decorated on graphene sheets through liquid arc discharge approach with enhanced photocatalytic performance under visible-light, Appl. Surf. Sci. 342 (2015) 112–119. doi:10.1016/j.apsusc.2015.03.030.

[86] J. Li, H. Li, Y. Xue, H. Fang, W. Wang, Facile electrodeposition of environment-friendly Cu_2O/ZnO heterojunction for robust photoelectrochemical biosensing, Sensors Actuators B Chem. 191 (2014) 619–624. doi:10.1016/j.snb.2013.10.060.

[87] C. Luo, D. Li, W. Wu, C. Yu, W. Li, C. Pan, Preparation of 3D reticulated ZnO/CNF/NiO heteroarchitecture for high-performance photocatalysis, Appl. Catal.

B Environ. 166–167 (2015) 217–223. doi:10.1016/j.apcatb.2014.11.030.

[88] B.J. Liu, X. Li, L. Dai, Water-Assisted Growth of Aligned Carbon Nanotube–ZnO Heterojunction Arrays, Adv. Mater. 18 (2006) 1740–1744. doi:10.1002/adma.200502346.

[89] J. Ma, K. Wang, L. Li, T. Zhang, Y. Kong, S. Komarneni, Visible-light photocatalytic decolorization of Orange II on Cu_2O/ZnO nanocomposites, Ceram. Int. 41 (2015) 2050–2056. doi:10.1016/j.ceramint.2014.09.137.

[90] C.W. Li, M.W. Kanan, CO_2 Reduction at Low Overpotential on Cu Electrodes Resulting from the Reduction of Thick Cu_2O Films, J. Am. Chem. Soc. 134 (2012) 7231–7234.

[91] T. Hatsukade, K.P. Kuhl, E.R. Cave, D.N. Abram, T.F. Jaramillo, Insights into the electrocatalytic reduction of CO_2 on metallic silver surfaces, Phys. Chem. Chem. Phys. 16 (2014) 13814–13819. doi:10.1039/c4cp00692e.

[92] D. Kolbe, W. Vielstich, Adsorbate formation during the electrochemical reduction of carbon dioxide at palladium-A DEMS study, Electochimica Acta. 41 (1996) 2457–2460.

[93] J.H. Montoya, A.A. Peterson, J.K. Nørskov, Insights into C-C Coupling in CO_2 Electroreduction on Copper Electrodes, ChemCatChem. 5 (2013) 737–742. doi:10.1002/cctc.201200564.

[94] D.D. Zhu, J.L. Liu, S.Z. Qiao, Recent Advances in Inorganic Heterogeneous Electrocatalysts for Reduction of Carbon Dioxide, Adv. Mater. 28 (2016) 3423–

3452. doi:10.1002/adma.201504766.

[95] E. Andrews, M. Ren, F. Wang, Z. Zhang, P. Sprunger, R. Kurtz, J. Flake, Electrochemical Reduction of CO_2 at Cu Nanocluster/(1010) ZnO Electrodes, J. Electrochem. Soc. 160 (2013) H841–H846. doi:10.1149/2.105311jes.

[96] R.A. Geioushy, M.M. Khaled, A.S. Hakeem, K. Alhooshani, C. Basheer, High efficiency graphene/Cu_2O electrode for the electrochemical reduction of carbon dioxide to ethanol, J. Electroanal. Chem. 785 (2017) 138–143. doi:10.1016/j.jelechem.2016.12.029.

Vitae

Name	:Ramadan Abdelmonem Rabie Mohamed Geioushy
Nationality	:Egyptian
Date of Birth	:6/10/1983
Email	:r_gushy@yahoo.com/ rgeioushy@kfupm.edu.sa
Address	:Central Metallurgical R&D Institute (CMRDI), Egypt
Academic Background	:Click here to enter text.

- **PhD degree in Chemistry**, King Fahd University of Petroleum and Minerals, KSA, 2017. *Research Focus:* Fabrication of electro-catalysts for the electrochemical conversion of carbon dioxide into value-added products.
- **M.Sc. degree in Chemistry,** Beni-Suef University, 2010, in physical chemistry entitled "Synthesis and Characterization of Low Dimensional Thin Films Based on Ti-O-C-N System by Chemical Vapor Deposition Technique".

  Research Focus: Synthesis and Characterization of Ti-O-C-N Thin Films by Chemical Vapor Deposition Technique.
- **B.Sc. in Chemistry**, Faculty of science, Cairo University, Fayoum branch, May 2004, Excellent with the honor degree.

AWARDS AND FELLOWSHIPS

- Saudi Arabian Government Graduate Fellowship for International Scholars tenable at King Fahd University of Petroleum & Minerals (KFUPM), KSA.
- Runner-Up Award for poster presentation at 'Chemistry Students Research Poster Day 2017' Chemistry Department, KFUPM, January 3-4, 2017.
- International Summer Course in Materials Processes for two months at the Royal Institute of Technology (KTH), Stockholm, Sweden, June 2006.

EXPERIENCES

Lecturer; Chemistry department, King Fahd University of Petroleum & Minerals (KFUPM), KSA; (2013-2017).

- Engaged in full-time electrochemical conversion of CO_2 research.
- Taught several classroom and lab-based chemistry courses allotted by the registrar.
- Assisted in administering (including grading) freshmen chemistry and other school examination.
- Assisted in other departmental duties and student course registrations.

Assistant Researcher, Nanomaterials and Nanotechnology Department, Advanced Materials Division, Central Metallurgical R&D Institute (CMRDI), Egypt, 2005 to Dec., 2012.

- Synthesis and characterization of nanostructured materials, thin films, and development of advanced catalytic materials and processes for energy related applications.
- Synthesis of TiO_2-Graphene nanocomposite for photocatalytic application.

- Synthesis of Ti-O, Ti-O-C and Ti-O-C-N system by MOCVD.
- Synthesis of ZnS and SiC by CVD technique.
- Synthesis of Ni nanopartciles by simple wet method.
- Synthesis of ZnO nanorod by thermal evaporation.

SELECTED RESEARCH PUBLICATIONS

- ***R.A. Geioushy**, Mazen M. Khaled, Khalid Alhooshani, Abbas S. Hakeem, A. Rinaldi, '**Graphene/ZnO/Cu_2O electrocatalyst for selective conversion of CO_2 to n-propanol**' Electrochimica Acta 2017, http://dx.doi.org/ 10.1016/j.electacta.2017.05.185.*
- ***R.A. Geioushy**, Mazen M. Khaled, Abbas S. Hakeem, Khalid Alhooshani, Chanbasha Basheer, ' **High efficiency graphene/Cu_2O electrode for the electrochemical reduction of carbon dioxide to ethanol** ' journal of Electroanalytical Chemistry 785 (2017) 138-143.*
- *Adel A. Ismail, **R.A. Geioushy**, Houcine Bouzid, Saleh A. Al-Sayari, Ali Al-Hajry, Detlef W. Bahnemann, "**TiO_2 Decoration of Graphene Layers for Highly Efficient Photocatalyst: Impact of Calcination at Different Gas Atmosphere on Photocatalytic efficiency**" Applied Catalysis B: Environmental 129 (2013) 62-70.*
- *O.A. Fouad, **R.A. Geioushy**, S.M. El-Sheikh, M.H. Khedr, I.A. Ibrahim, "**Metalorganic chemical vapor deposition of Ti–O–C–N thin films using TBOT as a promising precursor**" Journal of Alloys and Compounds* 509 (2011) 6090-6095.

CONFERENCES

- The "International Conference on Powering a Greener Future: Nanomaterials for Solar energy Conversion" [Solar 09], 10-14 January 2009, Luxor, Egypt.
- International Conference on Materials imperatives in the new millennium [MINM 2010] 29 Nov. – 2 Dec., 2010 CMRDI, Cairo, Egypt.
- Poster presentation at the 4th Saudi International Nanotechnology Conference (SINC 2016), KFUPM, 25th – 26th October, 2016.

WORKSHOPS

- The Egyptian-Italian workshop on Nanotechnology applications, February 23-24, 2009, American University in Cairo, Egypt.
- The US-Egypt Advanced Studies Institute "Nanomaterials & Nanocataylsis for Energy Petrochemicals and Environmental Applications", March 28- April 4, 2010, National Research Centre, Cairo, Egypt.
- Workshop on Introduction to Nanomaterials Development for Petro-Catalytic Applications. Center of Research Excellence in Nanotechnology (CENT). KFUPM, 27 October, 2016.

REFEREES (available on request)